BRAIN NETWORK, MODELLING AND CORRESPONDING EEG PATTERNS FOR HEALTH AND DISEASE STATES

A Thesis Submitted by

Auhood Hadi Jabbar Al-Hossenat

For the award of

Doctor of Philosophy

2020

Dedication

To

God who gave me the power

Mum and Dad who prayed for me day and night

My husband, Dr. Ammar and my children, Leelas and Joud, who supported me

Without whom this thesis would not have been completed and received success and honour

Auhood Hadi Jabbar

University of Southern Queensland 2020

Abstract

EEG is a significant tool used to capture normal and abnormal cerebral electrical activities in human brain. To understand and test complex hypotheses about the mechanisms of their generation, various model and modelling approaches have been proposed and developed.

Among these models and approaches, a new type of network model has emerged known as large-scale brain network model (LSBNM). LSBNM is becoming increasingly important in understanding, studying and testing the mechanisms of the generation of normal and abnormal oscillatory activities of the human brain. It also offers unique predictive tools for studying disease states and brain abnormalities. However, there are still many limitations in the existing LSBNM approaches. Hence, developing novel methods for LSBNM leads to the exploration, generation and prediction of a new and rich repertoire of healthy and disease rhythmic activities in the human brain.

The aim of this project is to develop LSBNM to include new versions of network models comprising various human cerebral areas in the left and right hemispheres. First, two network models at multi scale are developed to generate EEG patterns for health states: alpha rhythms with a low frequency at 7Hz and, and the alpha band of EEG rhythms at different ranges of frequencies 7–8 Hz, 8–9 Hz and 10–11 Hz. Second, a new network model for simulating multi-bands of EEG patterns: delta–range frequency of (1-4 Hz), theta at a frequency of (4-7Hz) and diverse narrowband oscillations ranging from delta to theta (0-5Hz) is introduced. Third, novel brain network models are simulated and used to predict the abnormal electrical activity such as oscillations observed in the epileptic brain.

The design and simulation of each of the network models are implemented using the unique neuro informatics platform: The Virtual Brain (TVB).

This project made significant contributions to brain modelling, in particularly to the understanding of neural activity in the human brain at multi levels of scale. Further, it emphasises the role of structural connectivity of the connectome on emerging normal and abnormal dynamics of brain oscillations, as well as affirming that modelling with TVB can provide reliable neuroimaging data such as EEG_S for the healthy and diseased brain. In particular, the results of this study help researchers and physicians studying large-scale brain activity associated with lower and higher alpha oscillations and the delta waves of Stages 3 and 4 of the sleep and theta waves of Stages 1 and 2 of sleep. Moreover, they will be able to assist researchers and clinical doctors in the field of epilepsy to understand the complex neural mechanisms generating abnormal oscillatory activities and, thus, may open up new avenues towards the discovery of new clinical interventions related to these types of activities.

Certification of Thesis

This thesis is entirely the work of Auhood Hadi Jabbar Al-Hossenat except where otherwise acknowledged, with the majority of the authorship of the papers presented as a Thesis by Publication undertaken by the Student. The work is original and has not previously been submitted for any other award, except where acknowledged.

Peng (Paul) Wen: Principal Supervisor

Yan Li: Associate Supervisor

Student and supervisors signatures of endorsement are held at USQ.

Statement of Contribution

This section presents details of contributions by the various authors for each of the paper presented in this thesis by publication. The following detail is the agreed share of contributions for the candidate and co-authors in the published articles and the ones to be published.

Chapter 3, Al-Hossenat, et al., (2017, 2019a)

Al-Hossenat, A., Wen, P. and Li, Y, 2017, ' Simulation α of EEG using brain network model', in *Proceedings of the 1st MoHESR and* HCED Iraqi Scholars Conference in Australasia 2017 (ISCA 2017), Melbourne, Australia, 5th-6th December, 2017, pp. 336-345.
https://scholar.google.com.au/scholar?hl=en&as_sdt=0%2C5&q=Simulation+%CE%B1+of+EEG+using+brain+network+model&btnG=.

Al-Hossenat, A, Wen, P & Li, Y 2019a (in press) , 'Large-scale brain network model and multi-band Electroencephalogram rhythm simulations', *International journal of Biomedical Engineering and Technology*. http://www.inderscience.com/info/ingeneral/forthcoming.php?jcode=IJBET.

Author	Percent contribution	Tasks Performed
Al-Hossenat, A	70%	Designed the method, simulation, analysis, interpretation, wrote entire draft of paper.
Wen, P., Li, Y	30%	Significantly improved the manuscript, interpretation, and analysis.

Chapter 4, Al-Hossenat, et al., (2018, 2019b, 2020a)

The contents of this chapter was published in the Proceedings of ResearchFora 34th International Conference on Science, Engineering & Technology - ICSET 2019, Brisbane, Australia (Al-Hossenat, 2018) and was chosen as an excellent paper. It was then published in the in the International Journal of Electrical, Electronics and Data Communication as an excellent paper (Al-Hossenat, 2019b). Also, the contents of this chapter have been submitted to the journal of computer methods and programs in biomedicine, Q1, (under review) for publication.

Al-Hossenat, A., Wen, P. and Li, Y, 2018, 'Modelling and simulating different bands of EEG signals with the virtual brain', in *Proceedings of the Research Fora, 34th International Conference on Science, Engineering & Technology - ICSET 2019,* Brisbane, Australia, 8th -9th November, 2018, pp. 25-29.

Al-Hossenat, A, Wen, P & Li, Y 2019b, 'Modelling and simulating different bands of EEG signals with the virtual brain', *International Journal of Electrical, Electronics and Data Communication*, vol. 7, no. 5, pp. 66-70. https://scholar.google.com.au/scholar?hl=en&as_sdt=2005&sciodt=0%2C5&cites=13562361217473426022&scipsc=&q=%27Modelling+and+simulating+different+bands+of+EEG+signals+with+the+virtual+brain%27&btnG=

Al-Hossenat, A., Wen, P. and Li, Y 2020a, 'New brain network models for generating delta and theta rhythms'. Journal of *computer methods and programs in biomedicine,* Q1, *(*under review).

Author	**Percent contributio**	**Tasks Performed**
Al-Hossenat, A	70%	Designed the method, simulation, analysis, interpretation, wrote entire draft of the paper.
Wen, P., Li, Y	30%	Significantly improved the manuscript, interpretation, and analysis.

Chapter 5, Al-Hossenat, et al., (2020b)

Al-Hossenat, A., Wen, P. and Li, Y 2020, 'EEG epileptic patterns regeneration using novel brain network models', submitted to the Journal of Expert Systems with Application, Q1.

Author	**Percent contribution**	**Tasks Performed**
Al-Hossenat, A	70%	Designed the method, simulation, analysis, interpretation, wrote entire draft of the paper.
Wen, P., Li, Y	30%	Significantly improved the manuscript, interpretation, and analysis.

Acknowledgements

First, I would like to give my thanks to God for giving me good health, guidance, courage, knowledge and strength to complete my PhD study.

Next, the challenging work described in this thesis would not have been possible without the support and assistance of many people.

I would like to express my sincere gratitude and deepest appreciation to my principal supervisor, Professor Peng Wen (Paul Wen) for his guidance, remarks and continuous engagement and great patience throughout my PhD journey in the field of modelling and simulation. Without his suggestions, confidence, discussions, support, respect and patience, it would not have been possible to finish my PhD program. Also, my foremost gratitude goes to my co-supervisor Professor Yan Li for her support during my PhD study journey.

I would like to thank the Iraqi government and the University of Southern Queensland for giving me this opportunity. I would like to acknowledge the support of the Australian Commonwealth Government through the Research Training Program (RTP) Fees Offset scheme during my research. Special thanks go to the Faculty of Health, Engineering and Sciences and the ICT Service team of USQ.

I would like to show my deep personal gratitude to Sandra Cochrane for proofreading my thesis.

My special gratitude goes to my beloved family members. My thanks go my parents, Hadi and Mooda, for giving me unconditional love and support and always believing in me. Further, my brothers Thaer, Idel and Ali and their families, and my sisters Intesar and Kloud and, and Kloud's family especially her husband Bassem. Their support and encouragement are greatly appreciated.

My special thanks go to my lovely Aunt Fozeh for her encouragement and support through the study time and her daughter Hanan and her family.

I cannot forget my relatives as well as my friends here in Australia (Neale, Del, Kev Cottam, and Wendy Scott as well) and there in Iraq.

Finally, and most importantly, I would like to thank my husband, Dr. Ammar Shareef Kadhim for his love, standing beside me and encouraging me constantly at every step of my PhD study journey. Without his love and support, I couldn't have achieved my study goals. My deepest gratitude and massive thanks go to my lovely children, Leelas and Joud, for all their love and moral support necessary to achieve this success.

Table of Contents

List of Figures

List of Tables

List of related publications

The following papers, associated with this project and included in this thesis, have been published or submitted for publication.

JOURNAL PAPERS

Al-Hossenat, A, Wen, P & Li, Y 2019, 'Modelling and simulating different bands of EEG signals with the virtual brain', *International Journal of Electrical, Electronics and Data Communication*, vol. 7, no. 5, pp. 66-70.

Al-Hossenat, A, Wen, P & Li, Y 2019, 'Large-scale brain network model and multi-band Electroencephalogram rhythm simulations', *International journal of Biomedical Engineering and Technology* (in press).

PEER-REVIEWED CONFERENCE PAPERS

Al-Hossenat, A., Wen, P. and Li, Y, 2017, ' Simulation α of EEG using brain network model', in *Proceedings of the 1st MoHESR and* HCED Iraqi Scholars Conference in Australasia 2017 (ISCA 2017), Melbourne, Australia, 5th-6th December, 2017, pp. 336-345.

Al-Hossenat, A., Wen, P. and Li, Y, 2018, 'Modelling and simulating different bands of EEG signals with the virtual brain', in *Proceedings of the ResearchFora, 34th International Conference on Science, Engineering & Technology - ICSET 2019,* Brisbane, Australia, 8th -9th November, 2018, pp. 25-29.

JOURNAL PAPERS SUBMITTED

Al-Hossenat, A., Wen, P. and Li, Y 2020, 'New brain network models for generating delta and theta rhythms', submitted to the Journal of *computer methods and programs in biomedicine.*

Al-Hossenat, A., Wen, P. and Li, Y 2020, 'EEG epileptic patterns regeneration using novel brain network models', submitted to the Journal of *Expert Systems with Application*.

Abbreviations

AAL	Automated Anatomical Labelling
AD	Alzheimers Disease
AP	Action Potentials
BNM	Brain Network Model
BOLD	Blood-Oxygen-Level-Dependent
CM	Connectivity Matrix
CV	Conduction Velocity
DFT	Discrete Fourier Transform
DSI	Diffusion Spectrum Imaging
E	Excitatory
ECoG	Electrocorticography
EEG	Electroencephalogram
EIN	Excitatory Interneurons
EPSP	Excitatory Post Synaptic Potentials
FC	Functional Connectivity
FFT	Fast Fourier Transform
FH-N	FitzHugh-Nagumo
FMRI	Functional Magnetic Resonance Imaging
HCPS	Human Connectome Projects
HFOS	High-Frequency Oscillations
Hz	Hertz
I	Inhibitory
IIN	Inhibitory Interneurons
ILAE	International League against Epilepsy
IPSP	Inhibitory Post Synaptic Potentials
JR	Jansen and Rit
LSBNM	Large-Scale Brain Network Modelling
MEG	Magnetoencephalography

MRI	Magnetic Resonance Imaging
NM	Neural Mass
NMM	Neural Mass Model
ODES	Ordinary Differential Equations
P2SW	Poly 2 Spike Waves
PC	Pyramidal Cell
PSP	Post Synaptic Potentials
Q-S	Quasi-Sinusoidal
R	Ripples
SC	Structure Connectivity
S-J2D	Stefanescu-Jirsa 2D
SR	Spikes Ripples
SSW	Sharp Spikes Waves
SW	Spike Waves
S-W	Spike and Wave
SWD	Spike Wave Discharges
TMS	Transcranial Magnetic Stimulation
TVB	The Virtual Brain
WT	Wavelet Transform
α	Alpha
β	Beta
γ	Gamma
δ	Delta
θ	Theta

CHAPTER 1

INTRODUCTION

1.1 Background

The human brain is an extremely complex network system consisting of approximately 10^{10} neurons which are closely interconnected via synapses. Neurons, the essential component of the brain, transmit and process information and interact with large numbers of other neurons (Purves et al., 2004). Dynamic brain activities, which contain a wealth of information for brain function, are mostly generated by mean of neural cartels composed of inhibitory and excitatory neural populations. These rhythmical electrical activities can be monitored using techniques such as electroencephalography (EEG), electrocorticography (ECoG), magnetic resonance imaging (MRI), and functional magnetic resonance imaging (fMRI).

EEG is a significant tool used to capture cerebral electrical activities in the brain because of its non-invasiveness, excellent temporal resolution and usability (Grosse-Wentrup et al., 2009). Furthermore, it is a crucial instrument for diagnosing a person's state of health (whether asleep, awake or anaesthetized), and for diagnosing and treating different neural disorders and diseases such as Alzheimer's disease (AD), dementia and epilepsy (Adeli et al., 2003).

Normal EEG activity can be classified into specific bands at different frequencies: gamma-frequency typically higher than 30 Hz, beta-range frequency of 12-30 Hz, alpha-range frequency of 8–12 Hz, theta-range frequency of 4–8 Hz and delta–range frequency of 1–4 Hz) (Lally et al., 2014; Nunez et al., 2006). Abnormal activity that is characterized by different morphology patterns such as high-frequency oscillations (HFO_S) of ripples on spikes, spikes and waves, continuous and sporadic spikes, and ploy2 spikes (Medithe and Nelakuditi, 2016).

Understanding, studying and exploring the oscillatory activity of the human brain is a complicated but necessary task. One approach to achieving this task is simulating brain activity using mathematical models. These models do not use any live biological samples. Instead, they employ mathematical model with different parameters. Mathematical modelling offers many distinct advantages. It does not have side effects like real experiments performed under non-ideal conditions. One can study brain oscillatory activity without bothering about effects from outside, for example, incidence of the errors whether the errors were made by machine or researcher during experiments. Moreover, one can modify parameters easily while this is very difficult or even impossible in real experiments. Thus, mathematical models offer a useful tool for studying and testing complex hypotheses and solving large and complex problems easily, and without the need for high set-up costs and lengthy periods of time like those associated with real experiments.

Among these mathematical models, especially with the availability of detailed quantitative data of anatomical connections, a new type of network model (Spiegler & Jirsa, 2013) has emerged. It is known as large-scale brain network modelling (LSBNM). LSBNM incorporates biologically realistic, large-scale connectivity of brain regions, the so-called connectome with dynamic network models, known as neural mass model (NMM). NMMs absorb an important amount of biophysical parameters that describe properties and dynamic activity generated from connecting a local population of neurons. It is developed approximating the mesoscopic (local level) and macroscopic (global level) dynamic of cortical neural activity and allows for explorations of its local and global parameters and their impact on system behaviours. Hence, developing LSBNM has been essential in the area of biomedical research seeking to understand, simulate and predict the spatiotemporal dynamics of the brain's electrical activity at the multi-scale (Sanz Leon, 2014; Breakspear, 2017). So, a natural question is: Do we have a chance of exploring and understanding the complex neural mechanisms generating normal and abnormal large-scale brain activity without network brain simulation?

In this thesis, we focus on the development of a brain network model (BNM) that includes new versions of network models of the human brain to investigate the influence of local parameters and global parameters modification on behaviours of

novel network models. This research focuses on studying and modifying two of the most important local NMMs: the Jansen and Rit model (JR) and the Stefanescu-Jirsa 2D (S-J2D) model (Jansen and Rit, 1995; Stefanescu and Jirsa, 2008). Moreover, we investigate our own structural connectivity of the human brain by building connectivity matrices which represent coupling strengths, and consider time delay between brain areas at various brain lobes in both hemispheres on emerging normal and abnormal dynamics of brain oscillations. Our own structural connectivity is derived from a biologically realistic, large-scale connectivity connectome. The network models are proposed for simulating and predicting EEG brain activities at different levels of scale: normal electrical activity as well as abnormal electrical activity as observed in the epileptic human brain.

This study is the first network model to simulate and predict multi-alpha bands of rhythms at different ranges of low and high frequencies and multi-bands of patterns (delta and theta and diverse narrowband oscillations ranging from delta to theta), as well as predict epileptic patterns, and corresponding EEG patterns for healthy and diseased states. This study contributes to a better understanding of the complex neural mechanisms generating rhythmic activities at multi-scale for healthy and diseased human brains. Thus, it can support the diagnosis of brain disorders and the development of individualized medicine for brain diseases, as well as helping to improve the quality of life of patients with brain disorders.

1.2 Aim and objectives

The aim of this research is to develop LSBNMs to investigate how its local and global parameters affect the behaviour of developed network models' corresponding EEG patterns for healthy and diseased states. The objectives of this research are multi-fold.

The first objective is to develop a new LSBNM model to include four human cerebral areas at the left hemisphere of brain lobes to generate EEG patterns for healthy state alpha rhythms with the low frequency at 7Hz.

The second objective is to further improve the above LSBNMs at different levels of scale, including six cerebral areas to simulate multi-alpha band EEG rhythm frequency ranges of 7–8 Hz, 8–9 Hz and 10–11 Hz.

The third is to further investigate the LSBNM using a new network model comprising eight cerebral areas in the left hemisphere and different brain lobes to simulate more multi-bands of EEG patterns on different scales: delta–range frequency of (1-4 Hz), theta at a frequency of (4-7Hz) and diverse narrowband oscillations ranging from delta to theta (0-5Hz). Data from the time series generated from the network model are also validated using wavelet transform (WT).

The fourth is to develop novel LSBNMs comprising different numbers of cerebral areas in the left and right hemispheres of different brain lobes for simulating and predicting the EEG epileptic patterns: regular or irregular dynamic oscillations. Analysis of the simulated epileptic patterns is also achieved using WT. In addition, these novel network models are evaluated by comparing their outputs: different morphology patterns of abnormal with epileptiform abnormal pattern in EEG and other computational models.

1.3 Research strategy

We develop a set of LSBNMs that include multi-regions at multi-scale. Each model is comprised of different numbers of cerebral areas in the left and right hemispheres. We used these models to investigate how these proposed network models' behaviour changes if one or more of their local and global parameters are modified. A brief description of the research strategy is provided below.

First, a simplified LSBNM comprising four human cerebral areas at the left hemisphere is developed. A connectivity matrix representing the connection strength between four regions is built and embedded into an oscillator JR model with its original parameters. From here, the network model is extended and improved to include six cerebral areas by linking modified parameters of the JR model with the connectivity

matrix via specific connections. The time-delay is also considered in this network model. All outputs of the simplified and improved LSBNMs are validated using FFT.

Later on, a new model consisting of eight cerebral areas in the left hemisphere is developed based on further modifications on JR equations to include new values for parameters, representing interconnected excitatory and inhibitory populations at the local level. Global parameters adjustments that take into account structural connectivity are also considered in the model. The model outputs are validated using WT.

Another series of novel LSBNMs is introduced to investigate how the biophysical parameters of the S-J2D local mass model can affect the proposed model's behaviour via an imbalance between excitatory and inhibitory coupling strength at the local network. The results are compared with the epileptiform abnormal pattern in EEG and those obtained from other BNMs.

The design, implementation and simulation of each of our network models is carried out using the basis of the unique neuroinformatics platform: The Virtual Brain (TVB).

1.4 Research Outcomes and Significance

The proposed network models are evaluated in simulation and successfully predict various EEG brain activity patterns for healthy and diseased states.

First, from a simplified BNM, alpha rhythms with the low frequency at 7Hz are generated. These are associated with relaxation.

Second, from the improved BNM, the alpha bands of EEG rhythms at different ranges of 7–8 Hz, 8–9 Hz and 10–11 Hz are simulated. These indicate wakefulness with eyes closed that often precedes sleep.

These results of simplified and improved BNM will help researchers and physicians to understand the general mechanism of EEG rhythms and to accurately diagnose, especially with lower and higher alpha frequency ranges for cognitive and creative tasks, as well as diagnose patients who have neurocognitive disorders such as AD and dementia.

Third, from the new network models, multi-bands of EEG patterns: delta–range frequency of (1-4 Hz), theta at a frequency of (4-7Hz) and diverse narrowband oscillations ranging from delta to theta (0-5Hz), are simulated. These are associated with deep sleep (dreamless) and loss of awareness. These outcomes could be helpful to researchers and clinicians studying slow oscillation activity associated with the delta waves of Stages 3 and 4 of sleep and theta waves of Stages 1 and 2 of sleep.

Finally, from the novel $LSBNM_S$, different morphology patterns such as ripples on spikes, continuous spikes, sporadic spikes and ploy2 spikes ranging from 94-144 Hz, as observed in epileptic patients, are predicted. These results will assist researchers and clinical doctors in the field of epilepsy to understand the complex neural mechanisms of generating abnormal oscillatory activities and, thus, may open up avenues towards the discovery of new clinical interventions related to these types of activities.

This study makes a significant contribution to better understanding of neural activity in human brain at multi levels of scale. Further, it emphasises the role of structural connectivity of the connectome on emerging normal and abnormal dynamics of brain oscillations as well as affirming that modelling with TVB can provide reliable neuroimaging data such as EEG_S for the healthy and diseased brains.

1.5 Outline of the thesis

This thesis is organised into six chapters. It starts with Chapter 1: **Introduction** which provides an overview of the research study and the entire thesis including its aim and objectives, a brief description of the research strategy as well as a summary of the most

important outcomes and the significance of the work. The rest of this thesis is organised as follows:

Chapter 2 provides an overview of existing BNMs or LSBNMs and related background knowledge. It briefly introduces the fundamental knowledge and surrounding information related to this research including, the structure and functions of the human brain and the fundamentals of EEG and normal and abnormal neuronal activity. Next, the chapter briefly introduces brain network modelling and then a comprehensive literature review of existing BNMs at multi-scale. At the end of this chapter, the problem statements are defined.

Chapter 3 introduces the simulation and the development of multi-alpha band EEG rhythms at different frequency ranges 7Hz, 7–8 Hz, 8–9 Hz and 10–11 Hz using new LSBNMs. The first LSBNM model incorporates our own structural connectivity derived from a human brain connectome with a JR NMM in its standard parameterization. The second model focuses on modifying the parameterization of the JR model and investigates the integration of own structural connectivity via specific connection weights and time delays with modified parameters of the JR model. The chapter explains the architecture of each model, describes them mathematically, and provides the sequential steps of pipeline simulations used to develop network models. The results of each network model are analysed using FFT.

Chapter 4 presents a new network model for simulating different bands of EEG patterns: delta–range frequency of (1-4 Hz), theta at a frequency of (4-7Hz) and diverse narrowband oscillations ranging from delta to theta (0-5Hz). This work includes further modifying the JR model's equations, and adjusts and analyses their influence on proposed LSBNM behaviour. The results of the network models are evaluated using WT.

Chapter 5 introduces another novel network models for simulating and predicting EEG epileptic patterns on a different scale. This chapter investigates links of patterns and the parameters of S-J 2D using our own structural connectivity derived from the biological data. The outputs of the network models are analysed using WT and

compared with epileptiform abnormal patterns in real EEGs and with those obtained from other BNMs.

Chapter 6 provides the major outcomes and contributions of the study and discusses future research directions in this area.

CHAPTER 2

BRAIN AND BRAIN NETWORK MODELS

The Chapter presents a short introduction to the background knowledge and general concepts related to brain network modelling, including the structure of the human brain and its functions, background knowledge about EEG, and normal and abnormal neuronal activities. It provides a general description of brain network modelling and its components: general concepts, and background knowledge and a literature review on NMM and the human connectome. A comprehensive literature review of existing BNMs also is covered in this chapter.

2.1 Fundamentals of the human brain

The human head consists of multiple layers: the scalp, skull and brain. The scalp is the outer layer which covers the skull. The skull is a shaped hard bone layer and its purpose is to protect the brain. The brain is the deeper part of the human head and a remarkable object.

2.1.1 Structure of the human brain and its functions

The human brain is an amazing organ and is the essence of the central nervous system. It controls all functions of the human body including receiving, interpreting, processing and communicating information which, after processing, is sent to either parts of the brain or other parts of the body. Anatomically, the human brain is composed of three major parts: cerebrum, cerebellum and brainstem (Gray, 2002; Kahle and Frotscher, 2003), as shown in Figure 2.1 (Purves et al., 2004).

Cerebrum: The largest part of the human brain and performs important functions such as thoughts, movements, emotions and motor functions as well as interpreting touch,

hearing, vision and speech. It is divided into two hemispheres called left hemisphere and right hemisphere (Mayfield Clinic-online[1]). Each hemisphere is divided into four lobes and is split into several cerebral regions that serve specific functions (Purves et al., 2004) as shown in Figure 2.2:

- **Frontal lobe (pink):** The largest lobe in healthy human brains and located at the front of each cerebral hemisphere. Several areas of this lobe are important for cognitive functions, personality, emotions, motor development, planning, problem solving, parts of speech and movement
- **Parietal lobe (green)**: Sits behind the frontal lobe and several of its areas are responsible for sensations such as pain and touch, as well as processing visual signals and interpreting these signals from vision, hearing, sensory and memory
- **Occipital lobe (purple):** Contains most of the anatomical region of the visual cortex and is involved with visual processing such as colour, light and movement.
- **Temporal lobe (blue):** Located beneath the parietal and occipital lobes on the underside of the cerebrum and is involved in auditory processing as well as processing of semantics in both speech and vision

Cerebellum: Under the cerebrum at the back of the human head is the second-largest-part of the brain. It is responsible for important functions such as learning, coordinating movement and balance, and other senses

Brainstem: Located under the brain and connects the cerebrum to the spinal cord. It performs several automatic functions such as breathing, movement of the eyes and mouth, body temperature, wake and sleep cycles and digestion.

[1]Available: https://mayfieldclinic.com/pe-anatbrain.htm[Accessed 2017]

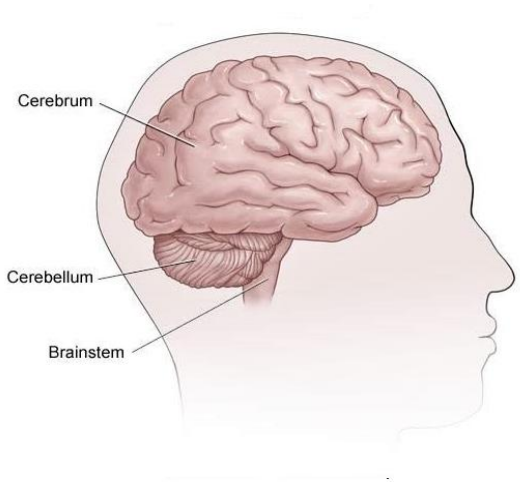

Figure 2.1: Anatomy of the human brain (Gray, 2002)

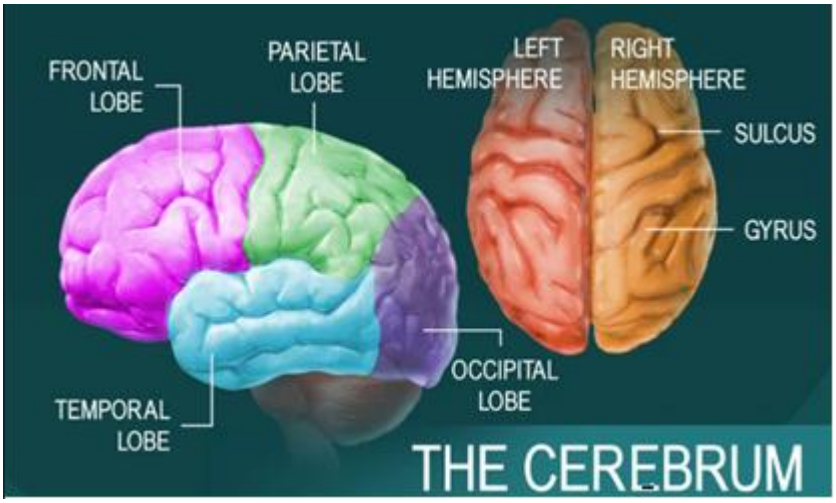

Figure 2.2: The two cerebral hemispheres of different brain lobes

Each cerebral hemisphere consists largely of grey matter that contains around 70 % of the brain's 100 billion neurons, and white matter that consists of myelinated fibers that connect the cortical areas with each other.

2.1.2 The neurons and their anatomical structure

Neurons are the basic functional unit of the brain. They receive and send electrical signals quickly over long distances. Although the shape and size of neurons vary, they

possess the same structure (Vanrumste et al., 2002). Figure 2.3 shows the anatomical structure of a neuron: a cell body (also called soma), the dendrites and an axon. The cell body is the main part of the neuron and contains indispensable components such as the nucleus. This cell body processes information (incoming signals) and determines whether or not the information has to be transmitted to the axon. The dendrites receive inputs from other cells. The axon extends from a few millimetres (in the brain) to a metre (from the spinal cord to the foot) and conveys signals to other nerve cells in the brain or to the spinal cord or to glands and muscles in the periphery of the body (Carlson and Braun, 1995; Carlson, 2005; Purves et al., 2004). Thus, electrical signals travel in one direction starting from the dendrite to the cell body, ending at the axon to its terminal which conducts electrical signals to the nerve synapse (the gap between nerve cells). Then the signals move across the synapse to another axon by means of a neurotransmitter.

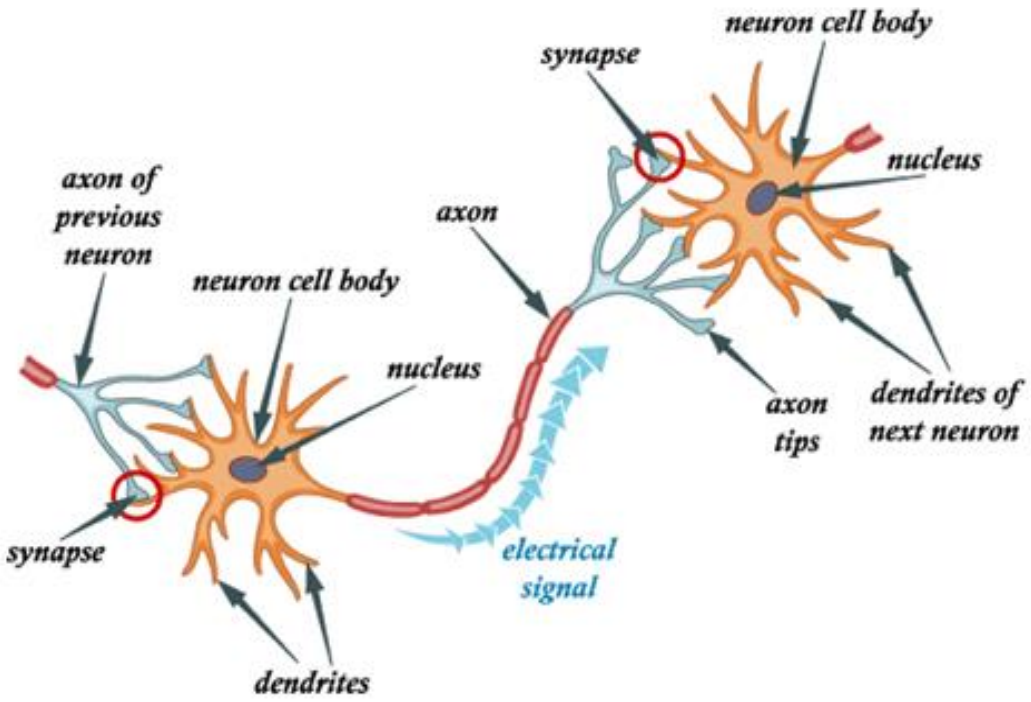

Figure 2.3: Anatomical structure of neuron and information transmission (Sanei and Chambers, 2007)

For communication between neurons, neurophysiological electrical events within a neuron are generated from both an external stimulus and chemical diffusion of ions (Atwood and MacKay, 1989). This electrical activity of neurons can be split into two subsets: action potentials (AP) and postsynaptic potentials (PSP). PSP are categorised into excitatory (or EPSPs) if they increase the probability of a postsynaptic action potential occurring, and inhibitory (or IPSPs) if they inhibit the likelihood of postsynaptic action occurring (Kingsley et al., 2000; Webster, 2014). Unlike the nerve cell AP's, PSPs are considered to be the main contributors to the EEG, that is recording these potentials from scalp surface, because nerve cell AP's have a much smaller potential field distribution and are much shorter in duration than PSPs. It is for these reasons that a large number of interacting neural ensembles (populations), the so-called neural mass (NM), generate fluctuations of electrical activity that are recordable on the head surface. Most of the neurons can receive inputs from both excitatory and inhibitory synapses, e.g. the pyramidal cell which is the most prevalent neuron cell in the cerebral cortex (see Figure 2.4) (Purves et al., 2004; Holmes and Khazipov, 2007; Sanei and Chambers, 2007; Webster, 2014).

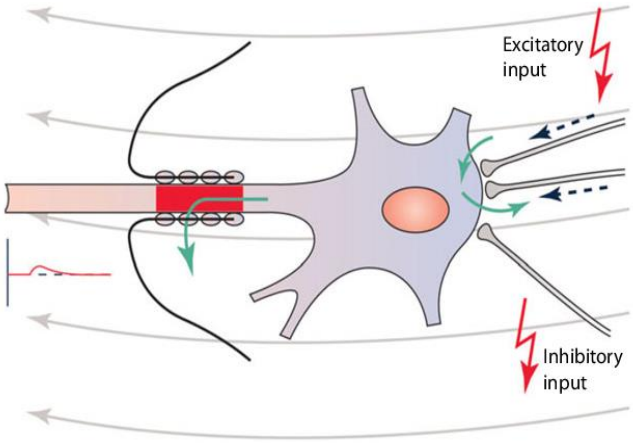

Figure 2.4: A cortical pyramidal cell is depicted with two somatic excitatory and one inhibitory synapse (pyramidal cell-online[2])

[2]Available: https://www.semanticscholar.org/paper/Membrane-resistance-and-shunting-inhibition%3A-where-Paulus-Rothwell/c99f31ead357a4aaef233f59c6def873dd356839/figure/2[Accessed1.01.2016](Paulus and Rothwell, 2016)

Among a group of electro biological measurements, EEG involves recording the brain electrical potentials generated by the brain structure.

2.1.3 Electroencephalography (EEG)

Electroencephalography (EEG) was the first of the electrobiological measurements and has undergone tremendous advance. In 1875, the first known neurophysiologic recordings of an animal were made by an English physician, Richard Caton, who observed the EEG from the exposed brains of rabbits and monkeys. In 1912, the first recorded animal (dog) EEG was made by the Russian physiologist, Vladimirovich.

In 1914, the first photographed EEG recordings of induced seizures (see Figure 2.5) were made by Cybulsky–Macieszyna. During 1914, the first human EEG recordings were made and these were published in 1929 by German physiologist and psychiatrist, Hans Berge. Berge invented the term EEG and discovered the alpha wave rhythm, also known as the “Berger" wave. He also described the nature of EEG alterations in brain diseases such as epilepsy (see Figure 2.6). In 1934, Adrian and Matthews verified the concept of “human brain waves" and identified regular oscillations around 10 to 12 Hz which they termed “alpha rhythm". In 1935 Gibbs, Davis and Lennox described interictal spike waves and the three cycles/patterns of clinical absence seizures. In 1953, the first EEG recordings of REM sleep were made by Aserinsky and Kleitman (Collura, 1993; Bronzino, 1995; Swartz & Goldensohn, 1998; Britton et al., 2016).

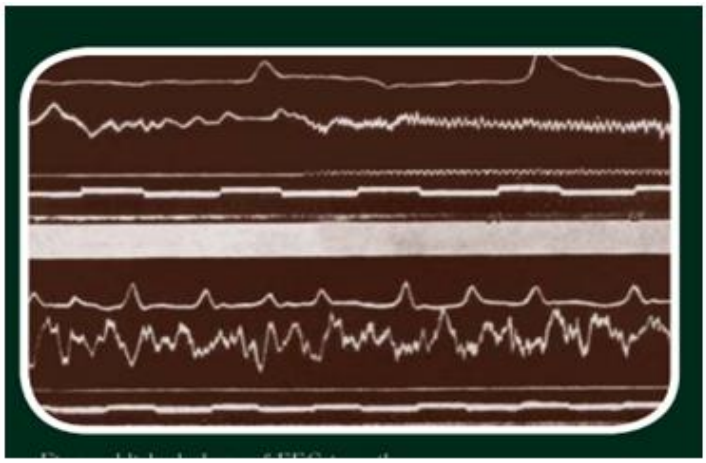

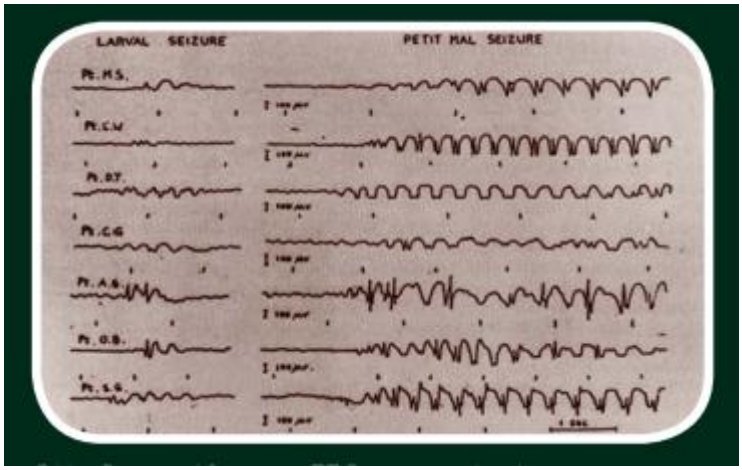

Figure 2.5: Top: the first photographed EEG recordings of experimental seizures. Bottom: EEG in petit mal epilepsy (EEG-online[3])

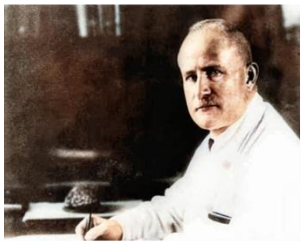

Hans Berger(1924)

One of Berger's first attempts to record the EEG in male patient

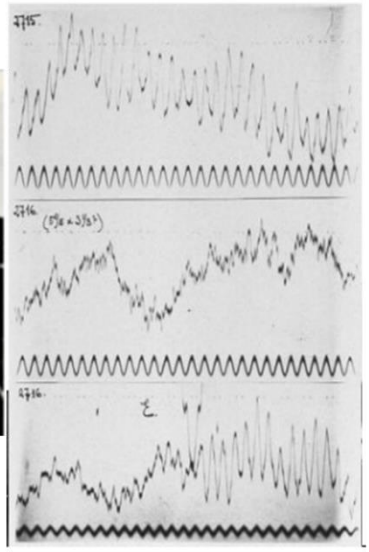

Recordings of EEG were made by Berger

Figure 2.6: The first human EEG recordings made by Hans Berger (Collura, 1993)

[3]Available: https://www.ilae.org/files/dmfile/Epi_poster17-26_PRESS6.pdf [Accessed 2017].

Current EEG testing uses electrode caps, conductive jelly, a ruler, injection and aid for disinfection, an EEG amplifier unit and a personal computer (PC)/laptop. The basic EEG system in a typical laboratory consists of electrodes, amplifiers with filters, converter (A/D) and device (PC or laptop) to record and store the data (see Figure 2.7) (Webster, 2014). EEG activity is recorded by electrodes positioned at different locations of the head surface (scalp). Each electrode is connected to an amplifier that transports the microvolt, and the A/D converter changes analog signals to digital signals which are finally stored or reviewed on a computer. The standard method for scalp electrode localization is the International 10-20 Electrode System (Jasper, 1958a).

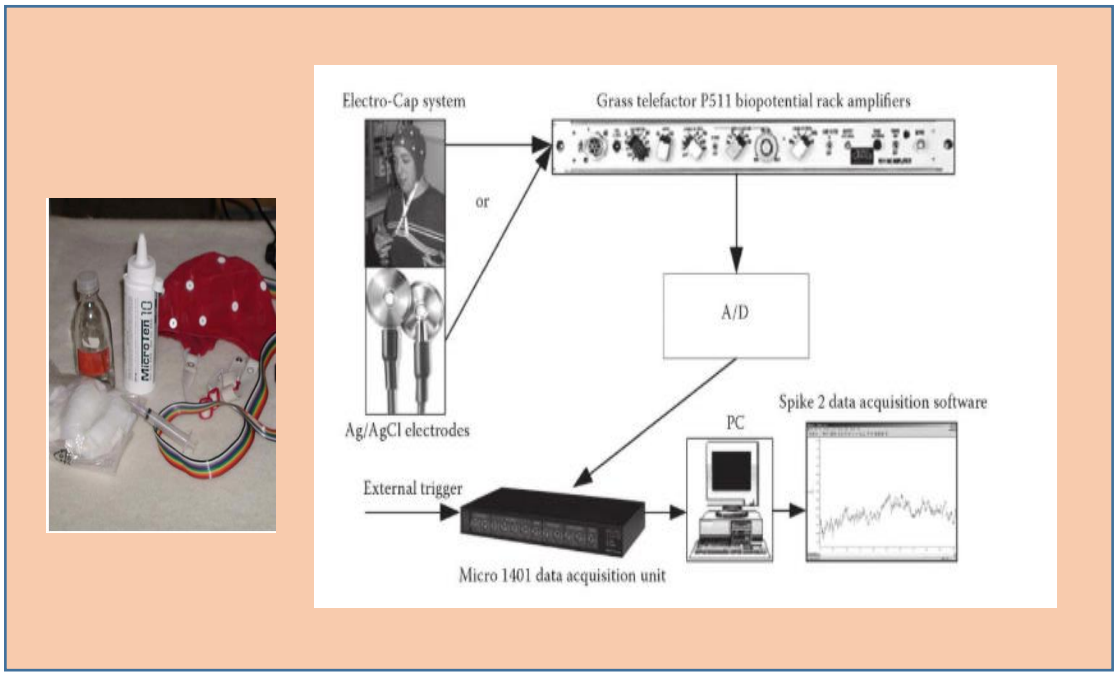

Figure 2.7: Illustrations of typical EEG components (left panel) and the basic EEG system in a typical laboratory (right panel) (Webster, 2014).

Each location uses a letter to identify the lobe and a number to identify the hemisphere location: F (Frontal), T (Temporal), C (Central) and O (Occipital) , and these letters are accompanied by odd numbers for electrodes on the left side, even numbers for electrodes on the right side as shown in Figure 2.8 (Jasper, 1958b; Webster, 2014). Additional electrodes are placed in the 10-20 system and termed an extension of 10-20 system because this number of electrodes is inadequate for clinical purposes which need to obtain a more accurate EEG and require 64 or 128 dipoles.

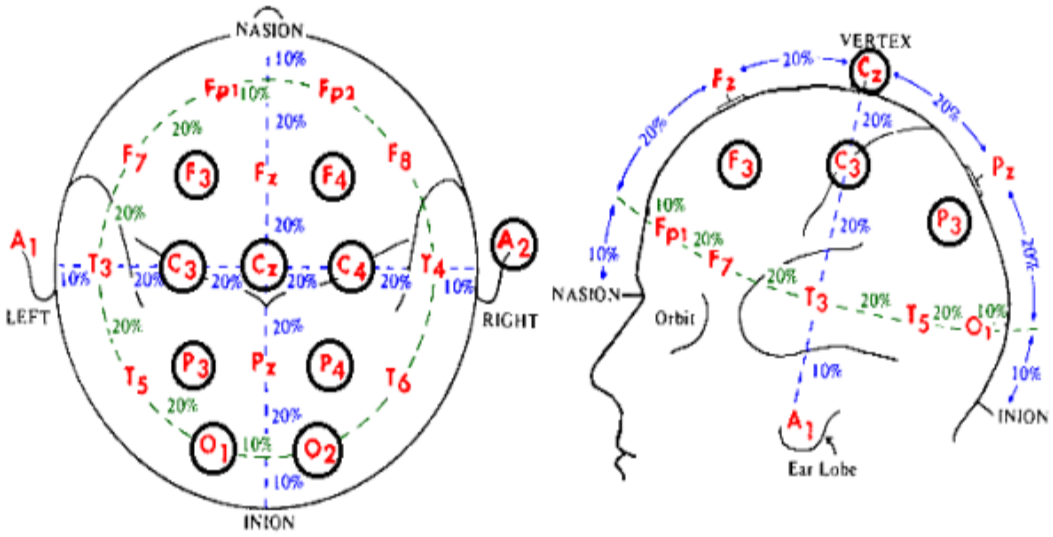

Figure 2.8: The 10-20 International Electrode System for the placement of electrodes at the head surface: top and side views (Jasper, 1958b; Webster, 2014)

The EEG patterns of rhythmic brain activity are an important source for studying brain functional behaviour in cognitive research and for diagnosing different neural diseases and disorders.

2.1.3.1 Normal EEG rhythms

Brain oscillations refer to a rhythmic or repetitive activity that can be organized in complex patterns based on the state of the brain, e.g. at sleep, awake or on task. In a normal person, this rhythmic activity has a number of characteristics in common such as synchronization that occurs locally between neurons within an area or over longer distances between areas within a wider network (Jansen et al., 2002; Tallon-Baudry, 2004; Womelsdorf and Fries, 2007). Other typical EEG rhythm characteristics are amplitude, location, shape, and frequency which is one of the most important for understanding functional behaviours in cognitive research and a key characteristic used to define normal or abnormal EEG rhythms (Stern, 2005; Webster, 2014).

Rhythm oscillations range from 0.05 to 600Hz according to Buzsáki and Draguhn (2004), with slow-wave activity being associated with sleep, and faster oscillations with the awake state. Typically, they can be classified into several oscillatory bands at

different frequencies: gamma-frequency typically higher than 30 Hz, beta-range frequency of 12-30 Hz, alpha-range frequency of 7-12 Hz, theta-range frequency of 4-7 Hz and delta-range frequency of 1–4 Hz, as described below (Fisch and Spehlmann, 1999; da Silva, 2005; Da Silva, 2005; Nunez et al., 2006; Lally et al., 2014):

- **Gamma rhythms** can be decomposed into different frequency ranges: slow gamma, typically defined as a frequency from 30 to 80 Hz with an amplitude usually less than 2 μV peak to peak, and high-frequency oscillations (HFOs) with a frequency >80 Hz. They are associated with the simultaneous processing of information from different brain areas
- **Beta rhythms** are of two basic types: Beta I wave which are lower frequencies which disappear during mental activity, and Beta II waves which are higher frequencies that appear during tension and intense mental activity. The greatest amplitudes are found on the parietal and frontal regions of the scalp
- **Alpha rhythms** include sub-bands of frequency range: low-alpha band (7.6-9.4Hz) and high-alpha band (9.6-11.4Hz) while awake (Tanaka et al., 1997). The greatest amplitude (30-50m μV) of alpha rhythm can be found in the occipital and parietal regions of the cerebral cortex when the subject has their eyes closed or is in a state of relaxation
- **Theta rhythms are** normally be seen in sleep with an amplitude usually greater than 20 μV. They mainly occur in the temporal and parietal region of the head
- **Delta rhythms** contain the largest amplitude and slowest frequency of all waves. They are normally seen in deep sleep and lightly anaesthetised adults, infants and children. Figure 2.9 shows the five frequency bands of normal EEG rhythm.

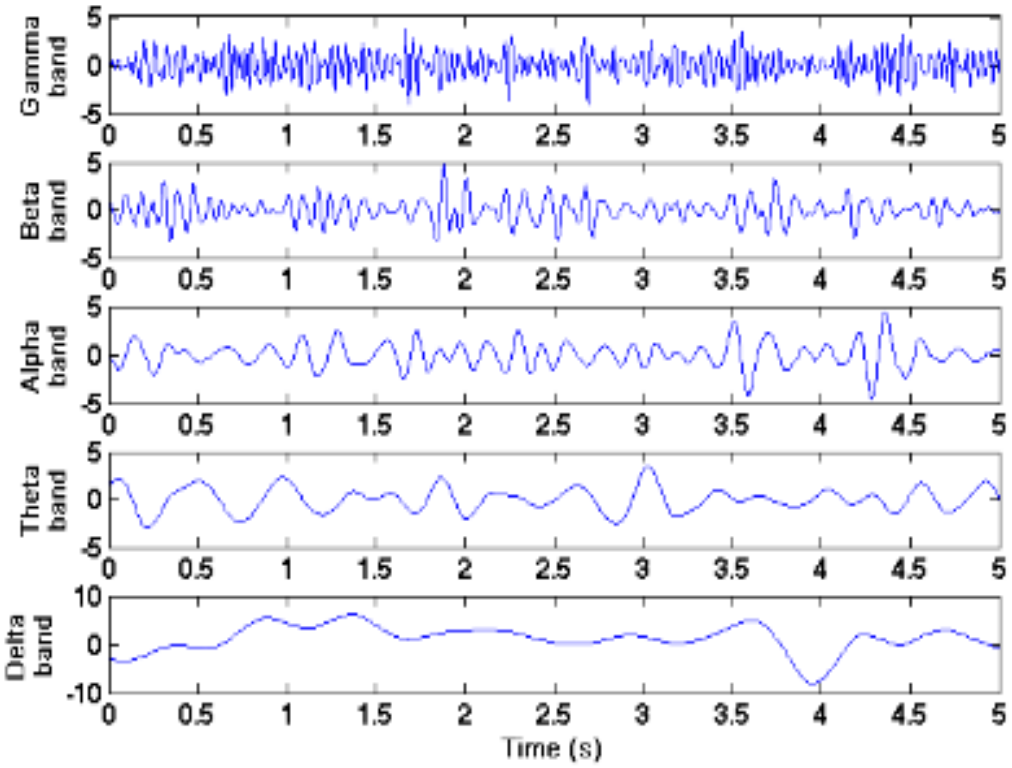

Figure 2.9: The five frequency bands of normal EEG rhythm (atwoodhhad et al, 2015)

2.1.3.2 Abnormal EEG rhythms

Unlike normal EEG activity, abnormal activity can cause seizures that are defined as sudden changes in the normal activity resulting in altered behaviours. Abnormal activity is characterized by different morphology patterns which can be recognised primarily by their wave shape and form, and secondarily by their frequency. These are the most important criteria for assessing abnormalities in clinical EEGs. Morphology patterns observed in the epileptic patient are high-frequency oscillations (HFOs) of ripples on spikes, spikes and waves, continuous and sporadic spikes, and ploy2 spikes (clinical data[4] of EEG, Chatrian, 1974; Barlow, 1993; Westmoreland, 1996; Noachtar

[4] Epileptic events extracted from EEG data in a patient with temporal lobe epilepsy used in the previous study (Wending et al., 2012).

et al. 2004; Chang and Drislane, 2007; Jacobs et al., 2008, 2009, 2012; Mathews et al., 2015).

HFOs are in the high frequency range of 80Hz to 500Hz and serve as a biomarker in clinical epilepsy. For example, Jacobs et al. (2008) reported that HFOs can assist in the identification of abnormal EEG patterns found in the seizure onset zone of human ictal and interictal recordings. These HFOs can be further divided into sub-categories depending on their frequency, ripples (80-250Hz) and fast ripples (250-500Hz), some of which are irregular oscillations (Bragin et al., 1999).

Other patterns that are the most characteristic features on epileptic HFOs are spikes and sharp waves which are recognised by their shape and form. Spikes are very fast oscillations. By definition, they have a duration less than 70ms (from 20-70ms) while sharp waves, that is sharply contoured, have a duration between 70 and 200ms according to the Mayo Clinic for Medical Education and Research and researchers in the field of epilepsy (Westmoreland et al., 1994; Westmoreland, 1996; Barlow, 1993; Chang and Drislane, 2007). Spike-and-wave HFOs that consist of a spike immediately followed by one or two slow-waves, polyspikes waves that are characterized by a run of two or more spikes, and quasi-sinusoidal waves that include a repetitive spike pattern. Figure 2.10 provides examples of the morphology of patterns observed in epilepsy.

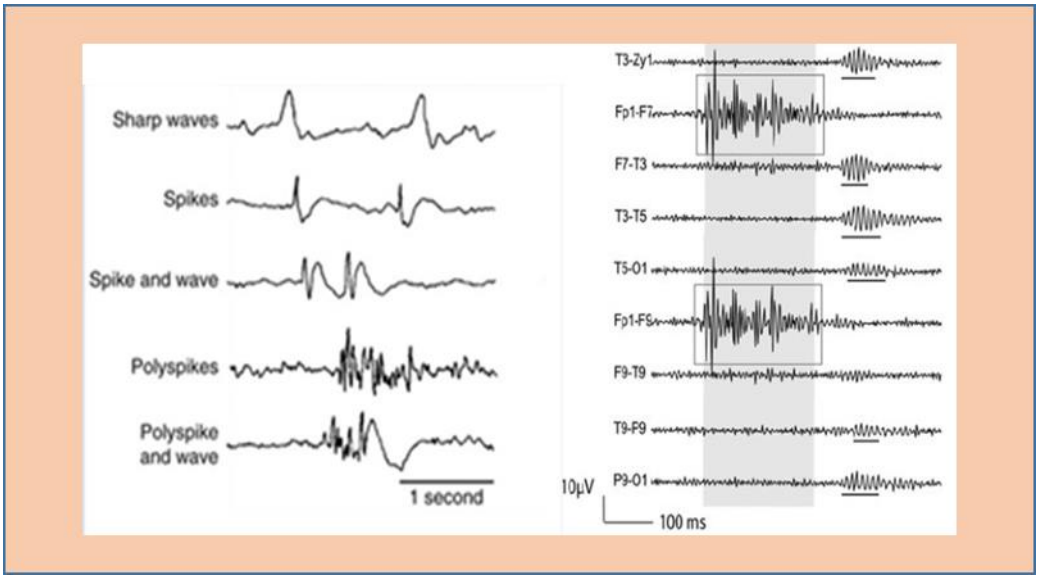

Figure 2.10: Examples of morphology of patterns observed in epilepsy (A) and ripples on epileptic spikes which are underlined (B) (Tamilia et al., 2017; clinical-electroencephalography-online[5])

These types of abnormal EEG patterns commonly arise anywhere in the temporal and occipital lobes, and their emergence can depend upon the areas involved such as the amygdala and hippocampus (Noachtar and Rémi, 2009). If they affect the whole brain (both hemispheres), seizures are called generalized seizures, while those effecting a specific part of the brain (right or left hemisphere) are defined as focal seizures, previously called partial seizures (Stafstrom and Carmant, 2015). Figure 2.11 illustrates patterns of EEG activities for normal, focal and generalized seizures.

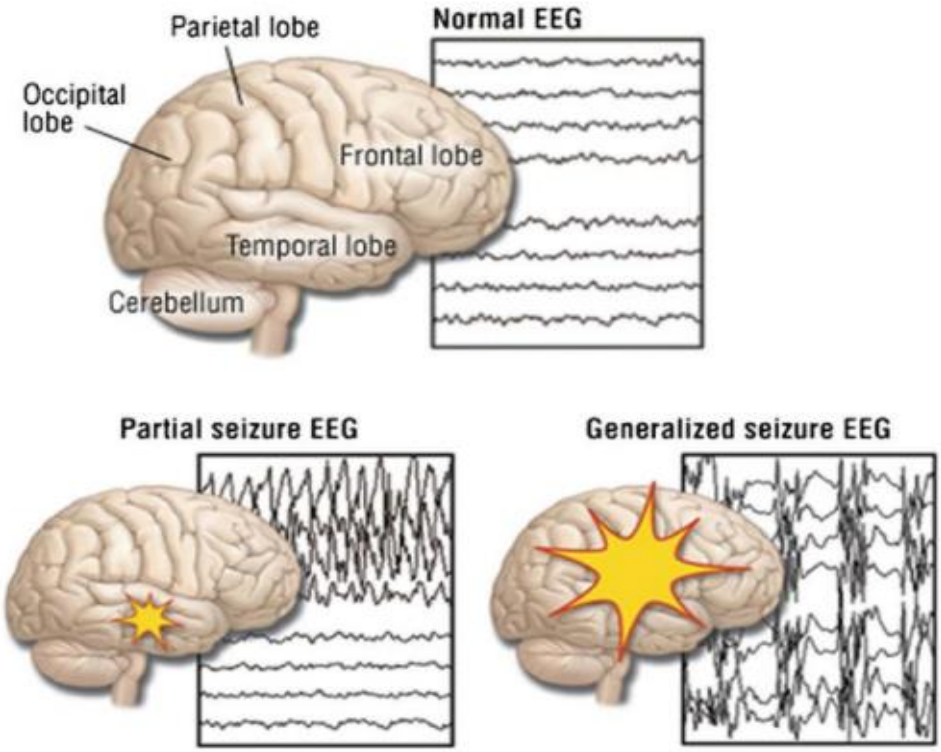

Figure 2.11: Illustrations of typical patterns of EEG activities for normal, focal and generalized epileptic seizures (epilepsy- Drugs.com[6])

[5]Available:https://neupsykey.com/clinical-electroencephalography-and-nocturnal-epilepsy [Accessed 2017].

[6] Available: https://www.drugs.com/health-guide/partial-seizures-focal-seizures.htm[Accessed 2017].

In this project, we are interested in modelling the brain network to simulate normal EEG rhythmic activity e.g. multi-band of alpha, theta and delta, as well as abnormal EEG epileptic patterns such as HFOs of ripples on spikes, spikes and waves, continuous and sporadic spikes, and ploy2 spikes.

2.2 An overview of BNM and its components

Theoretical and simulation research modelling of the whole brain as a network (Jirsa et al., 2002, 2009; Deco et al.,2011b) depends on the information provided by the structural connectivity of human connectome (Sporns et al., 2005) and has provided significant contributions to the understanding of the space-time structure of network dynamics of electrical activity. Further, the BNM approach has offered a wide range of biomedical applications ranging from resting-state activity (Schirner et al., 2018) to stimulation (Kunze et al., 2016; Spiegler et al., 2016) to disease states (Falcon et al., 2016a; Jirsa et al., 2017; Proix et al., 2017).

2.2.1 The generic concept of modelling the brain network

The full brain network modelling approach is composed of two main components: the human connectome, and NNMs as the network's nodes. It is a dynamic system of coupled NMMs where the coupling is informed by the human connectome, as shown in Figure 2.12. The connectome provides a network map of the human brain in which regions and inter-regional connections are rendered into the nodes and edges of a graph (Bohland et al., 2009). The construction of this connectome is based on different methods such as tractography methods or tract-tracing methods. For example, one of the connectomes compute from diffusion MRI data, as adapted from Daducci et al. (2012) (Figure 2.12(a)), while the other is characterized by complex topological features and an ever changing geometry (Roberts et al., 2016), or from cortical parcellation and the CoCoMac neuroinformatics database (Kötter and Wanke, 2005).

NMMs that have proven especially useful in understanding brain rhythms activity (Jansen and Rit, 1995) are used to model the activity of neurons (pyramidal cells, excitatory and inhibitory cells) in local populations organized as cortical columns (Figure 2.12 (left, b)) using mathematical representation (Figure 2.12 (centre, b)).

NMMs are often used to reduce the population's dynamic activity to the low dimensional differential equation (Figure 2.12 (right, b)). Travelling the scale to the large-scale network-contain infinite of nodes, BNM (Figure 2.12(c)) describe the local dynamics generated by NMM, within nodes (brain regions) and global dynamics between nodes (brain regions). Thus, the output of the BNM provides neuroimaging data that represent simulated time series such as M/EEG, BOLD and Raw (Figure 2.12(d)).

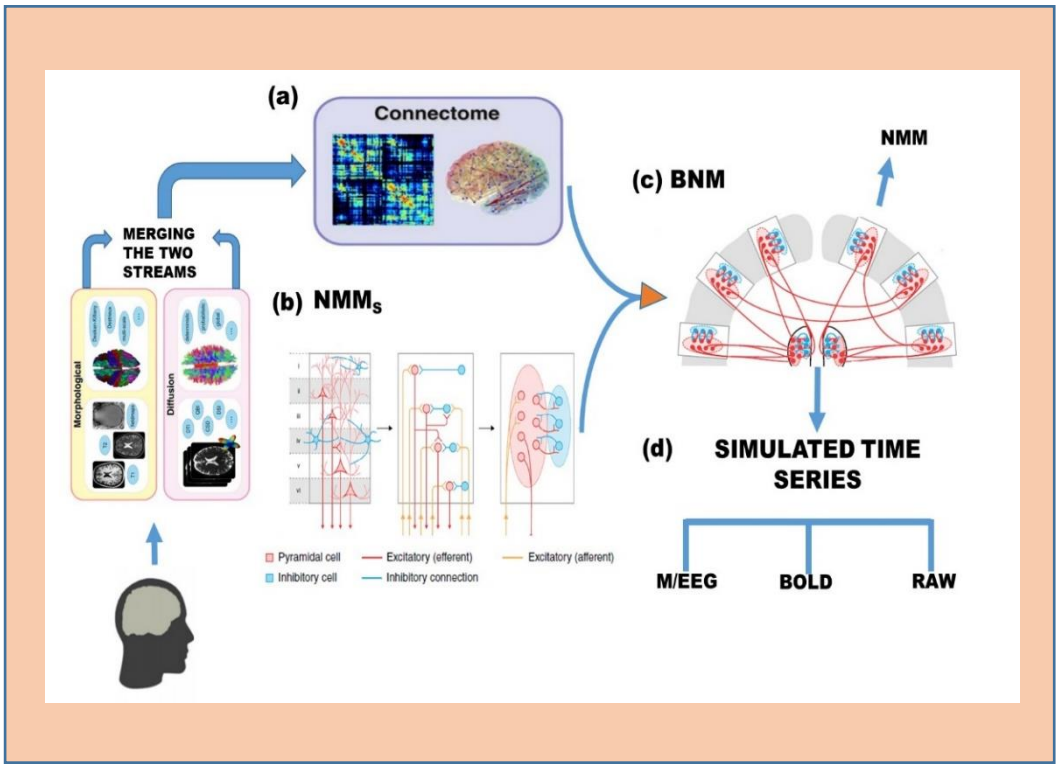

Figure 2.12: The generic concept of brain network modelling at multi scale (adapted from Breakspear, 2017)

2.2.2 The general principle of NMMs

With the BNM framework, it is possible to capture local dynamics that are generated from NMMs. The general principle of NMMs makes it possible to reduce the complexity of the cortical connection to relatively simple circuits. These quantify the mean firing rates *m(t)* and mean membrane potential *u(t)* of the neural mass (NM) that is a lumped representation of neurons by using ordinary differential equations (ODES)

according to Freeman's approach (Freeman, 1975). Freeman used the name NM action model. In models of NM, this *u(t)* is the result of diverse inputs. These inputs that represent *m(t)* can come from other NMs or from external inputs, and outputs of NM which are also *m(t).* For each NM, a rate-to-potential operator that captures the Post Synaptic Potential (PSP) describes the activities of the cell bodies and dendrites, while the potential-to-rate operator describes the actions of the axons. Figure 2.13 shows a schematic drawing of a NM.

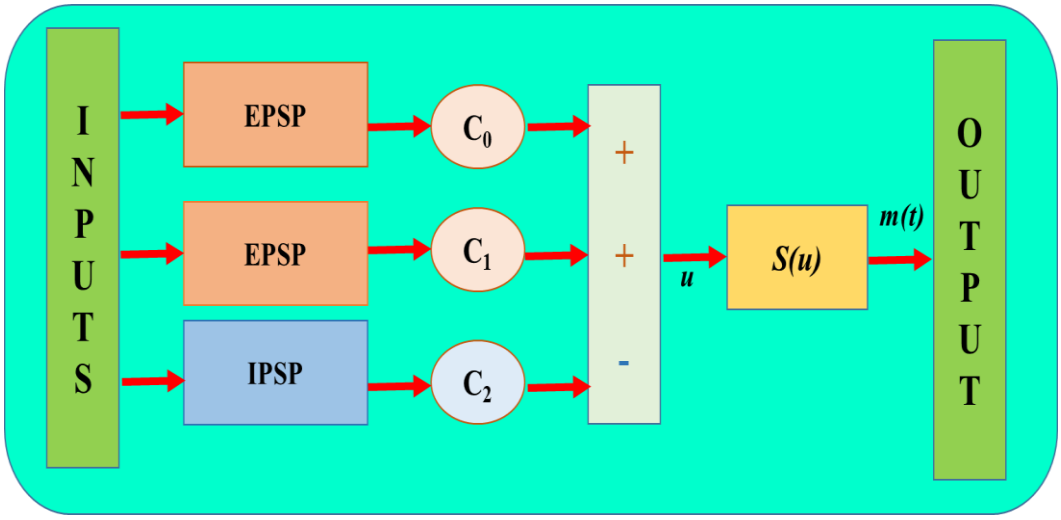

Figure 2.13: A schematic drawing of a NM. Different inputs convert to potentials: excitatory PSP (EPSP) or inhibitory PSP (IPSP) via PSP transforms. Each potential is multiplied by a constant, the average number of the synapse from this input to the population. By summing all excitatory potential and subtracting all inhibitory potential, the mean membrane potential u is produced. Then, applying potential-to-rate transformation which is defined by sigmoid function to *u* in order to achieve the mean firing rates *m(t)* that this population produces

2.2.3 A brief overview of NMMs

NMMs have been widely used to simulate the coarse grained activity of large populations of neurons and synapses, and are designed to strike a balance between mathematical simplicity and biological realism (Spiegler, 2011). NMMs mainly describe the neural function of the brain at a mesoscopic level and their equations model brain activity at large scales. They have become increasingly important in explaining experimental data such as those of EEG, fMRI, MEG (Coombes, 2010).

The first NMM established by Beurle (1956), used differential equations to describe activity patterns in bulk neural matter. Another attempt was the point-like NMM made

by Nunez (1974) who used the concept of a neural mass to quantify the dynamics of the interaction of a large number of neurons and analysed the brain wave with a mathematical framework. A similar idea was developed by Lopes Da Silva and colleagues who modelled the lumped-parameter enabled the generation of an alpha rhythm (Lopes Da Silva et al., 1974; Da Silva et al., 1976). Later, Freeman (1978) made a substantial contribution as part of a study of perceptual processing in the olfactory neuron. One year later, Zetterberg et al. (1978) attempted to model a local neuron population to produce signals that resembled EEG background activity and certain types of paroxysmal activity, in particular, spikes. Years later, Van Rotterdam et al. (1982) extended the theoretical model proposed by Lopes Da Silva et al. to the spatial domain to explain properties of EEG, especially the dynamics underlying EEG. Nearly five years later, Freeman (1987) simulated the chaotic patterns of the EEG, including the normal low-level background activity, and the high-level relatively coherent "bursts" of oscillation in the olfactory system using the second order ordinary differential equation (2ODE).

In 1993, and in a similar direction as previous work, Jansen et al. (1993) modified the local model of Zetterberg and colleagues to study visual event-related potentials. Two years later, Jansen and Rit (1995) introduced further development and exploration of the neurophysiological based model of the cortical column to include a slightly different version of this model proposed by Jansen et al. (1993). The mathematical framework of Jansen and Rit (1995) has been widely used to explain epileptic EEG brain signals (Wendling et al., 2000, 2002) and various narrowband oscillations of EEG ranging from delta to gamma (David and Friston, 2003) and to study connectivity between cortical areas with a similar framework (David et al., 2004). Subsequently, new advances in NMMs (Assisi et al., 2005; Deco et al., 2008; Stefanescu and Jirsa, 2008) have rediscovered the mathematical structure of the Fitz-Hugh Nagumo model which modelled the current signal observed in a living organism's excitable cells. For example, Stefanescu and Jirsa, (2008) introduced a novel, computationally parsimonious, mathematical representation of clusters of neurons, providing a low-dimensional description of complex neural population dynamics, including synchronization, multi-clustered solutions in phase space, and oscillator death. This model has been widely and successfully used by researchers in BNM to produce a wide range of neural activity due to its characteristic feature that takes into account the

parameter dispersion, giving rise to a rich repertoire of behaviours. In contrast, some traditional neural mass descriptions allowed for only a very limited repertoire of behaviours, which ultimately rendered their descriptions biologically unrealistic.

The strengths of these models, especially the Jansen-Rit model, have enabled researchers to explain the various range of phenomena in electric brain activity and to demonstrate which the simplest model is. Therefore, types of research have been devoted to the description of the oscillatory behaviours of NMMs by using the bifurcation theory of nonlinear systems which is a useful tool for investigating the dynamical behaviour in NMMs.

Grimbert and Faugeras (2006**)** used the bifurcation analysis of Jansen's NMM to investigate the effect of the input parameter of the NMM on the dynamics of the model and found that alpha rhythm activities and epileptic waves are related to the structure of a set of periodic orbits and their bifurcation. Also, the underlying mechanisms of rhythms were identified by Spiegler et al. (2010) who described the first complete account of the dynamics behaviour of a NMM (Zetterberg et al., 1978) by using bifurcation analysis of the impact of extrinsic input and dendritic time constants. This analysis can be useful for applications such as sleep and epilepsy. Furthermore, Geng et al. (2014) proposed a modified NM that incorporates a time delay, and this study presented a detailed description of the model's behavior with bifurcation diagrams. This research reported that bifurcation in this model could provide a theoretical reference for the understanding of the neurodynamics in epileptic seizures. Other researches introduced a general framework for studying the bifurcations of neural mass models and explaining the essential difference between the topology of the global bifurcation diagram of absence, and tonic-clonic seizures were introduced by Touboul et al. **(**2011**)** and Breakspear et al. (2005).

2.2.4 Structural data: human connectome

About 100 years ago, researchers analysed and wrote about the brain based on its cytoarchitecture. Cytoarchitecture is the process of describing the brain through its different areas which vary in cellular composition that can be detected under the microscope. In 1909, Brodmann was the first researcher to undertaken a parcellation

scheme that defined the link between nodes. He distinguished 43 different areas on the cerebral cortex by the organizating the characteristic of the cell under the microscope (Brodmann, 1909).

Later, the automated anatomical labelling of brain regions (AAL) was performed by Tzourio-Mazoyer et al. (2002). Since then many researches such as Salvador et al. (2005); Achard et al. (2006); Achard and Bullmore (2007); Liu et al. (2008); Supekar et al. (2008); Lynall et al. (2010); Sanz-Arigita et al.(2010); Braun et al. (2012) have used AAL parcellation. Another parcellation scheme was introduced by Hagmann et al. (2007) to study large-scale brain connectivity. He proposed an efficient methodology to generate large, comprehensive and individual white matter connectional datasets of the living or dead, human or animal brain, based on diffusion MRI.

Despite this early work, many scientists continue to work on projects which aim to map the human brain. This is so-called connectome which is exactly the great goal and much attention recently with the human connectome projects (human connectome projects-online[7]) (HCPs), which are combined in a systematic effort to make thousands of quality datasets freely accessible (Van Essen et al., 2012a, 2012b; Glasser et al, 2013).

The anatomical structure of the human connectome allows us to explore neural dynamics, cognition and behaviour. It also provides an important tool for mechanistic modelling. Additionally, it could potentially have a major impact on our understanding of brain damage such as traumatic brain injury and neurodegenerative disease (Sporns et al., 2005; Sporns, 2011).

The connectome was first defined for structural connectivity as a comprehensive structural description of the network of elements and connections forming the human brain by Sporns et al. (2005). They argued that the connectome is fundamentally important in cognitive neuroscience and neuropsychology, and that it will also be critically important for understanding brain function. It was also considered to be able to provide new mechanistic insights including how brain function is affected if this structural substrate is disrupted. Later, the concept of connectome was extended to

[7] Available :http://www.neuroscienceblueprint.nih.gov/connectome/[Accessed 2018]

include functional connectivity, i.e. the functional connectome (Biswal et al., 2010, Zuo et al., 2011). However, only a few researchers were focused on the structure–function connectivity relationship (for reviews see Rykhlevskaia et al.(2008); Bassett and Bullmore (2009); Damoiseaux and Greicius (2009); Honey et al.(2010); Sporns (2011)).

Despite the connectome accomplishments so far, a number of significant challenges remain. Empirical and theoretical challenges include the issue of capturing network connectivity across multiple spatial scales, accounting for individual variability and structural plasticity, as well as clarifying the role of the connectome in shaping brain dynamics (Sporns et al., 2013). A significant current need for understanding is the organisation of human brain connectivity according to three scales: the microscale of individual neurons (single neurons) and synapses, the macroscale of brain regions and pathways, and the mesoscale of neuronal groups or populations (Kötter, 2007, Sporns et al., 2011; Sporns, 2007, 2010). Computational models of BNM encompass two levels of spatial scale: the macroscopic, where the synaptic interaction are given by the long-range white-matter tracts of the order of a few centimetres and the mesoscopic scale which describes the connection between nodes embedded within one cortical patch (Sanz-Leon et al., 2015).

Network science provides a unique tool for modelling and analysing connectome data sets and bringing valuable insights into the principles underlying the structural connectivity of the brain. The fundamental concept of structural network organization in the brain is based on the anatomical linkage of its neurons that are connected locally by synapses from short axons. This organization can be described mathematically as a network or graph; a collection of nodes interconnected by a set of “edges” (Sporns et al., 2004; Bassett and Bullmore, 2006; Bullmore and Sporns, 2009; Van den Heuvel et al., 2010; Sporns, 2010; Fornito et al., 2013).

Nodes represent brain regions and the edges represent the connections formed between pairs of nodes represented by some measure of interaction between them, as inferred from neuroimaging data (Rubinov and Sporns, 2011). From this graph representation, the structural connectivity of the connectome can be succinctly described as a connectivity matrix where its elements consist of rows and columns corresponding to

different brain regions. The connectivity matrix is obtained using different techniques or parcellation schemes. For example, an anatomical matrix from the CoCoMac database (Kötter, 2004) that contains the results of about 300 published axonal tract-tracing studies, referring to one hemisphere, comprising 38 nodes (brain regions), and a link having only three scales of weighting. This CoCoMac database, created by Rolf Kotter, represents one of the first attempts to obtain a large-scale anatomical connectome of the human brain. Figure 2.14 shows the connectivity matrix weights and the strength of connections between brain areas based on the CoCoMac database (Kötter and Wanke, 2005).

Another matrix, introduced by Hagmann et al.(2008), is comprised of 66 brain regions of the cortex including both hemispheres (left and right), derived by the white matter tractography of diffusion spectrum imaging (DSI) weighted magnetic resonance imaging MRI images. In spite of this, the optimum number of structural regions in a connectome is still subject to controversy, with connectomes including different nodal sizes, e.g. cortical and subcortical regions represented in the connectivity matrix used to explore brain dynamics (Zalesky et al., 2010). More, recently, new approaches conducted by Glasser and Essen (2011), Glasser et al (2013), Glasser et al. (2014) and Glasser et al. (2016) have provided a dense connectome to determine regions of interest on the cortical surface.

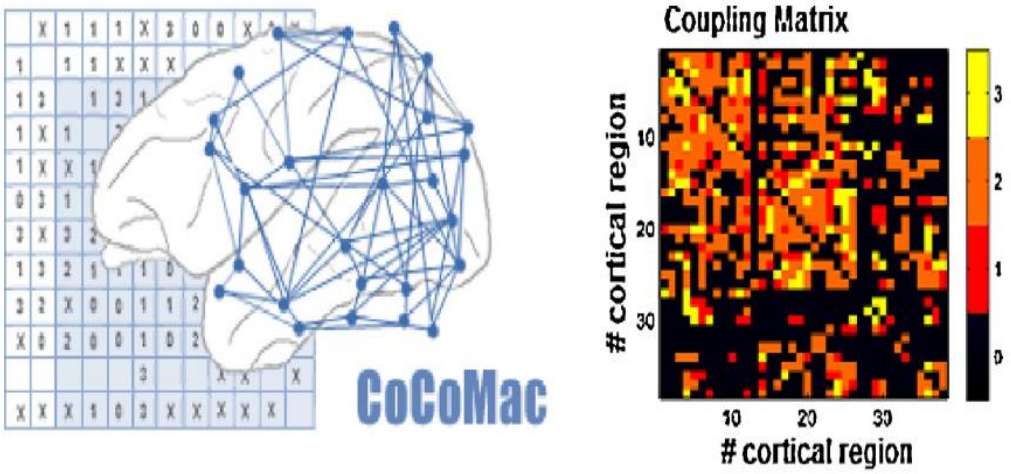

Figure 2.14: Example of a realistic connectivity map of one hemisphere of the human brain introduced by Kötter and Wanke (2005)

However, the default connectivity of the connectome in BNM (Leon et al., 2013; Sanz-Leon et al., 2015) is a bio-hemisphere (each of hemisphere consisting of 38 brain cortical areas) which is a hybrid fusion of the CoCoMac database and DSI data whose two matrices represent the strength of the connections between regions and white matter fibre lengths. Any of these matrices can be either directed graphed, in which case the edges point from one node to another or undirected, in which case the edges have no directionality (Bullmore and Bassett, 2011).

With the availability of both the NMM that describes brain activity at the mesoscopic level (Section 2.2.2) and brain structural connectivity known as the connectome (Section 2.2.4), existing network models have been emerging as important topics leading to the generation, prediction and testing of large-scale brain activity and testing, and comparing and refuting models when incorporating the connectome into NMM.

2.3 Existing BNMs

Different studies of BNM methods have been used previously and the main difference between them is the type of dynamics assumed at the local level generated from NMM and the selected model structure. This difference in study has led to different results. Honey et al. (2007) introduced the first such studies attempting to investigate the relationship between structure–functional connectivity (SC-FC) and develop an understanding of resting-state dynamics by combining the availability of structural connectivity with computational models of the brain's large-scale neural dynamics. Their network model included the NMM of Breackspear et al. (2003) which displayed oscillatory behaviours and dynamics determined by voltage- and ligand-gated ion channels and feedback between a population of interconnected excitatory and inhibitory neurons. Their model structure was SC derived from a macaque cortex (Kötter, 2004). These NM dynamics were derived from Morris and Lecar (1981) and were extended for neural population activity Larter et al. (1999). This model was successful in reproducing functional connectivity patterns recorded during rest.

Later, Honey et al. (2009) extended Honey et al. (2007), but their model components are different. Their model was developed from the structural model of the human cerebral cortex and based on a diffusion spectrum imaging (DSI) data set described by

Hagman et al. (2008) which allowed an extension of the model to the scale of the entire human cerebral cortex, and the NMM of Breackspear et al. (2003). This model simulated human resting state fMRI data and compared it to actual fMRI data obtained from the same subjects. The model results showed that large-scale anatomical structure of the human cerebral cortex constrained the characteristics of resting state activity.

Other efforts by Ghosh and colleagues (2008a, 2008b) investigated the role that noise and conduction delays play in shaping large-scale neural dynamics at rest. They used the FitzHugh-Nagumo model which represents neural population activity with two state variables namely the membrane potential and the recovery variable (FitzHugh, 1961; Nagumo, 1962) coupled according to the anatomical connectivity of one hemisphere. The anatomical connectivity used in this model was obtained from the CoCoMac database (Kötter, 2004) that is collected from published reports of experimental tracing studies and comprises 38 nodes with weights ranging from 0 to 3. Their method investigated the stability of rest state and tested multiple oscillation types including Hop oscillators, Wilson-Cowan systems (Wilson, 1972), FitzHugh-Nagumo systems (1961, 1962), and finally mixed populations of coupled FitzHugh-Nagumo neurons (Assisi, 2005); all providing similar results. The model showed that the structural connectivity and other factors such as time delays or noise may play an important role in the shape the dynamics of the brain at rest; giving damped oscillations (10Hz).

One important application of large-scale models of brain activity has been the investigation of the effects of variations in anatomical connectivity. Knock and his colleagues (Knock et al., 2009) used two different sets of connectivity structure: one extracted from the CoCoMac database (Kötter, 2004) and a second derived from Hagman et al. (2008). In this study, these two different connectivity matrices were compared to clarify which structural details are more relevant than others. Their results clearly showed that brain dynamics derived from the CoCoMac database were more complex and more biologically realistic than connectivity structural that based on the DSI database. The reason for this difference was the directionality weights in the CoCoMac connectivity matrix. As a result, this study provided a skeleton for the construction of future large-scale models of neural dynamics.

Another important modelling approach extended the previous model of resting state activity. Deco et al. (2009) used a comparable model to that of Honey et al. (2009) and investigated the key role of coupling, delay and noise in resting brain fluctuations, and showed that resting state dynamics is strongly based on all of these factors. The network dynamics were periodic oscillations (40Hz). The simulation and analyses of this model were performed using the neural model of the Wilson-Cowan formulation (Wilson-Cowan et al., 1972) that described dynamics at the node level with a set of differential equations, while the structural model used a realistic connectivity matrix of the primate brain depending on data from the CoCoMac neuroinformatics database with time delays derived from a human template. Furthermore, this model studied the role and relevance of noise on the collective dynamics of the brain network by systematically simulating the behaviour of that network for different levels of noise.

More whole-brain models have provided a mechanistic explanation of the origin of a normal resting state network and showed that different local dynamics are shaped by underlying structural connectivity (Deco et al., 2011a, Deco et al., 2011b; Deco and Jirsa, 2012; Deco et al, 2013a,2013c). For example, Deco and Jirsa (2012) has given rise to the idea that the resting brain resides in a regime that is close to instability which allows it to continually explore a dynamic repertoire of noisy brain states. In other word, the model considered that noise is able to explain the generation of resting state activity with slow fluctuations which do not change if the time delays are neglected. However, Cabral et al. (2014) investigated the mechanisms of spontaneous MEG connectivity by using a simple model of coupled oscillators adapted to incorporate realistic whole-brain connectivity and conduction delays. The structural brain networks used in the model were estimated from DTI data introduced by Gong et al. (2009), a modified version of already published methods, whilst the model utilized the original Kuramoto model to explore the spontaneous behaviour of coupled brain areas, (Acebron et al., 2005, Kuramoto, 1984). Simulation results revealed slow and structured envelopes similar to the real MEG data. Further, Deco and colleagues published a study that has been used to model important features of sleep (Deco et al., 2013b).

Additionally, Cabral et al. (2011) investigated the structure-function relationship using large-scale neural modelling. They utilized a simple neural model, called the

Kuramoto model (Kuramoto, 1984, 2003; Acebrón et al., 2005) which had been used extensively to investigate the behaviour of coupled oscillatory systems, while the structural model, a key ingredient of this model, was the same as that used in Honey et al. (2009). They used the SC of the connectome between 66 regions of the human brain. The time delays between brain regions were considered in this model. The model investigated the assumption that merging neural dynamics at the local level with large-scale structural connectivity can produce slow resting-state fluctuations observed in the blood-oxygen-level dependent signal (BOlD).

Overall, these studies of BNM have pointed out that spontaneous brain activity at rest as well as task-related activity is strongly based on the properties of the underlying structural connectivity (Deco and Corbetta, 2011a). Therefore, any damage to the structural connectome can potentially have a very acute effect on the functional connectivity. Indeed, changes in the structural connectivity of the human brain can emerge in many situations such as traumatic brain injury, neurosurgical lesions, stroke and neuropsychiatric disorders, while much less severe examples can be seen in ageing, and learning.

An example of modelling the impact of lesions in the human brain was introduced by Alstott et al. (2009) and van Hartevelt et al. (2014). Alstott et al. (2009) used the same structural and neural models as those used by Honey et al. (2009), i.e. the structural connectivity based on a DSI data set obtained from five healthy participants described by Hagman et al. (2008) and the neural model used by Breackspear et al. (2003). The Alstott et al. method modelled the structural lesion by removing the network's nodes representing the brain areas from the connectomes of the macaque brain. The findings showed that research can predict the effect of structural alterations on brain dynamics as well as making the model a unique tool for the comprehension of brain diseases.

Whole-brain computational models have also offered unique predictive tools in studying disease states with altered structural connectivity, as in people with schizophrenia, a disease long associated with connectivity deficits (Cabral et al., 2012a; Cabral et al., 2012b; Cabral et al., 2013). Cabral et al. (2012b) focused on an investigation of the effects of structural disconnection on resting state functional connectivity. This investigation used a large-scale neural modelling framework

consisting of the local neural populations introduced by Mattia and Del Giudice (Mattia and Del Giudice, 2002) and the large-scale healthy anatomical connectomes structural model. The connectome, derived from DIT, was acquired from 21 healthy subjects using automated anatomical labelling (AAL) and an anatomical connectome based on DSI averaged over five healthy subjects described by Hagmann et al. (2007). In contrast with the model of Cabral et al. (2012a), this model considered the role of noise in shaping the resting state activity and neglected the role of delays between brain areas. Interestingly, model results proposed a general scenario including an understanding of the elements of schizophrenia and dynamical and functional connectivity studies.

BNM at multiscale is a complex neural model and may seem difficult for neuroscientists to use, However, this has become a lot easier with the exciting development of TVB which is a unique predictive neuroinformatics platform for the simulation of the neural dynamics of large-scale brain networks (Ritter et al., 2013; Sanz-Leon, 2014; Woodman et al., 2014). With this interactive tool. A whole-brain computational model, based on multiple choices of modelling assumptions, can be built. Its typical framework involves managing project information, uploading data, setting up simulation parameters (model, integration scheme, output modality), launching simulations, analysing and visualizing, and finally storing results and sharing output data. Also, the framework maintains a dataset from the different operations performed by the user in each project**.** Thus, researchers from computational, theoretical and clinical neuroscience can benefit from this tool.

2.4 The research gaps

From the literature, it is seen that there are many BNM studies using different methods for exploring the mechanisms of the generation of oscillatory activity of the human brain but, there are still many limitations in the existing BNM methods. To the best of the author's knowledge, no prior study has integrated the modifications of the neural mass of the JR model with our own structural connectivity. Hence, this new method of BNM will lead to the exploration and generation of a new and rich repertoire of multi-alpha, delta and theta rhythmic patterns of EEG of which no study has been

reported in the literature. Moreover, no previous network modelling study has linked unbalancing excitatory and inhibitory coupling strength at the local network of the Stefanescu-Jirsa 2D model with realistic biological data, using different structural connectivity to predict different morphology patterns such as ripples on spikes, spikes, continuous spikes, sporadic spikes and ploy2 spikes ranging from 94-144 Hz. Hence, the development of BNM at different scales is required to explore, generate and predict a new and rich repertoire of healthy and disease rhythmic activities for the human brain.

2.5 Summary

This chapter has provided an overview of BNM and the necessary background related to the BNM. First, it presented an outline of human brain fundamentals including its structure and functions, the fundamentals of EEG, the normal and abnormal neuronal activity. Next, it discussed BNM and its components. After that, a comprehensive literature review of existing BNMs was covered.

CHAPTER 3

LARGE-SCALE BRAIN NETWORK MODEL AND MULTI-ALPHA BAND EEG RHYTHM GENERATION

EEG alpha oscillations play a considerable role in understanding cognitive and physiological aspects of human life, and in diagnosing neurocognitive disorders such as AD and dementia. particular (Dauwels et al., 2010; Lizio et al., 2011; Al-Qazzaz et al., 2014; Sharma et al., 2016; Houmani et al., 2018).They also play a role in cognitive processes (Klimesch et al., 1993; Klimesch, 1997a, 1999, 2012; Jensen et al., 2002), perceptual learning (Sigala et al., 2014) and their application in seizure suppression has created enormous interest for some researchers (Kraft, 2006).

In this chapter, we developed LSBNMs to generate multi-alpha band EEG rhythms. This development is introduced in two LSBNM models. The first network model (basic model) is comprised of a network of four cortical areas in the left hemisphere. Each area is modelled by an oscillator Jansen and Rit (JR) model, with its standard parameterisation on all four cortical areas.

The second network model extends the first one to include six cortical areas in the left hemisphere of different lodes, with each area implemented as a local JR network but with modified parameters. The proposed models of local neural populations of JR dynamically coupled via the biologically realistic, large-scale connectivity connectome is an essential step in developing our more realistic network models.

3.1 Method

Figure 3.1 shows the different steps of the proposed method for modelling the multi-alpha band of EEG rhythms at different ranges of frequencies. Input of each of proposed model uses a connectome which is hybrid input of DSI and the CoCoMac

neuroinformatics database (Kötter, 2004; Kötter and Wanke, 2005). The connectome and the local neural population of the JR model are linked. Here we use the original parameterisation of JR which is composed by coupling three interconnected neural masses: Pyramidal cell (PC) and two interneurons–one excitatory (EIN), and the other inhibitory (IIN). Form this linking, the LSBNM (basic model) is built, incorporation of global and local dynamics. The second model is built as an incorporation of the JR model with its modified parameterisation and with that connectome data. Obtained outputs from these network models represent the simulated large-scale brain activities of EEG multi-alpha. Validation of the simulated activities is done using FFT.

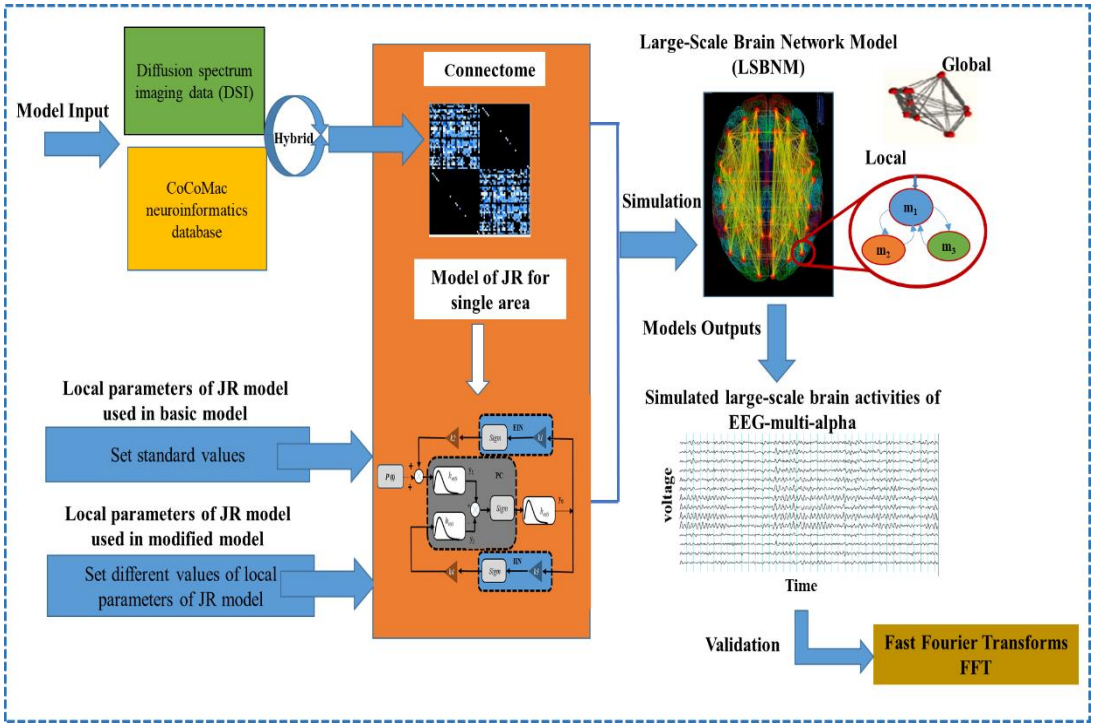

Figure 3.1: The architecture of the proposed method

3.1.1 Structural connectivity of the human connectome

In this study, the connectome is default in The Virtual Brain (TVB-online[8]) which is open source (Leon et al., 2013), and corresponds to a biologically realistic, large-scale connectivity of the brain regions. This connectome includes both left and right hemispheres, with each hemisphere consisting of 38 cortical regions as listed in Table 3.1. The connectomes of the network models (discussed in this chapter) include the cortical regions in the left hemisphere; the occipital, parietal and temporal lobes (see Figure 3.2). These have a characteristic frequency of alpha rhythm and alpha waves of the greatest amplitude which can be detected and recorded from occipital, parietal regions of the cerebral hemisphere by using EEG (Teplan, 2002). Further, the functional role of the left hemisphere dominates the functions of speech, language processing and comprehension, and logical reasoning. Accordingly choosing these cortical regions in the left hemisphere can be the construction of a realistic, anatomically accurate brain model that simulate alpha rhythms, as shown in the results section.

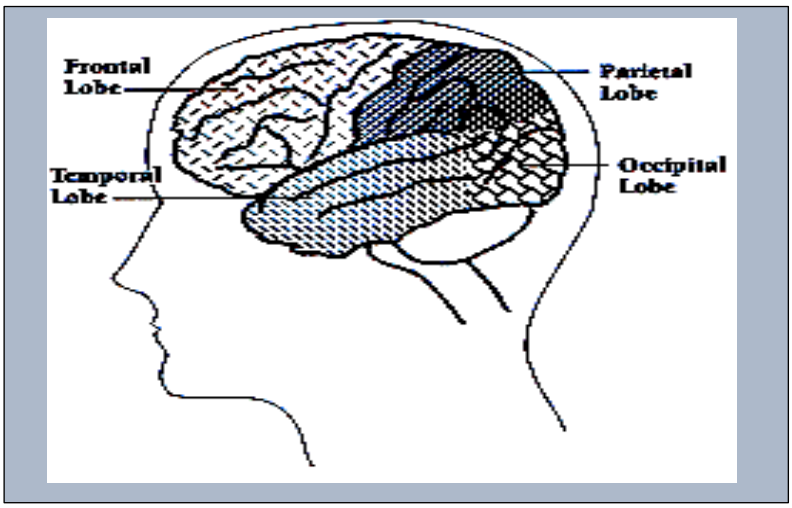

Figure 3.2: The left hemisphere lobe

[8] Available: http://thevirtualbrain.org/tvb/zwei/brainsimulator-software [Accessed 1.2 2016].

Table 3.1: Anatomical labels and names of cerebral areas

Label	Anatomical region	Label	Anatomical region
A1	Primary auditory cortex	PFCdm	Dorsomedial prefrontal cortex
A2	Secondary auditory cortex	PFCm	Medial prefrontal cortex
Amyg	Amygdala	PFCorb	Orbital prefrontal cortex
CCA	Anterior cingulate cortex	PFCpol	Pole of prefrontal cortex
CCP	Posterior cingulate cortex	PFCvl	Ventrolateral prefrontal cortex
CCR	Retrosplenial cingulate cortex	PHC	Parahippocampal cortex
CCs	Subgenual cingulate cortex	MCdl	Dorsolateral premotor cortex
FEF	Frontal eye field	PMCm	Medial premotor cortex
G	Gustatory cortex	PMCvl	Ventrolateral premotor cortex
HC	Hippocampal cortex	S1	Primary somatosensory cortex
IA	Anterior insula	S2	Secondary somatosensory cortex
IP	Posterior insula	TCc	Central temporal cortex
M1	Primary motor area	TCi	Inferior temporal cortex
PCi	Inferior parietal cortex	TCpol	Pole of temporal cortex
PCip	Cortex of the intraparietal sulcus	TCs	Superior temporal cortex
PCm	Medial parietal cortex (Precuneus)	TCv	Ventral temporal cortex
PCs	Superior parietal cortex	V1	Primary visual cortex
PFCcl	Centrolateral prefrontal cortex	V2	Secondary visual cortex
PFCdl	Dorsolateral prefrontal cortex	CC	Cingulate cortex

3.1.2 Structural connectivity used in the basic network model

Based on the default connectome in TVB, we have chosen four cortical areas in the left hemisphere from the connectome which are in different lobes: the primary auditory cortex (A1) and auditory cortex (A2) in the temporal lobe, and the posterior cingulate cortex (CCP) and retrosplenial cingulate cortex (CCR) in the parietal lobe (Figure 3.2 and Table 3.2). Then we built the connectivity square matrix *Wij*, where $1 \leq i \leq n$ and $1 \leq j \leq n$, and n is the number of nodes in the network comprising four (lA1, lA2, lCCP1, lCCR) left nodes. This matrix of connectivity defines the connection strengths and the time-delay of signal transmission between each pair of brain regions and weights the strength of the connection between the four brain areas by integer values from 0 to 3; with 0 representing the absence of a connection, 1 a weak connection, 2 a moderate connection and 3 a strong connection (see Figure 3.3). To quantify the connectivity characteristics and ensure the dissipation of activity in the network, we determined the connectivity measures for four nodes (lA1, lA2, lCCP, lCCR) including the in-and-out degree of connectivity - i.e. the in-out degree is the number of incoming and outgoing to/from a node, respectively.

Table 3.2: Labels and names of cortical areas in the left hemisphere included in this model

Label	Anatomical region	Lodes of the brain
A1	Primary auditory cortex	Temporal lobe
A2	Secondary auditory cortex	Temporal lobe
CCP	Posterior cingulate cortex	Parietal lobe
CCR	Retrosplenial cingulate cortex	Parietal lobe

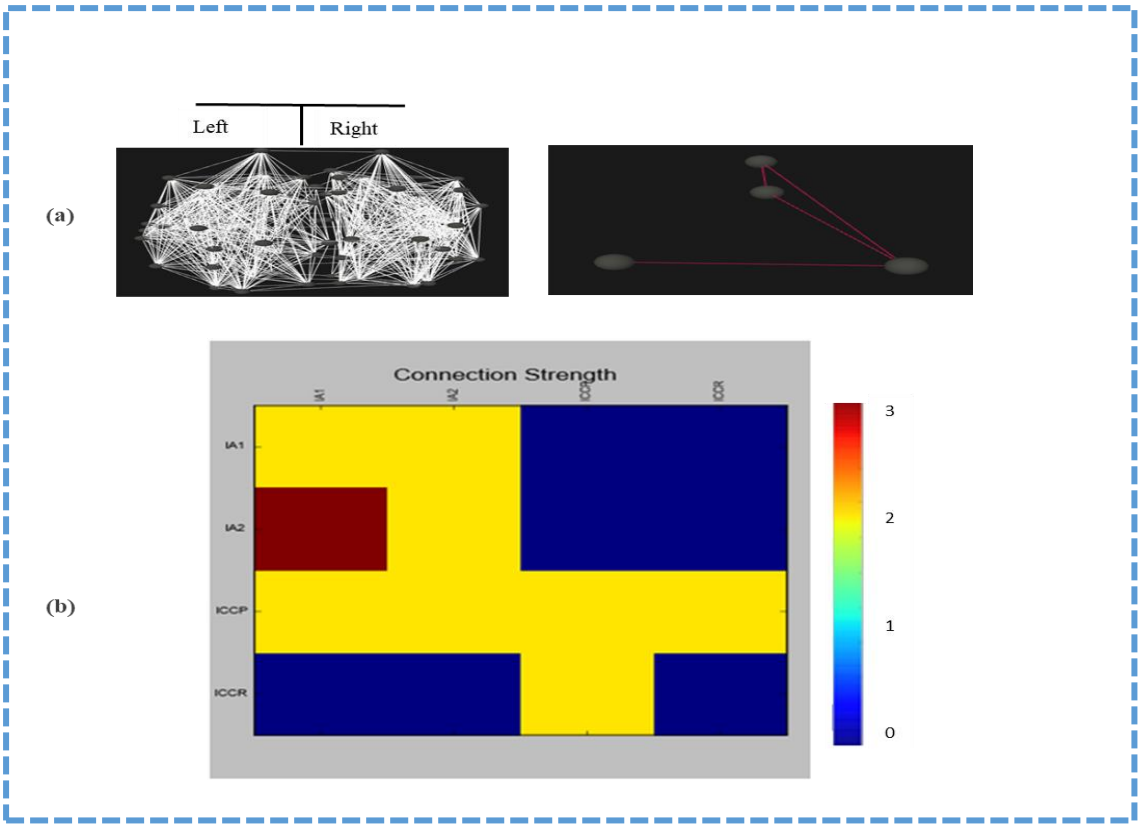

Figure 3.3: Structural connectivity datasets of the human for the structural layout of basic model. (a) Left, 3-dimensional representation of the brain network structure comprising a collection of 76 nodes (cerebral centers in black) with a collection of edges (white lines describing the long range neural fibre tracts). Right, shows the 2-dimensional view for the network, as projections of connectivity graph which can be represented as a connectivity matrix. (b) Connectivity matrix is arranged in columns and rows weighted to be absent, weak, moderate and strong which represent the connection strength between the four brain regions

3.1.3 Structural connectivity used in modified network model

We extended the first model network to include six cortical areas in the left hemisphere which are in different lobes: the primary auditory cortex (A1) and the auditory cortex (A2) in the temporal lobe, the posterior cingulate cortex (CCP) and retrosplenial cingulate cortex (CCR) in the parietal lobe and the primary visual cortex (V1) and the secondary visual cortex (V2) in the occipital lobe (see Table 3.3). From this default connectome in the TVB (see Figure 3.4(a)), we built the large-scale connectivity between the six regions and we determined the connectivity measures for all six nodes

including the in-out degree, i.e. the number of incoming and outgoing connections to/from a node, respectively (Figure 3.4(b)). From this connectivity network, two matrices were constituted, the weights of the connections (strength) and time delays between brain regions were created via finite signal transmission speed. The weighted matrix is represented in a square matrix (n × n), where n = 6 is the number of nodes (i.e., cortical areas) and represents the connection strength between the six cortical areas with integer values from 0 to 3 for no connection, weak, moderate and strong connection, respectively (Figure 3.4(c)). The delays matrix is computed by dividing the distance matrix, D, and the transmission speed, c.

Table 3.3: Labels and names of cortical areas in the left hemisphere included in modified network model

Label	Anatomical region	Lobes of the brain
A1	Primary auditory cortex	Temporal lobe
A2	Secondary auditory cortex	Temporal lobe
CCP	Posterior cingulate cortex	Parietal lobe
CCR	Retrosplenial cingulate cortex	Parietal lobe
V1	Primary visual cortex	Occipital lobe
V2	Secondary visual cortex	Occipital lobe

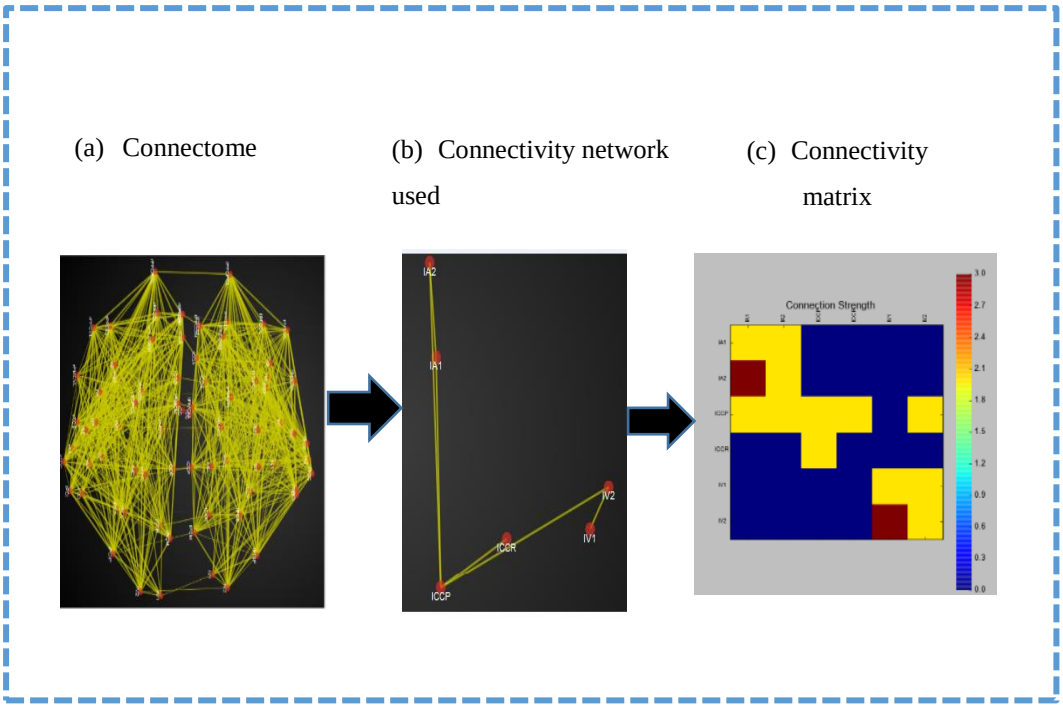

Figure 3.4: Brain's structural connectivity used in the model: (a) Connectome included in TVB, representation of the connectivity network, consisting of a collection of 76 nodes (cerebral centres in red) with its edges in yellow lines, (b) Representation of connectivity network between six brain nodes in the left hemisphere used in this study (lA1, lA2, lCCP, lCCR, lV1, lV2) including the in-and-out degree of connectivity, (c) Connectivity matrix is weighted by integer values from 0 to 3

3.2 Local dynamics of JR model of an area

The model of JR consists of three interconnected neural masses: pyramidal cell (PC) and two interneurons –one excitatory (EIN), and the other inhibitory (IIN). Each neural mass (NM) has two state variables, namely the mean membrane potentials *u(t)* and the mean firing rates *m(t)*. The dynamics of each neural population is modelled by two operators:

Rate-to-Potential Operator converts the average firing rate describing the input to population into an average postsynaptic membrane potential. This linear transformation is described by the function 3.1:

$$h(t) = \begin{cases} \alpha\gamma t e^{-\gamma t} & t \ \ for \ \ \geq 0 \\ 0 & for \ \ t < 0, \end{cases} \tag{3.1}$$

For the case $t \geq 0$ the function $h(t)$ gives the excitatory and inhibitory connections function, where α and γ are different parameters in the excitatory and inhibitory cases. The parameter α defines the maximum amplitude of the EPSP and IPSP, while γ defines time constant of excitatory PSP and inhibitory PSP. For both cases excitatory and inhibitory, we have $\alpha = A$, $\gamma = a$ (respectively $\alpha = B$, $\gamma = b$).

Potential-to-Rate Operator converts the average membrane potential of a population of neurons into the average firing rate by a nonlinear sigmoid function 3.2:

$$Sigm(V) = \frac{2eo}{1+e^{r(v0 - v(t))}} \tag{3.2}$$

According to previous studies (Jansen and Rit, 1995; Al-Hossenat et al., 2017), the parameters of e_0 determine the maximum firing rate of the neural population, v_0 is the value of the potential of PSP for which 50% firing rate is achieved, r is the slope of the sigmoid at v_0 ; v_0 (either the firing threshold or the excitability of the populations). In this study, we focused on set different values of A Parameter while keeping the other parameters with standard numerical values through different simulations (see Table 3.4). Thus, by applying a second order differential operator, the temporal differential operator reads as follows:

$$P: D_i = \lambda^2 + 2b_i\lambda + b_i^2 \tag{3.3}$$

With $b1$, $b2 = 1$ and $b3 = 1/2$ for pyramidal cells (i =1) with the feed loops represented by excitatory (i =2) and inhibitory (i=3) (see Spiegler and Jirsa, (2013) Appendix A for more details).

According to Figure 3.5, the post-synaptic boxes are labelled $h_e(t)$ and $h_i(t)$ characterised by a liner transfer system while the boxes are labelled *Sigm* representing the cell bodies of neurons and are characterized by a nonlinear sigmoid function. The four connectivity constants *K1*, *K2*, *K3* and *K4* represent the interactions between populations, and *y0=y1 - y2* represent the outputs of the three postsynaptic boxes (Jansen and Rit, 1995).

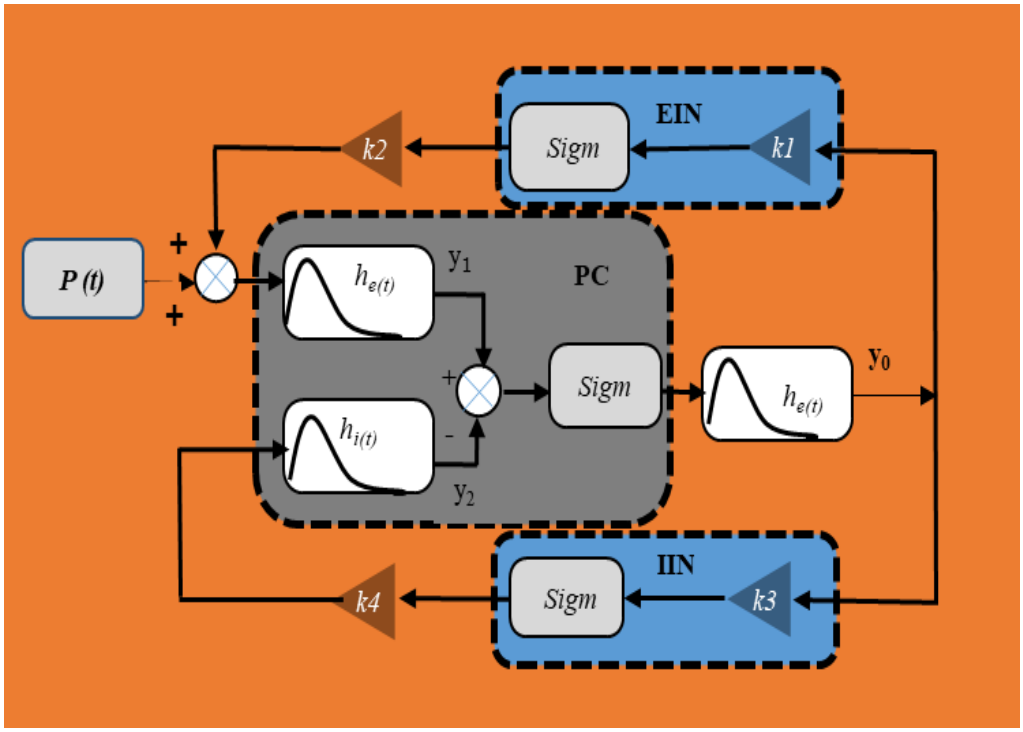

Figure 3.5: Block diagram of JR model which represents the mathematical operations performed inside a cortical area. The postsynaptic boxes labelled $h_{e(t)}$ and $h_{i(t)}$ in the figure correspond to liner synaptic integrations while the boxes labelled *Sigm* represent the cell bodies of neurons and correspond to the sigmoidal transformation that converts the membrane potential of a neural population into an output firing rate. The constants K_i model the strength of the synaptic connections between populations and y_0, y_1 and y_2 are three main variables in the model as the main outputs of the 3 postsynaptic boxes (Jansen and Rit, 1995)

Table 3.4: Numerical values of the JR model used in our model

Jansen's original model with its standard Numerical Values		
Parameter	**Interpretation**	**Numerical Value**
A	Average excitatory synaptic gain	3.25mV
B	Average inhibitory synaptic gain	22mV
a	Time constant of excitatory PSP	$100s^{-1}$
b	Time constant of inhibitory PSP	$50s^{-1}$
K	Average number of synapses between populations	135
K1, K2	Average Probability of synaptic contacts in the feedback excitatory loop	*K1=K k2=0.8k*
K3,K4	Average Probability of synaptic contacts in the slow feedback inhibitory loop	*k3=k4=0.25*
v_0	The value of the average membrane potential	6Mv
V_{max}	Threshold	$5s^{-1}$
r	Steepness of the sigmoidal transformation	$0.56mV^{-1}$
e_0	The maximum firing rate of the neural population	$2.5\ s^{-1}$
	Using different values of *A* parameter in this model	
4.5, 4.7, 4.9, 4.99, 5, 5.5, 6, 6.5, 7, 7.5, 8, 8.5, 9, 9.5, 10 mV and 10.5 mV		

3.3 Description of the models

The two models' architecture is based on combining both the JR NMM accounting for interaction of neural masses in one region and large-scale anatomical structure-or connectomes consisting of two matrices representing the strength and the time-delay of signal transmission between each pair of brain regions. The connectivity between the neural masses of a cortical patch is replaced by connections between the mean activity of populations. The general form of the BNM equation describes the evolution of activity of a certain node in the network. This equation is computed by summing its intrinsic local dynamics (often described by a NMM), short-range input, long-range input from connected regions, and external input which could be the noise and stimuli

(Sanz-Leon et al. 2015). According to such strengths and time-delay matrices, the long-range input is computed by summing the scaled and delayed activity of connected nodes while the short-range input does not have a delay and the signal transmission is instantaneous. The evolution equation for the BNM used in this study employs a similar notation to the above and the paper of Spiegler and Jirsa (2013) where this equation was described using a delayed differential system.

According to Spiegler and Jirsa (2013) the basic model of the brain network is mathematically described as follows: each area in network describes a neural mass of the JR model with its standard numerical values and each neural mass has two state variables, namely the mean membrane potential and mean firing rate which describes a set $\Phi = \{\varphi_1, \varphi_2\}$. For the JR model which has m=3 different neural masses (NM), namely PC and two for the excitatory and inhibitory interneurons, the state variables of a network of m=3 NM is formed as a vector $\Psi = [\Phi 1; \Phi 2 \ldots \Phi_m]$. To link state variables Ψ between 3 neural masses either excitatory or inhibitory, the square matrix of order $\sum_{i=1}^{m} ni$ is used, where n is the number of variables of neural mass. By considering the interconnection l=4 of the NMM in the spatial domain, representing a single cortical areas, the state variable of the resulting BNM is formed as a vector $\Omega = [\Psi 1; \Psi 2 \ldots \Psi l]$ according to $W_{het,}$ heterogeneous connectivity matrix. Thus, W_{het} can describe connectivity between four elements of the network (cortical areas). By applying a temporal differential operator $P\left(\frac{d}{dt}\right)$ of a network of coupled local mass of JR model, the temporal evolution equation of our BNM described below with the S (Ω) is transfer function:

$$P\left(\frac{d}{dt}\right)\Omega(t) = S\left(V_{loc}\Omega(t)\right) + W_{het}S\left(V_{loc}\Omega(t)\right). \quad (3.4)$$

The description of the modified BNM is as follows: the model consists of the six brain areas in the left hemisphere where each area describes an NM of the JR model setting its parameters with different values. Each NM has two state variables, n = 2; namely the average membrane potential and the average firing rate described by $\Phi = \{\varphi 1, \varphi 2\}$. Of each NM that is formed as a vector, $A = [\Phi 1, \Phi 2 \ldots \Phi m]$, describes the relationship between the state variables of m = 3 NM, namely PC and two for EIN and IIN. Thus,

the three NMs can be interconnected as a matrix depending on a local connectivity matrix, V_{loc}. By interconnection $l = 6$ such as NMM according to the W_{het}, heterogeneous connectivity matrix, the state variable of the resulting BNM is characterised as a vector $\Psi = [A1, A2 \ldots Al]$. Thus, W_{het} can describe connectivity between six elements of the network (cortical areas) and consider the signal transmission delays which are dependent on matrix inter-regional distanced, D and propagation speed, c between two neural masses. Using a temporal differential operator to Ψ, the temporal evolution equation of a network of a coupled Jansen and Rit local model is identified below with the $Z(\Psi)$ as the transfer function:

$$P\left(\frac{d}{dt}\right)\Psi(t) = Z\left(V_{loc}\Psi(t)\right) + W_{het}Z\left(V_{loc}\Psi(t - D/c)\right) \quad (3.5)$$

3.4 Implementation and Simulation using TVB package

To evaluate our proposed BNM, we implemented sequential steps using the platform TVB. Simulating with the TVB at the region level uses a coarse representation of the brain and involves five main components: structural long-range connectivity of the brain, a local population model which describes the dynamics of local neural populations (embedded in the platform), long-range coupling, an integration scheme, and monitors which record the output data (Leon et al., 2013). Depending on the structural connectivity matrix which represents the connection strength between the four brain regions used in the basic network model and six brain regions used in the modified network model, we performed the pipeline simulation within requirements (system requirement of TVB-online[9]) by integrating global dynamics with the local dynamics of the JR model that describe the dynamics within the brain regions.

The sequential steps of simulation for the basic model using the TVB are listed below:

[9] Available: file:///C:/Users/u1060978/Documents/decuments/TVB_Distribution/docs/UserGuide.pdf [Accessed 1.01. 2016].

I. Bringing structural connectivity through the connectivity matrix of the human connectome to determine the coupling strengths among 4 cerebral areas. (See Section 3.1.2)
II. Setting a long rang coupling function that is used to join the local dynamics at a distinct location over the connections' connectivity (i.e. it is applied to the activity propagated between regions before it enters the local dynamics equations of the model with its original parameter values. The coupling function used in this simulation is a linear function that rescales incoming activity to a level appropriate to the population model with a slope a = 4.2e-8 (0.0000000042).
III. Using the conduction speed. In this study we used 4mm/ms of speed of signal propagation through the network in all simulations
IV. After we defined our model's structure and dynamics, the numerical integration of the system was performed using Hen's method which is available for solving ordinary different equations (ODES) with an integration step size of 0.01220703125ms
V. Recording the relevant data from the simulation which is simply raw neural activity described by the state variables of the JR model using the temporal average monitor with sampling period 1ms
VI. Finally, the simulation length is1000ms.

Next, we performed the pipeline simulation of the second BNM by bringing together a NMM with different values of the *A* parameter and with structural data represented connectivity matrix between six brain regions. The next paragraph lists the sequential steps of the simulation for the modified model of the brain network:

I. Importing long-range connectivity given by two metrics which determined the coupling strengths and time delay between six cerebral areas (see Section 3. 1.3) into the TVB simulator
II. Setting of global parameters including the coupling function to transform the neural activity from source nodes (i.e. cortical areas) into the target node. In all simulations, the global coupling function was a linear function with a slope **a** = 4.2e-12 and the second global parameter was the conduction speed.

4mm/ms of speed of signal propagation was utilised through our network in all simulations

III. Selecting the local JR model with its original parameterisation. Then we used different values of the *A* parameter (see Table 3.4) by conducting different simulations. For each simulation, the parameters of the local dynamics were determined and tuned using the phase plane tool (already) included in TVB before embedding the JR model in a network and then conducting a simulation.

IV. Using the integration scheme. In this work, the Hen's method was used for solving model equations numerically with a small step size of 0.01220703125ms

V. Using the Temporal average monitor which records the relevant data from the simulation with sampling period 1ms

VI. Using simulation length. The simulation length used in all simulations was 1000ms.

3.5 Results and evaluations

3.5.1 The results from the basic model

The simulation results of this model showed that own structural connectivity with neural network dynamics generated from the JR model with its standard parameters is capable of generating a signal similar to spontaneous EEG alpha oscillation within low frequency of 7 HZ. The result of the model represents the time series of the mean PSP of the PC noted *y0*, in Figure 3.5. This time series constituted the output of each area in the network. Validating the simulated time series was done in terms of frequency (kilohertz, kHz) which is a key characteristic used to define EEG rhythms. We used the fast Fourier transforms (FFT) to compute the discrete Fourier transform (DFT) of the time series for each of the areas. DFT produces a frequency domain representation that is the sum of weighted sinusoids. Figure 3.6 showed that the time series of each area instantaneously transmitted the mean firing rate of its PC to other linked areas, and four left interconnected cerebral areas in the network.

(a)

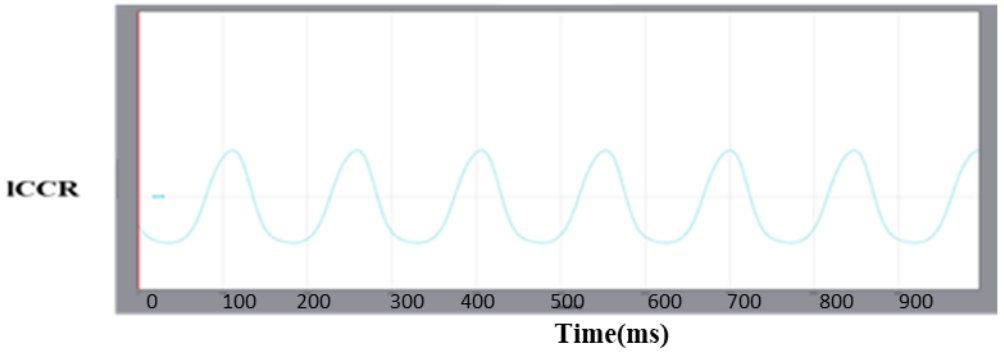
ICCR
0
100
200
300
400
500
600
700
800
900
Time(ms)

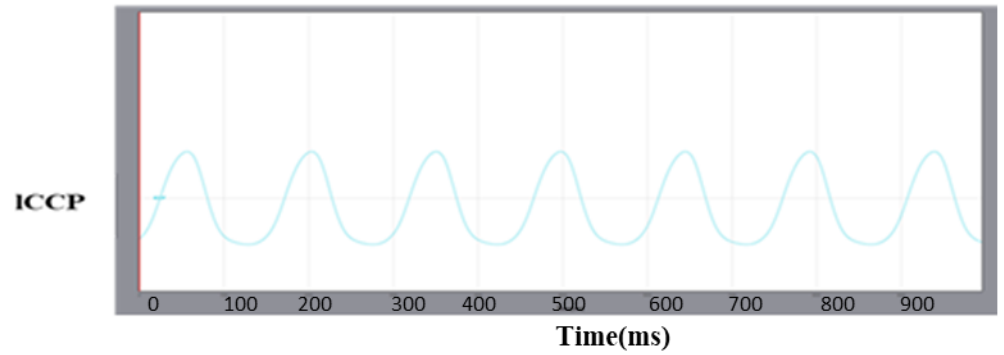
ICCP
0
100
200
300
400
500
600
700
800
900
Time(ms)

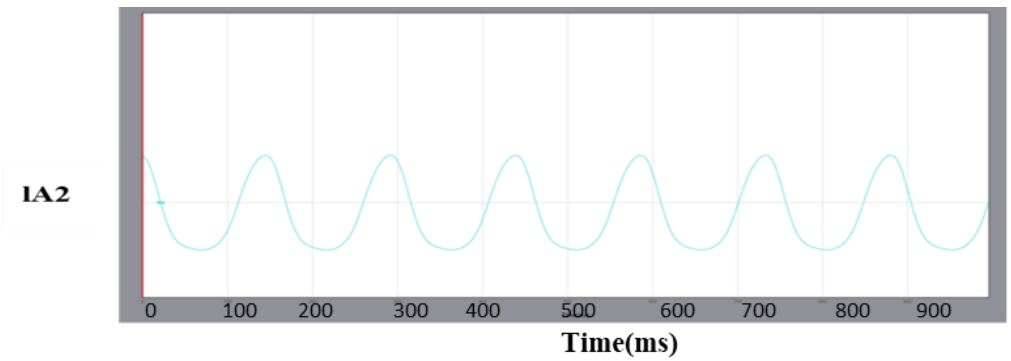
IA2
0
100
200
300
400
500
600
700
800
900
Time(ms)

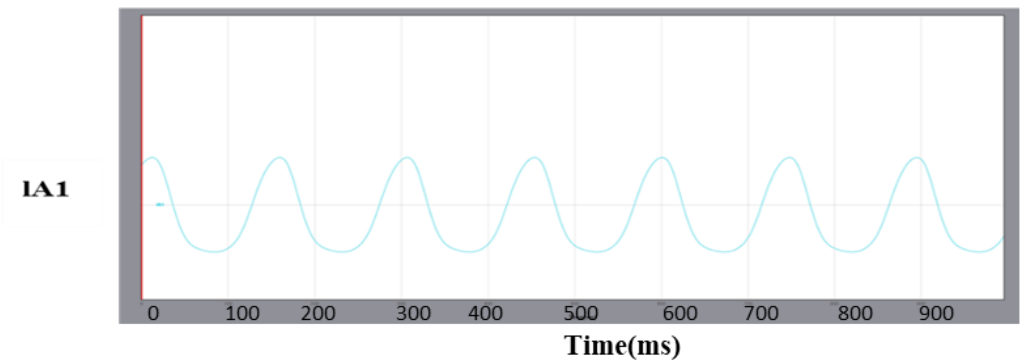
IA1
0
100
200
300
400
500
600
700
800
900
Time(ms)

(b)

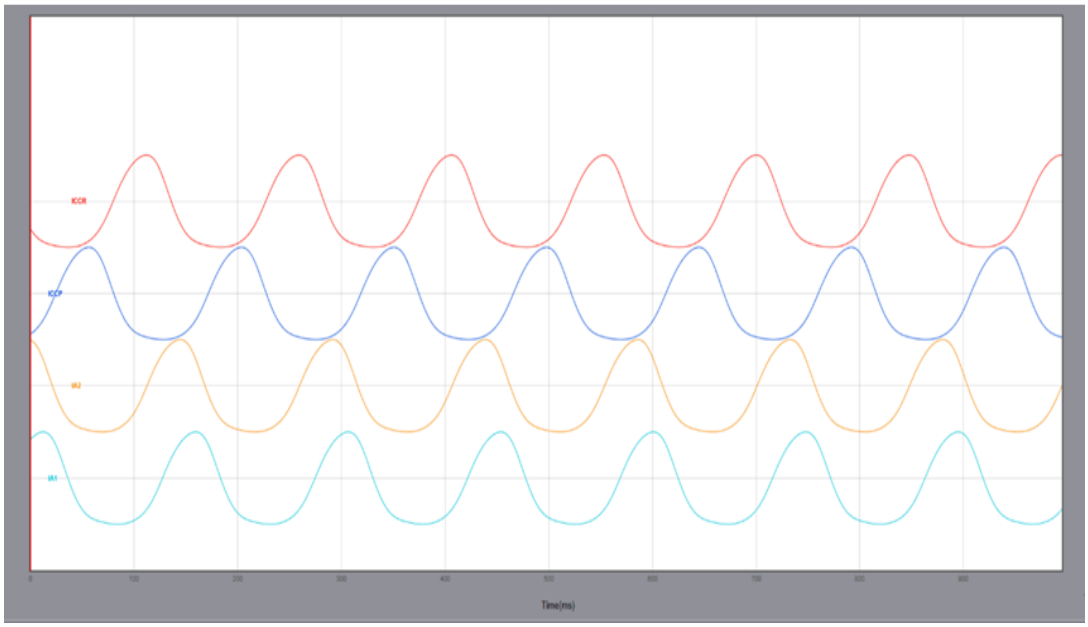

(b1)

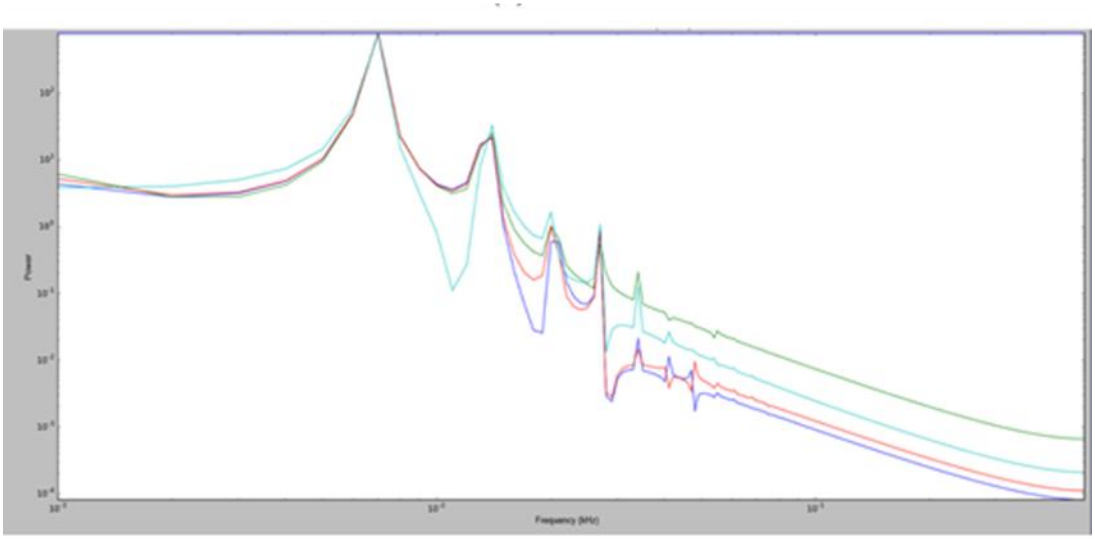

Figure 3.6: Simulated alpha rhythm (7 Hz): (a) Time series of each area constituted the output of the postsynaptic potential (PSP) noted y0, as shown in Figure 3.5 of each area in the network at the left hemisphere. From top to bottom: lCCR, lCCP, lA1 and lA2, (b) Time series show the simulated alpha activity for four left interconnected cerebral areas in the network. (b1) Frequency plot

3.5.2 Experimental results of modified model

A set of simulations for this BNM at different scales was performed using the sequential steps with TVB platform, as mentioned in Section 3.4. The results were evaluated on the capability of the proposed model to generate multi-alpha frequency EEG rhythms. Here, we studied variations of synaptic gains which were precisely the values of the *A* parameter. Changing parameter *A* to different values, while keeping the values of other parameters constant, led to the generation of a multi-alpha frequency band as shown in Table 3.5, which provides a summary of the simulation results for our model. These results represent the frequencies of the output of the model that signify the time series of each area. When the value of *A* = 4.5, 4.7, 4.9, 4.99 and 5 mV, respectively, the model can generate the alpha frequency of 7 Hz for each area (Figure 3.7(a)), while in the case *A* = 5.5, the oscillations have a frequency range (7–8) Hz (Figure 3.7(b)). Increasing the value of *A* from 5.5 to 6 mV, the alpha frequency range was (8.5–9) Hz (Figure 3.7(c)) and for *A* = 6.5 mV, the alpha frequency was 10 Hz for each area (Figure 3.7(d)). As the value of *A* increased to 7, 7.5, 8, 8.5 mv, many rhythms were generated within the frequency range of 10.5–11 Hz (Figure 3.7(e)), while in case *A* = 9, 9.5 and 10 mV, the model generated the alpha frequency of 11 Hz for each area (Figure 3.7(f)). Interestingly, if case *A* is more than or equal 10.5 mV, the model could cease oscillations (see Figure 3.7(g)).

Again, the simulated time series was validated using FFT. Figures 3.7(a1)–5(g1) show the frequency spectrum for the six cerebral areas in the left hemisphere corresponding to the simulated time series.

Table 3.5: Summary of simulation results

Parameter of *A*	**Frequency of alpha rhythms for each area**					
Numerical Values	**lV2**	**lV1**	**lCCR**	**lCCP**	**lA2**	**lA1**
4.5,4.7,4.9,4.99,5mV	7 Hz	7 Hz	7 Hz	7 Hz	7 Hz	7 Hz
5.5 mV	8 Hz	7 Hz	8 Hz	7 Hz	7.5 Hz	7 Hz
6 mV	9 Hz	8.5 Hz	9 Hz	9 Hz	9 Hz	8.5 Hz
6.5 mV	10 Hz	10 Hz	10 Hz	10 Hz	10 Hz	10 Hz
7,7.5,8,8.5mV	11 Hz	11 Hz	11 Hz	10.5 Hz	11 Hz	11 Hz
9,9.5,10mV	11 Hz	11 Hz	11 Hz	11 Hz	11 Hz	11 Hz
10.5 and more	**Ceased oscillations**					

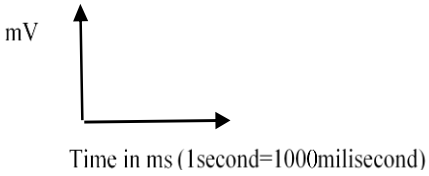

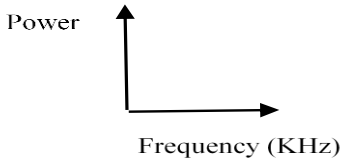

(a) (a1)

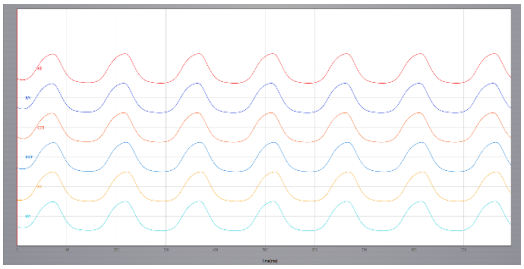

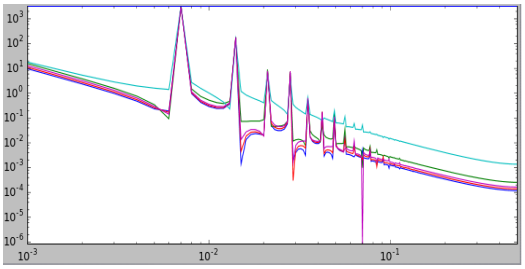

(b) (b1)

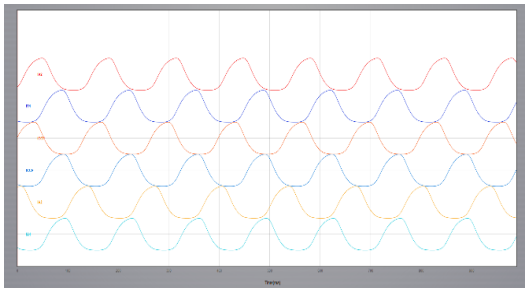

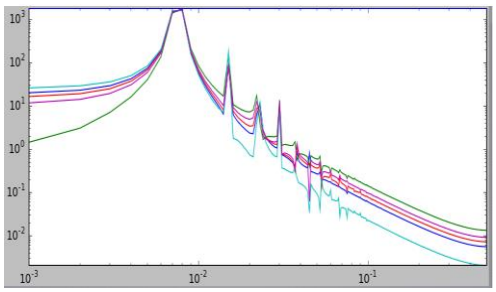

(c) (c1)

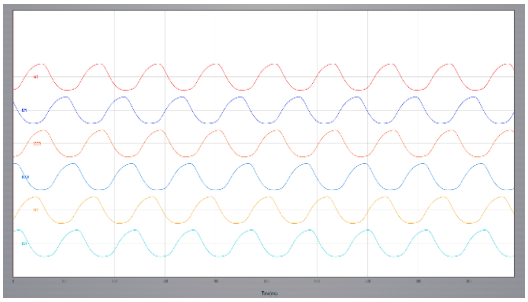

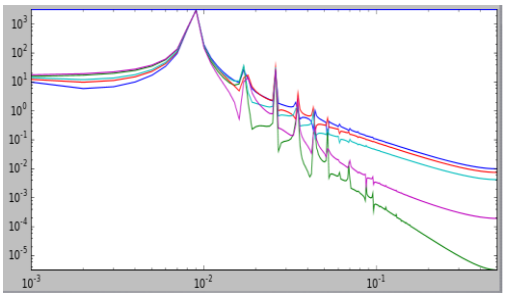

(d)

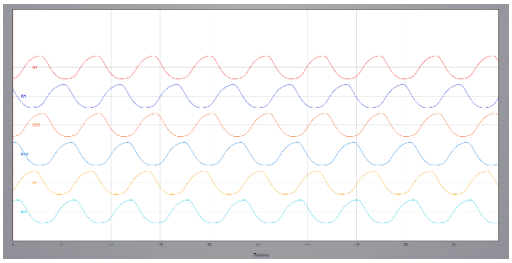

(d1

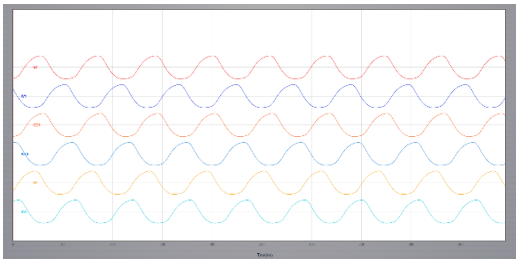

(e)

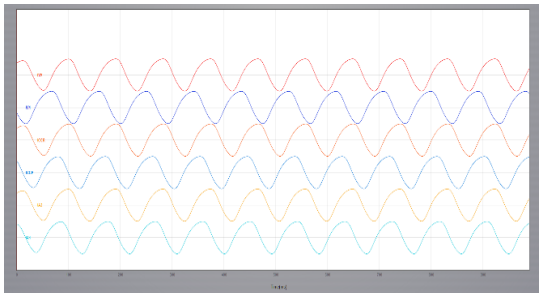

(e1)

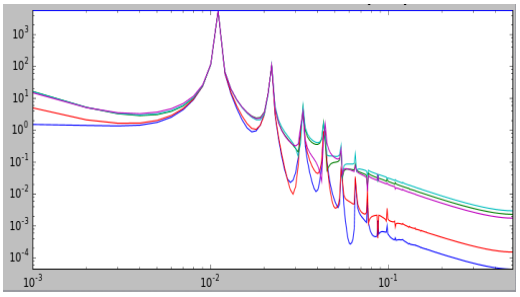

(f)

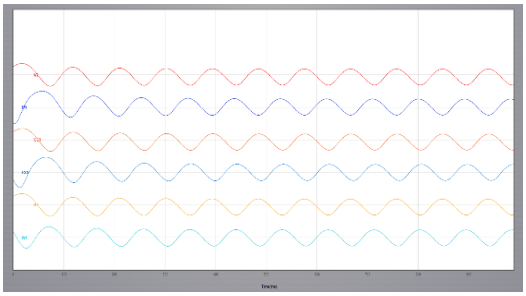

(f1)

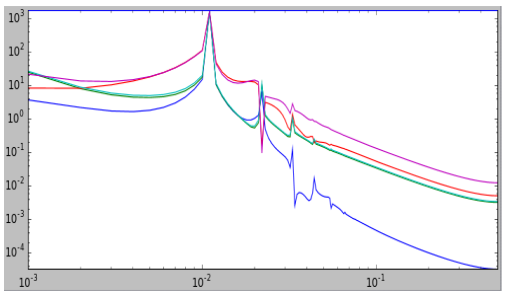

(g)

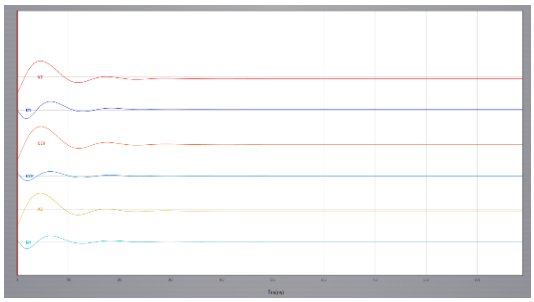

(g1)

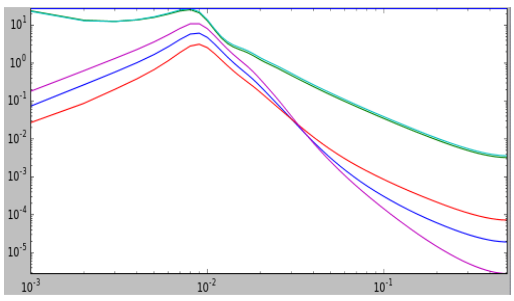

Figure 3.7 Simulation of multi-α-rhythms. Panel (a)–(g), simulated time series using different values of *A* parameter for six cerebral areas in left hemisphere (lV2: red, lV1: blue, lCCr: orange, lCCp: light blue, lA2: light orange, lA1: green, respectively). Panel (a1)–(g1): frequency plot.

In summary, the values of the average synaptic gain represented by local parameter *A* used in the modified network model were higher numerical values as compared with first BNM as well as the previous study of Jansen and Rit, (1995). As a consequence of slight increases in the values of parameter *A* in the modified network model, an increased frequency was observed (as demonstrated in Figure 3.8). Thus, this study showed that sensitivity of parameter *A* on modified network model' behaviours.

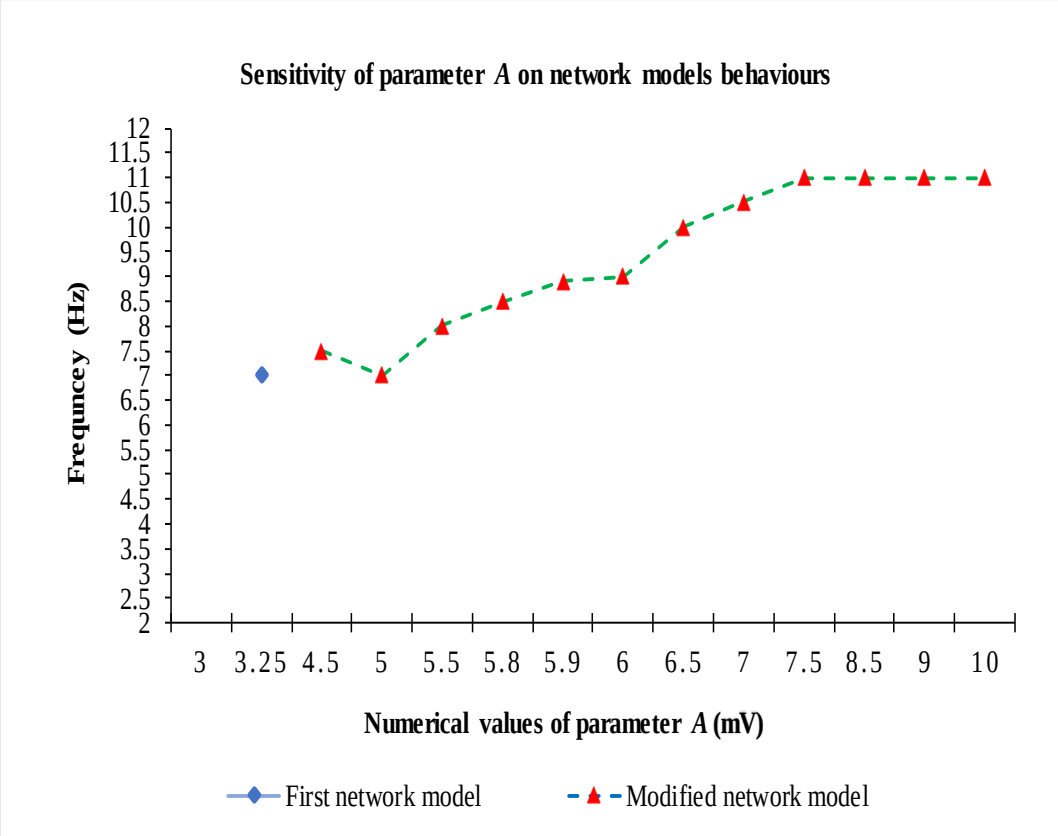

Figure 3.8: Sensitivity of paramter *A* on network models' behaviours

3. 6 Conclusions

This chapter focused on developing LSBNMs at different scales, the meso- and macroscopic scales of neural populations by combining the local dynamics of the JR model which accounts for the interaction network of neural masses in one area with structural connectivity that is defined by the human connectome. Two network models were proposed and developed. One generated low oscillations of EEG alpha rhythm with frequency 7 Hz by integrating structural connectivity that consisted of four brain areas in the left hemisphere with the local model of JR. Each area is modelled in its original parametrisation with the ability to oscillate within the low EEG. Another model is extended to include six brain areas in the left hemisphere. The local dynamic in each six brain areas is simulated using network composed of interconnected excitatory and inhibitory JR. Here, we modified the local parameters of JR and studied the influence of these modified parameters on the behaviour of BNM. By modifying these parameters, the model generated alpha rhythms of EEG at different low and upper frequency ranges of 7–8 Hz, 8–9 HZ and 10–11 Hz.

We used the TVB platform v1.5.4 for model implementation and simulation. Validation of the proposed models was undertaken in terms of frequency using FFT. The significance of these network models can help researchers and physicians to identify the general mechanism of EEG rhythms and accurately diagnose, especially with lower and higher alpha frequency ranges, for cognitive and creative tasks as well as patients who have neurocognitive disorders such as AD and dementia.

The contents of this chapter have been published in the *International Journal of Biomedical Engineering and Technology* (Al-Hossenat et al., 2019) and also in the *Proceedings of the First MoHESR and HCED Iraqi Scholars Conference in Australasia 2017: Melbourne, Australia* (Al-Hossenat et al., 2017).

CHAPTER 4

MODEL FOR GENERATING DELTA AND THETA RHYTHMS

This chapter focus on the study of other physiological parameters (i.e. local parameters) of these LSBNM models along with the global parameters which are two fundamental components of LSBNMs.

We investigate the influence of local physiological parameters of the JR model (the imbalance between excitatory and inhibitory neural populations) on the patterns of EEG delta and theta rhythms generated, especially the numerical values of average excitatory and inhibitory synaptic gain (*A, B)* and the time constant of excitatory and inhibitory PSP (*a, b*). This investigation is introduced via the development of a LSBNM consisting of eight brain areas in the left hemisphere by linking modified local parameters with global parameter changes that take into account structural connectivity. Each network node models the adjustments in the interconnected excitatory and inhibitory populations of JR that occur at the local level (local parameters) with global parameter changes. The coupling of network nodes is constrained by the structural connectome for constructing the structural layout of the adjusted network model.

4.1 Introduction

The delta and theta oscillations in EEGs play a fundamental role in human cognition (Klimesch et al., 1997b; Klimesch 1999; Klimesch et al., 2001; Jensen and Tesche, 2002; Hsieh and Ranganath, 2014) and have functional significance in cognitive processing (Harmony, 2013). Generally, in a normal person, these oscillations are characterized by frequency bands: delta rhythm (0-4 Hz) recorded during the slowest oscillatory activities of the brain and deep sleep, while theta rhythm (4-7 Hz) is recorded during low brain activities, sleep, or drowsiness (Bronzino, 1999).

Some of the mechanisms that generate these two activities can result from excitatory and inhibitory interactions within and between populations of neurons but the mechanism of emergence of these two types of EEG activities remain largely unknown or the subject of debate. Modelling studies have focused on the generation of human brain rhythms of EEG including delta and theta rhythmical oscillations with different approaches and at different scales (David and Friston, 2003; David et al. 2005, Grabska-Barwińska and Żygierewicz, 2006; Sotero et al, 2007; Dong and Liang, 2014). Until now, BNM has been used to help understand neuronal activity in the human brain and it has been uniquely capable of predicting and integrating neuronal activity at multi-scale. For an excellent review see Breakspear, 2017. It has also played an indispensable role in simulating functional magnetic resonance imaging (fMRI) data and investigating the effect of altered brain anatomical connectivity on fMRI functional connectivity (Horwitz et al., 2013) and understanding the structural–functional connectivity in the human brain (Honey et al., 2010).). More recently, works related to the BNM approach have been applied a wide range of applications such as disease state or resting state dynamics as well as stimulation using the TVB platform (Sigala et al., 2014; Roy et al., 2014; Adhikari et al., 2015; Ritter et al., 2015; Kringelbach et al., 2015; Schirner et al, 2015; Becker et al., 2015; Spiegler et al., 2016; Kunze et al., 2016; Falcon et al., 2015, 2016a, 2016b; Stefanovski, et al., 2016; Proix et al., 2016; Jirsa et al., 2017; Bezgin et al., 2017; Proix et al.,2017; Deco et al., 2017; Al-Hossenat et al., 2017; Deco et al., 2018; Schirner et al., 2018; Aerts et al., 2018; Zimmermann et al., 2018a; Zimmermann et al., 2018b; Proix et al., 2018; Stefanovski et al., 2019; Shen et al., 2019; Aerts et al., 2019, Al-Hossenat et al., 2019).

For example, Zimmermann et al. (2018b) introduced studying disease states, Falcon et al. (2015, 2016b) simulated the BOLD signal in stroke, Aerts et al. (2018) modelled large-scale brain dynamics in tumour patients, and Al-Hossenat et al. (2017, 2019) simulated the alpha band of EEG in the frequency range (7-12 Hz). So far, no network modelling studies have been presented to investigate the influence of modifying local and global parameters, derived from LSBNM, on the generation of regular delta–range at the frequency of (1-4 Hz) and theta at the frequency of (4-7 Hz) as well as diverse narrowband oscillations ranging from delta to theta (0-5 Hz).

4.2 Model and implementation with The Virtual Brain

The goal of this chapter is to develop a BNM to produce multi-bands of EEG patterns: regular delta–range frequency of (1-4 Hz), theta at a frequency of (4-7Hz) and diverse narrowband oscillations ranging from delta to theta (0-5Hz). The proposed model has a network of N = 8 nodes that represent eight cerebral areas at various brain lobes in the left hemisphere. Each node in the large-scale network is modelled as a local network comprising a modification of the interconnected excitatory and inhibitory populations of the JR model that describe brain neural activities at the local level (three neural masses: m1: pyramidal cell, m2: excitatory interneuron and m3: inhibitory interneuron). Neural activities generated from these local modifications of all brain regions are coupled according to structural connectivity which is represented by the global parameters using diverse examples of the global coupling and conduction velocity between brain regions. Figure 4.1 describes the network representation of our model.

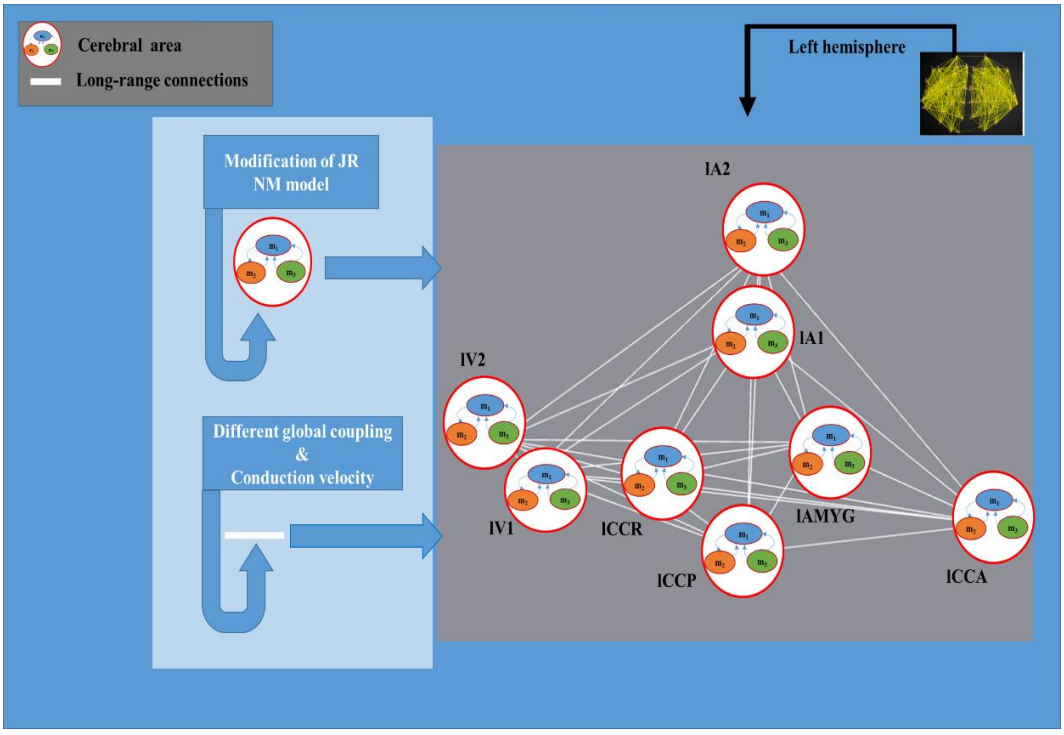

Figure 4.1: Network representation for our model

4.2.1 Model design and implementation

For simulating large scale brain activities with different rhythms (delta and theta) we modified the equation as in Sanz Leon (2014). That is a mathematical representation of the generic evolution equation of BNM described by a delayed differential system of a network of coupled neural populations. This equation is covered by local and global parameters and implemented in TVB.

TVB is embedded with several types of NMMs. For example, the JR model with its original parameters (Jansen et al, 1995), is embedded in the equation of the BNM (see Sanz- Leon, 2014). However, we modified JR's equations to include the use of new values for interconnected excitatory and inhibitory populations of the Jansen model, especially the maximum amplitude of the excitatory and other inhibitory, α=*A,B*, respectively as well as time constant of excitatory and inhibitory populations, γ=a, b, respectively (see Figure 4.2, Equations 4.2 and 4.4). Thus, the evolution equation of our BNM $\dot{z}_i(t)$ is computed by summing the intrinsic local dynamics of each area $f(z_i(t))$ generated by the modification in interconnected excitatory and inhibitory populations of the JR that occur at the local level (local parameters) with global parameters that connect the dynamics for each of the eight brain areas. These global parameters take into account the long-range connection, including long-range coupling, *c* and the time delay $\Delta t_{ij} = dij/cv$ between regions *i* and *j*, where, dij is a distance matrix and *cv* is a conduction velocity. Here, we utilized different global coupling (Sigmoid and linear coupling) and various values of conduction velocity ($cv = 4$ and 3 mm/ms) for long-range connectivity w. Figure 4.2 shows the evolution equation of our network model used in this chapter.

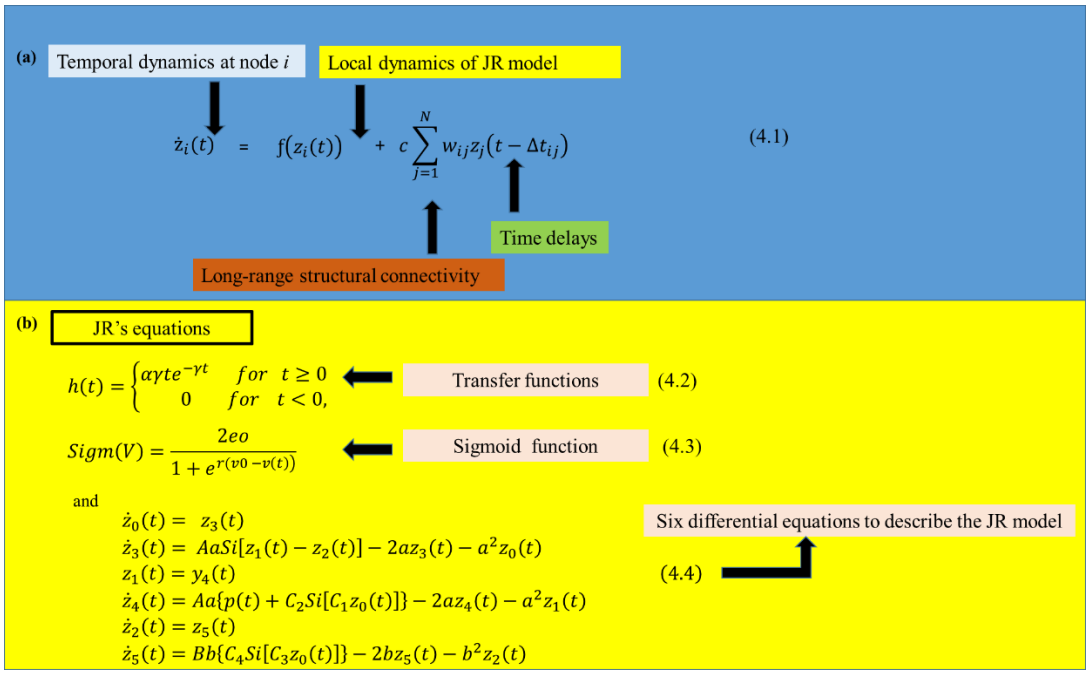

Figure 4.2: Our equation used to simulate EEG patterns (delta and theta). (a) Evolution equation representes temporal dummies of area *i* at time *t*. This equation depends on the local dynamics of JR model *f* (zi (t)) as well as long-range structural connectivity *w*. This *f* (zi (t)) is generated by modifying the values of the maximum amplitude of the excitatory and other inhibitory, α=*A* ,*B* respectively, as well as time constant of excitatory and inhibitory, γ=*a, b. w* links areas *i* and *j*, described by connectivity matrix (weights) and time delay(Δt_{ij}) between eight areas. Weights are scaled by global coupling c. (b) Jansen's equation comprising Eq. (4.2) is represented by transfer functions, Eq. (4.3) represents sigmoid function (Sigm) and Eq. (4.4) and describes the model outputs written as a set of six differential equations.

In this study, the pipeline implementation of our equations is conducted in several stages using TVB.

4.2.2 Structural network connectivity

The structural connectome discussed in Chapter 3 was again used to correspond with biologically realistic, large-scale connectivity of brain regions mediated by long-range neural fibre tracts (Sanz-Leon, 2014, 2015). Moreover, this large-scale connectivity is considered to be the time delay that plays a significant role in shaping large-scale dynamics (Deco et al, 2009). In this chapter, we extend the structural network connectivity used in Chapter 3 to include eight cerebral areas selected from the left cerebral hemisphere. This extension of the network structure included choosing

locations of cerebral areas at different cerebral cortex lobes that incorporate the parietal lobe, frontal lobe, temporal lobe and occipital lobe (see Figure 4.3 and Table 4.1). These areas were selected to generate theta and delta rhythms and relied upon some concepts such as the high-amplitude theta rhythms that are commonly located in various areas of the cerebral cortex such as the anterior cingulate cortex that is located in the frontal lobe and the amygdala in the temporal lobe (Leung and Borst, 1987). Delta rhythms are observed more in the frontal sites of both hemispheres, are very common in adult and are found in the posterior regions in children (Nunez and Srinivasan, 1982, 2006).

We found the strength of a structural link between the chosen areas (according to the dataset of the structural connectome) and this structure can determine the dynamic patterns of activities (Honey et al., 2010). Based on deductive concepts and the structural connectome, we built our own large-scale connectivity for eight cortical regions and then determined the incoming and outgoing edges from each region to ensure the dissipation of oscillatory activity in the network, as depicted in Figure 4.1. This connectivity is formalized by the weights matrix that shows the strength of the connection between the eight brain areas by integer values from 0, 1, 2 and 3 for no connection, weak connection, moderate and strong connection respectively (see Figure 4.4). The delays matrix ($\Delta t_{ij)}$ is computed by dividing the distance matrix dij and the transmission speed *cv* between brain regions.

Table 4.1 – Cortex regions names and their labels.

Label	Cortex regions
A1	Primary auditory cortex
A2	Secondary auditory cortex
AMYG	Amygdala
CCA	Anterior cingulate cortex
CCP	Posterior cingulate cortex
CCR	Retrosplenial cingulate cortex
V1	Primary visual cortex
V2	Secondary visual cortex

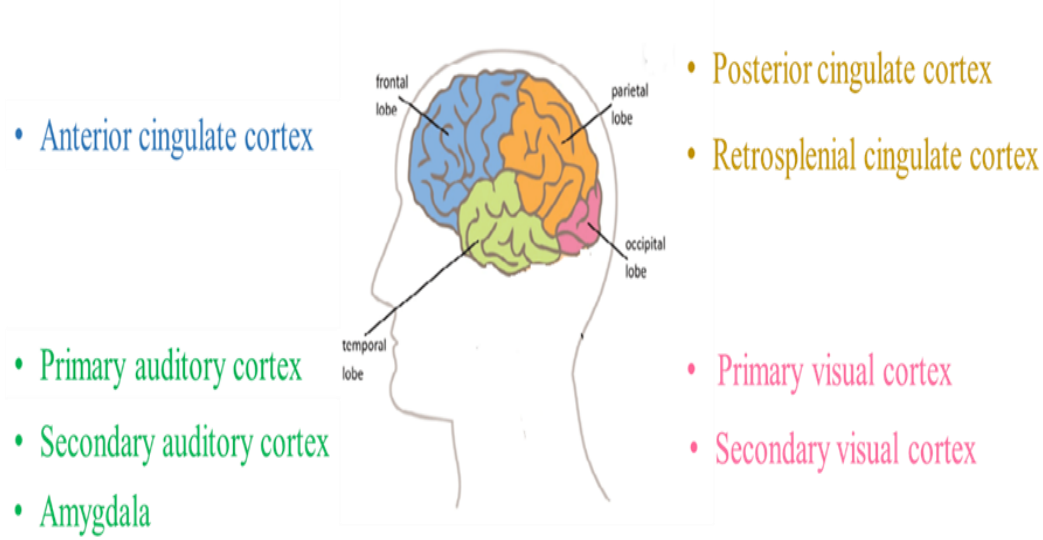

Figure 4.3: Anatomical regions in the left hemisphere of different lobes used in this study

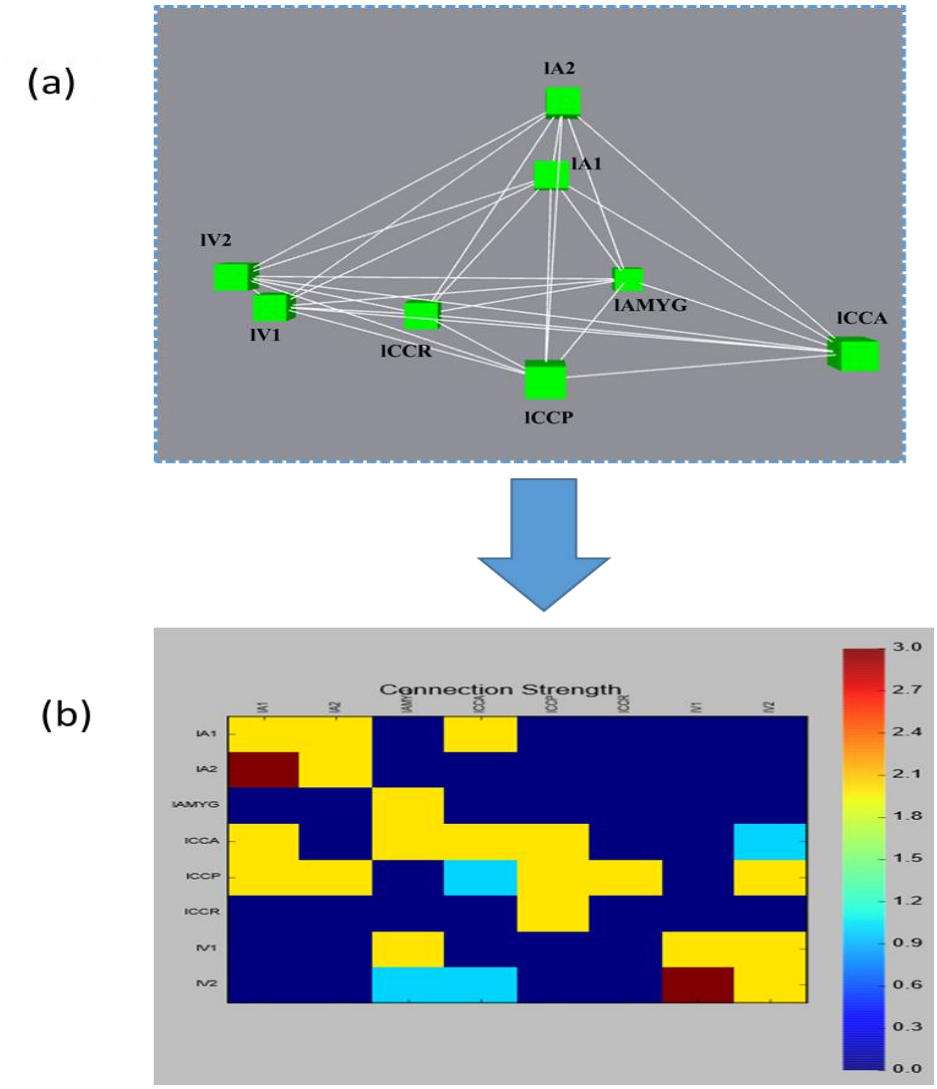

Figure 4.4: (a) Connectivity network between eight cerebral reiogns (green) at the left hemisphere of different brain lobes connected by long–range connections (white) used in this study (b) weighted connectivity matrix for eight cortical regions

4.2.3 Simulation

In the next stage, we imported our own structural connectivity representing connection strengths between the eight regions and time delays via signal transmission between the eight network nodes to TVB simulator to simulate the proposed model. By using TVB simulator that provides numerical methods, several simulations were conducted and each simulation included a number of steps.

Step 1. The local neural mass of the Jansen model was selected to simulate the temporal dynamics of each eight cortical area. The main idea of the JR model was to

produce oscillations, specifically with oscillatory activity in alpha, via three neural mass interactions; PC, EIN and IIN (see the simplified scheme of this model in Figure 4.5). We subsequently modified the Jansen's equation to use new values for interconnected excitatory and inhibitory populations, especially the maximum amplitude of the excitatory and other inhibitory, $\alpha = A, B$, respectively as well as time constant of excitatory and inhibitory, $\gamma = a, b$, respectively (see Equations 4.2 and 4.4). In previous studies, such as Kunze et al. (2016) and Al-Hossenat et al.(2017,2019), the parameters are set to the standard numerical values of the JR model (see Jansen and Rit, (1995)): the maximum amplitude of the excitatory *A*= 3.25mV and inhibitory *B*=22mV, time constant of excitatory, $a = 100^{s-1}$ and time constant of inhibitory $b=50^{s-1}$, the strength of synaptic connections between populations *k1=135,k2= 0.8k1,k3= k4= 0.25k1*, maximum pulse *e0* = 2.5 $^{s-1}$, the value of the average membrane potential v0=6mV, the steepness of the sigmoidal function $r = 0.56mV^{-1}$ and the external input that varies between 120 to 320Hz as noise entered the PC. But here we hypothesised the increase and decrease of both the maximum amplitude of the excitatory and other inhibitory, *A* and *B*, and time constant of excitatory and inhibitory, *a* and *b*. Moreover, external inputs that were modelled by a noise-band ranging from 120 to 320 pulses per second, were entered to all neural populations (PC, EIN, and, IIN) according to a similar notation to that was used in Spiegler and Jirsa (2013) and Sanz Leon (2014). Each simulation was included using different numerical values of parameters (see Table 4.2). To ensure the dynamics of this physical model change as a function of its parameter, we used the phase plane tool to set numerical values and then embedded that model into the network.

Step 2. To join the local dynamics of the JR model over the connection described in structural connectivity, and to transform the neural activity from source nodes (i.e. cortical areas) into a target node, the global coupling function was used to scale all connection strengths. This work was provided with two coupling functions to study their effect on model behaviour. One was a simple coupling function, a linear function whose slope affected the scaling of the oscillatory activity to every area. In the previous study the slope was from 0 to 0.042 (Sanz Leon, 2014) whilst in this work, we used small values, 4.2e-10 and 4.2e-12. A second coupling function, sigmoid coupling (Sigm), used the same default value in that reference. We subsequently set the conduction velocity (CV) in 4 and 3 mm/ms through our network (see Table 4.3).

Step 3. The selection integration scheme was applied to the coupled set differential equations. Here we used Hen's method with a step size of 0.01220ms that reduced its values in relation to those used in this study.

Step 4. The model output from the simulation was selected as a time series of EEG depending on the integration of local and global dynamics.

Step 5. Providing simulation length, we used the default values in TVB of 1000ms.

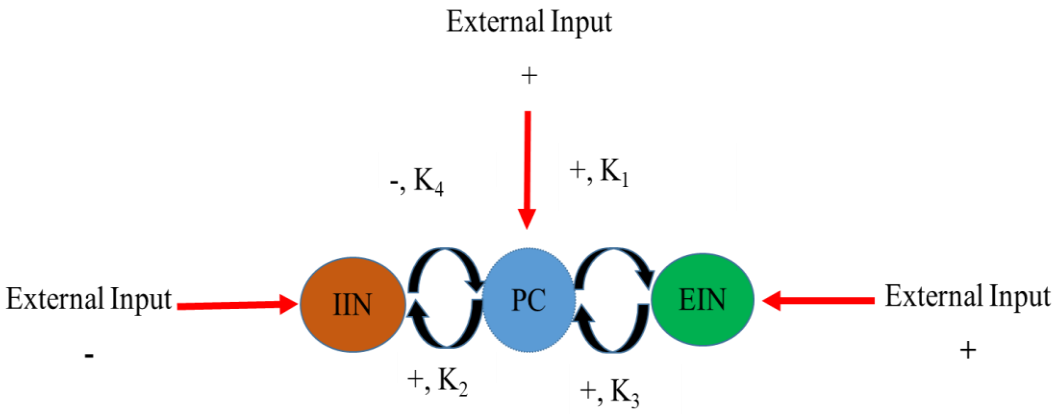

Figure 4.5: Simplified diagram of Jansen's original model. IIN and EIN both receive input from PC with connectivity strength k2, k1 respectively while PC receives input from both EIN and IIN with connectivity strength k3, k4 respectively and external excitatory input. Arrows are marked black with – inhibitory and + with excitatory

Table 4.2: Modified local parameters used in this model

Local parameters used in this model			
A	***B***	***a***	***b***
3.2 3.0	B=28.0, B=26.0 B=25.0 B=20.0	$40s^{-1}$ $30s^{-1}$ $10s^{-1}$,	$b=60s^{-1}$ $b=40s^{-1}$ $b=20s^{-1}$ $b=10s^{-1}$

Table 4.3: Modified global parameters used in this model

Global long-range parameters used in this model		
Global Coupling		Conduction Velocity
Linear coupling	Sigmoid coupling (Sigm)	
Slope=4.2e-12 ,4.2e-10,4.2e-8 and 4.2e-6	Default values in TVB	4 and 3 mm/ms

4.3 Results and evaluations

After modifying the local parameters and the global parameters of the LSBNM, different oscillatory rhythms of EEG were simulated, ranging in the regular band of delta (1-4 Hz), theta (4-7 Hz) and diverse narrowband oscillations ranging from delta to theta (0-5 Hz). These simulation results (see Table 4.4) were obtained using TVB version 1.5.3-8253 on a computer with an Intel (R) Core i7 CPU processor 16GB RAM. These different bands of EEG were represented as a time series of each brain area within the period of time from 0 to time1000ms. Validation of the simulated time series was undertaken using Continuous Wavelet Transform (CWT) which is a powerful tool for analysing signals infrequencies time domain.

4.3.1 Generating delta rhythms (1-4 Hz)

In the case of generating a band of delta rhythms from 1Hz to 4Hz for each of the eight brain areas at the left cerebral hemisphere (V2, V1, CCR, CCP, CCA, Amyg, A2, and A1), we conducted several simulations. In the first simulation, we modified the local parameter, *b* from $50s^{-1}$ to $10s^{-1}$, the global parameter was represented by the global coupling. Here, we set a linear function whose slope was changed from 0.042 to 4.2e-

10 with set conduction velocity in 3 mm/ms that was used in all simulations while setting the rest of the local constants. This led to the generation of a regular delta rhythm (1 Hz). Second, decreasing both local parameter *A* and parameter *b* from 3.25 to 3.0 and from $50s^{-1}$ to $10s^{-1}$, respectively and keeping the other parameters constant, the frequency at 2Hz of regular rhythm was seen for a period of time (1000ms). Third, when *A*=3.0, *B* =20.0, *a* = $100s^{-1}$ and *b* = $50s^{-1}$, a frequency at 3Hz of regular rhythm was observed, while when *A* =3.0, *B* =25.0, *a* = $10s^{-1}$ and b = $50s^{-1}$, rhythmic oscillation with regular frequency at 4Hz was observed. As shown in Figure 4.6 (a-d), the time series show the simulated delta rhythms (1-4 Hz) for eight left interconnected cerebral areas in the network and wavelet transform of the simulated time series (a1-d1).

Table 4.4. Summary of simulations results

Model parameters		Frequency of delta and theta rhythms for each area							
Local	**Global**	**V2**	**V1**	**CCR**	**CCP**	**CCA**	**Amyg**	**A2**	**A1**
A= 3.25,B=22.0,a=100$s^{-1}$and b=10s^{-1}	C=linear with a=4.2e-10 and CV=3mm/ms	1 Hz	1 Hz	1 Hz	1 Hz	1 Hz	1 Hz	1 Hz	1 Hz
A= 3.0,B=22.0,a=100s^{-1} and b=20s^{-1}	C=linear with a=4.2e-10 and CV=3mm/ms	2 Hz	2 Hz	2 Hz	2Hz	2 Hz	2 Hz	2 Hz	2 Hz
A= 3.0,B=20.0,a=100s^{-1} and b=20s^{-1}	C=linear with a=4.2e-10 and CV=3mm/m	3 Hz	3 Hz	3 Hz	3 Hz	3Hz	3 Hz	3Hz	3 Hz
A= 3.0,B=25.0,a=10s^{-1} and b=50s^{-1}	C=linear with a=4.2e-10 and CV=3mm/ms	4 Hz	4 Hz	4 Hz	4 Hz	4 Hz	4 Hz	4 Hz	4 Hz
A= 3.2,B=26.0,a=100s^{-1} and b=50s^{-1}	C=linear with a=4.2e-12 and CV=4mm/ms	5 Hz	5 Hz	5 Hz	5 Hz	5 Hz	5 Hz	5 Hz	5 Hz
A= 3.25,B=22.0,a=30s^{-1} and b=40s^{-1}	C=linear with a=4.2e-10 and CV=3mm/ms	6 Hz	6 Hz	6 Hz	6 Hz	6 Hz	6 Hz	6 Hz	6 Hz
A= 3.25,B=22.0,a=40s^{-1} and b=20s^{-1}	C=Sigm,CV=4mm/ms	4.4 Hz	4.5 Hz	2.2 Hz	3 Hz	2.8 Hz	2 Hz	2.5 Hz	2 Hz

A= 3.25,B=22.0,a=40s^{-1} and b=20s^{-1}	C=linear with a=4.2e-6 and CV=4mm/ms	4.2 Hz	4.2 Hz	5 Hz	5 Hz	4 Hz	5 Hz	4 Hz	5 Hz
A= 3.0,B=26.0,a=100s^{-1} and b=50s^{-1}	C=linear with a=4.2e-8 and CV=4mm/ms	stop	stop	4.2 Hz	5 Hz	5 Hz	4 Hz	5 Hz	4.8 Hz
A= 3.25, B=28.0,a=40s^{-1} and b=50s^{-1}	C=Sigm,CV=4mm/ms	stop	stop	7 Hz	7Hz	7 Hz	7 Hz	7 Hz	7 Hz
A=3.25,B=22.0,a=30s^{-1} and b=60s^{-1}	C=linear with a=4.2e-10 OR 4.2e-12 ,CV=3mm/ms	Stop							

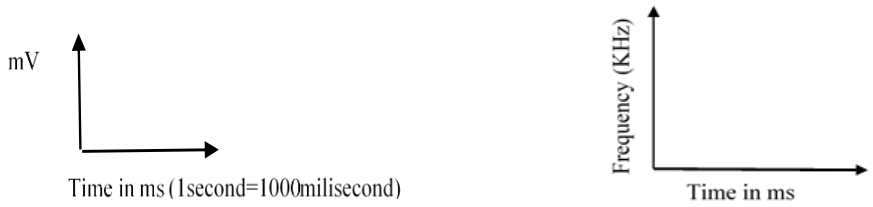
mV
Time in ms (1second=1000milisecond)
Frequency (KHz)
Time in ms

(a)

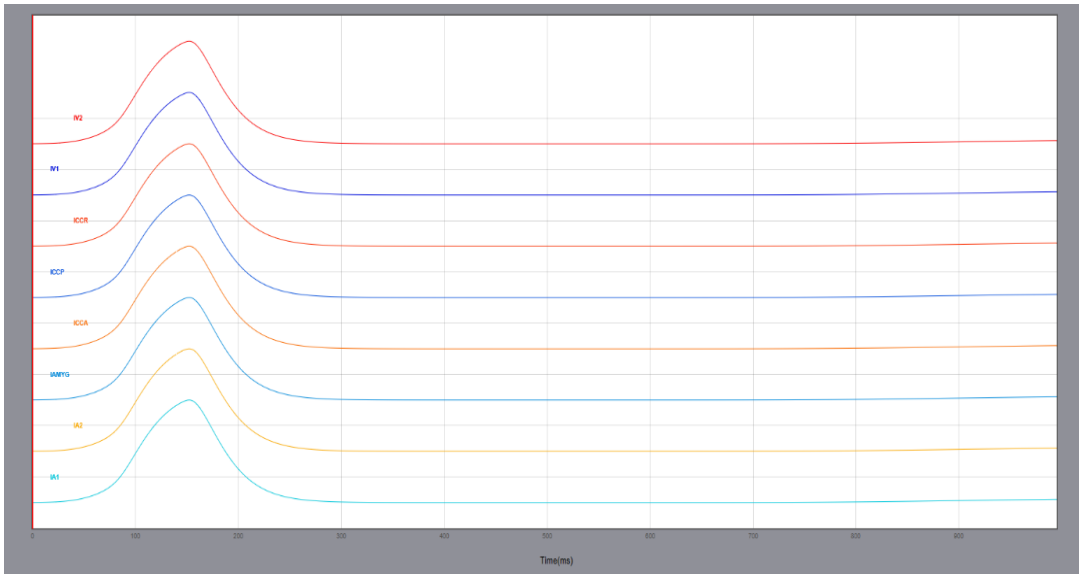
IV2
IV1
ICCR
ICCP
ICCA
IANYG
IA2
IA1
Time(ms)

(a1)

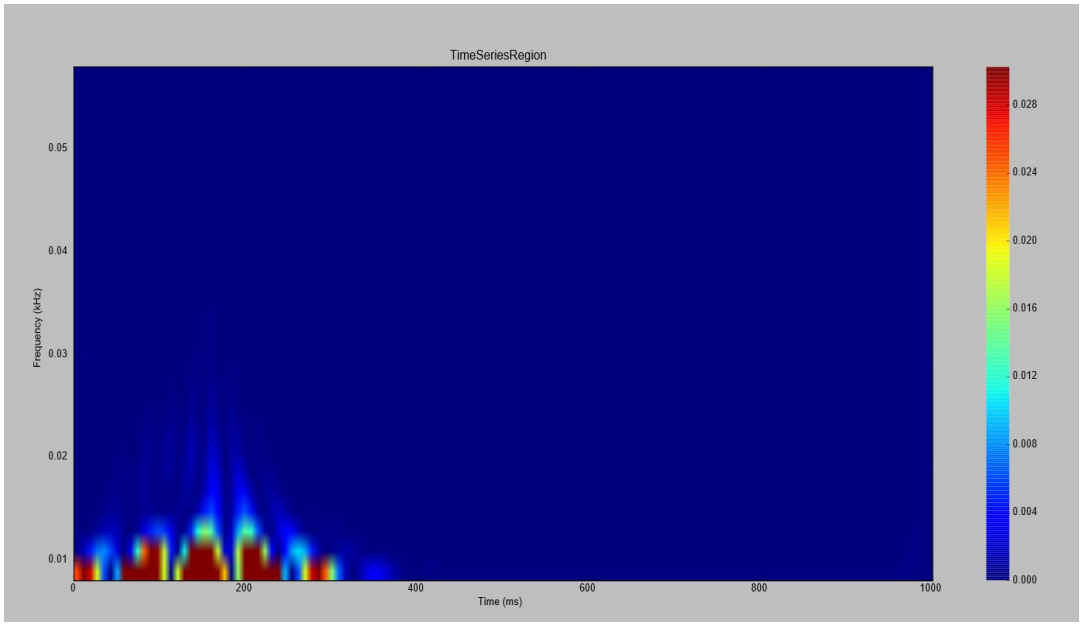
TimeSeriesRegion
Frequency (kHz)
0.05
0.04
0.03
0.02
0.01
0
200
400
600
800
1000
Time (ms)
0.028
0.024
0.020
0.016
0.012
0.008
0.004
0.000

(b)

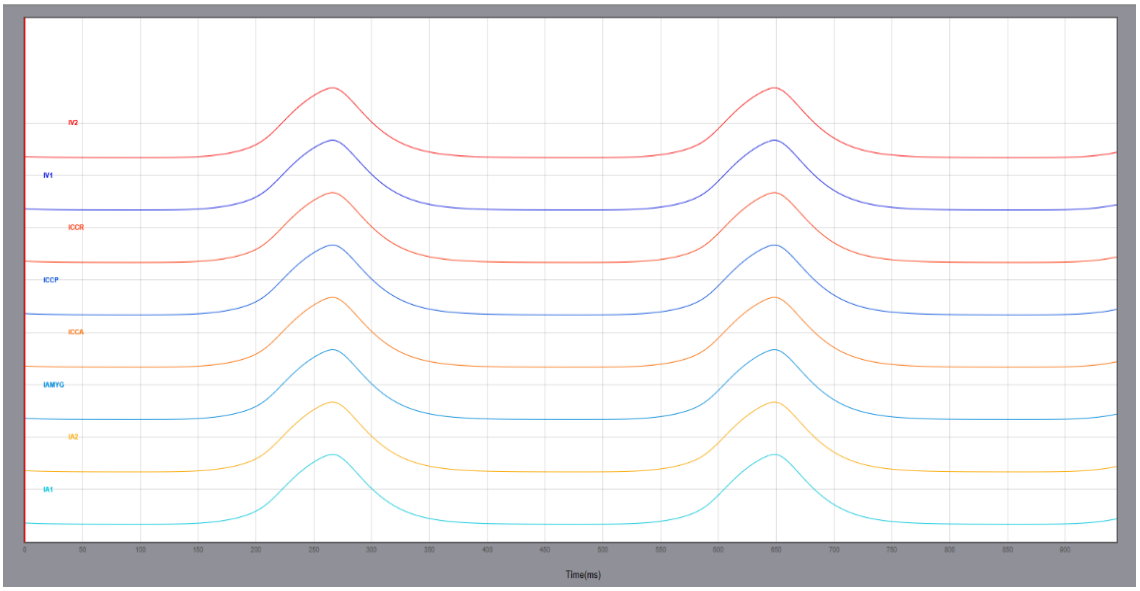
IV2
IV1
ICCR
ICCP
ICCA
IAMYG
IA2
IA1
Time(ms)

(b1)

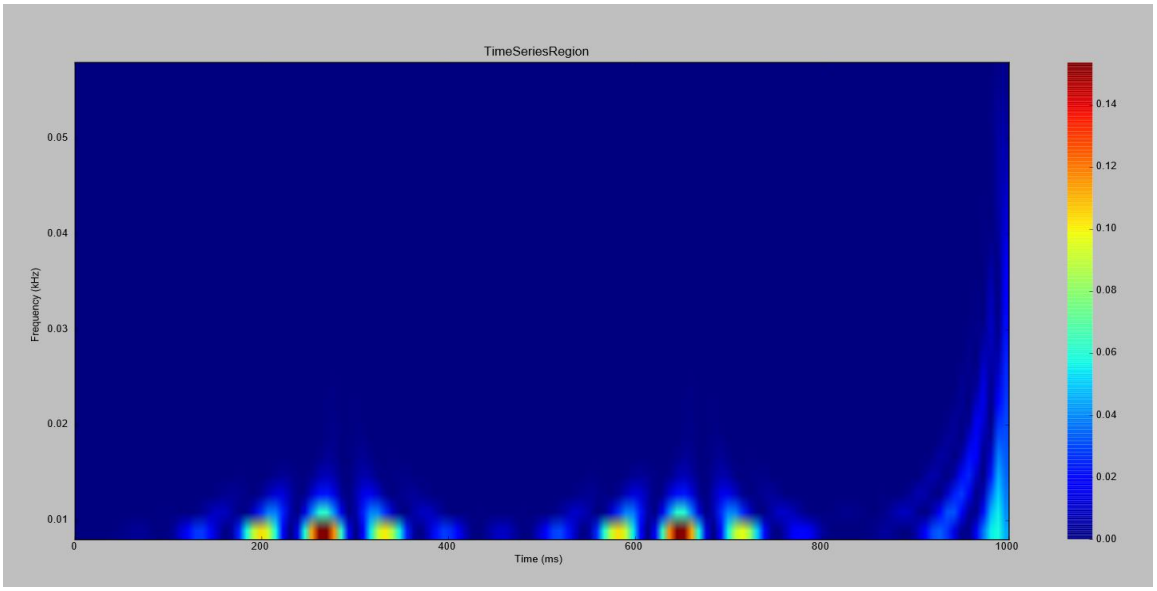
TimeSeriesRegion
Frequency (kHz)
0.05
0.04
0.03
0.02
0.01
0
200
400
600
800
1000
Time (ms)
0.14
0.12
0.10
0.08
0.06
0.04
0.02
0.00

(c)

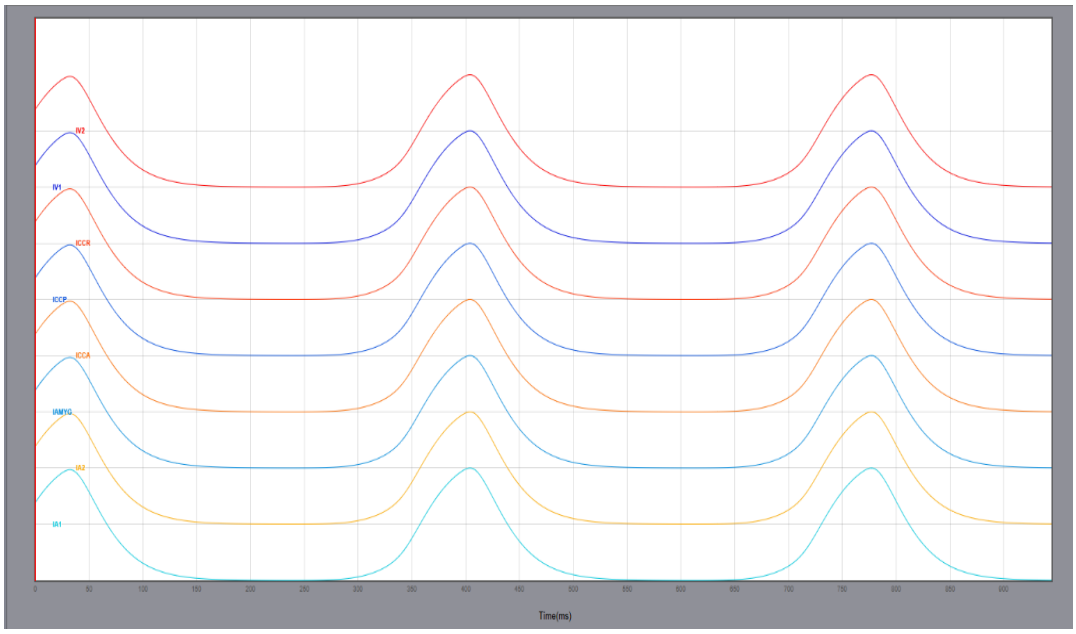
IV2
IV1
ICCR
ICCP
ICCA
IAMYG
IA2
IA1
Time(ms)

(c1)

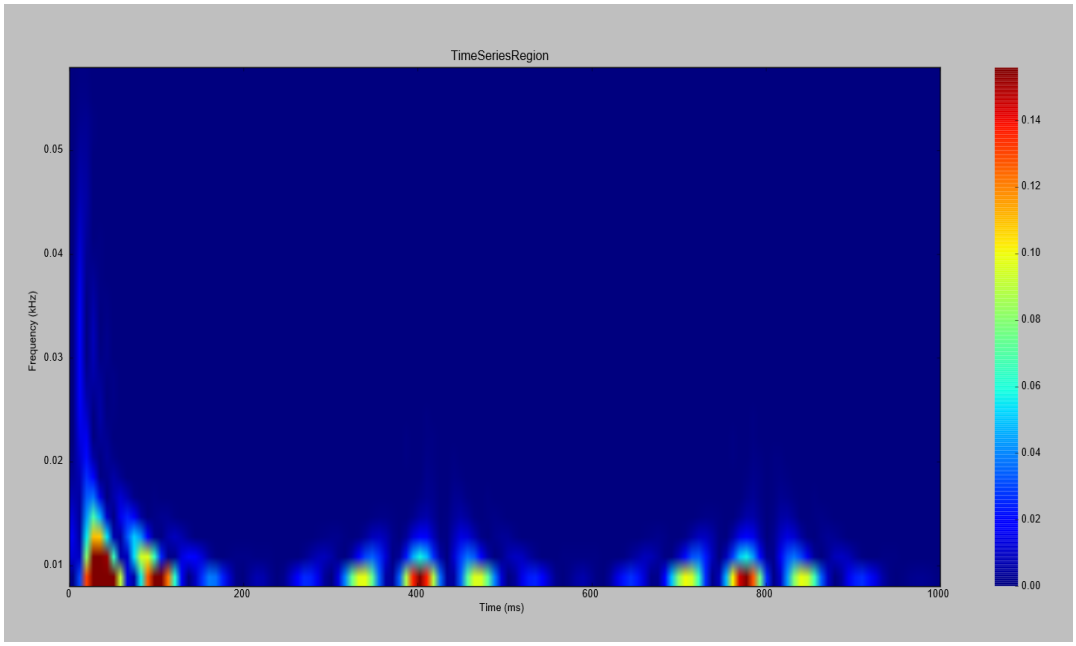
TimeSeriesRegion
Frequency (kHz)
0.05
0.04
0.03
0.02
0.01
0
200
400
600
800
1000
Time (ms)
0.14
0.12
0.10
0.08
0.06
0.04
0.02
0.00

(d)

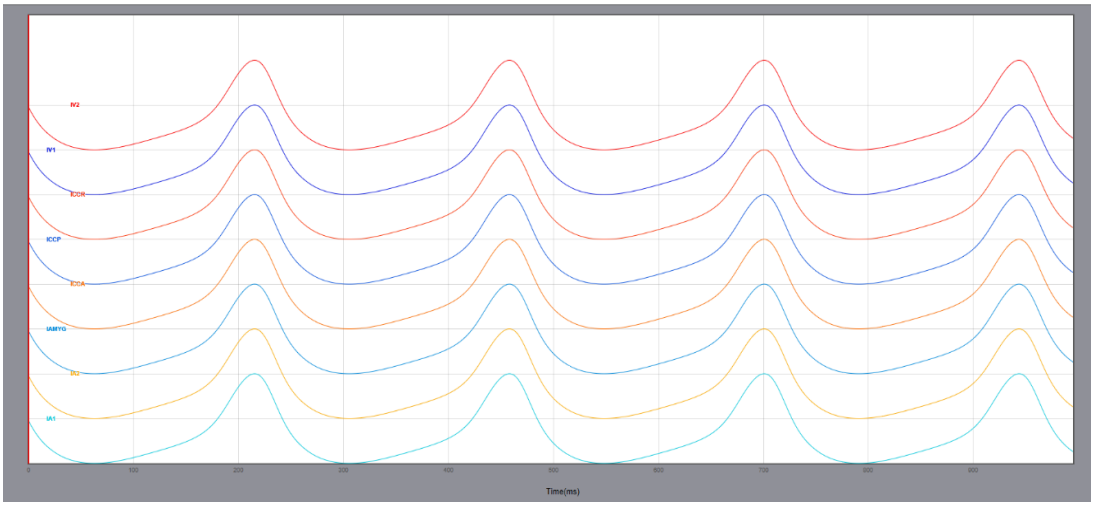

(d1)

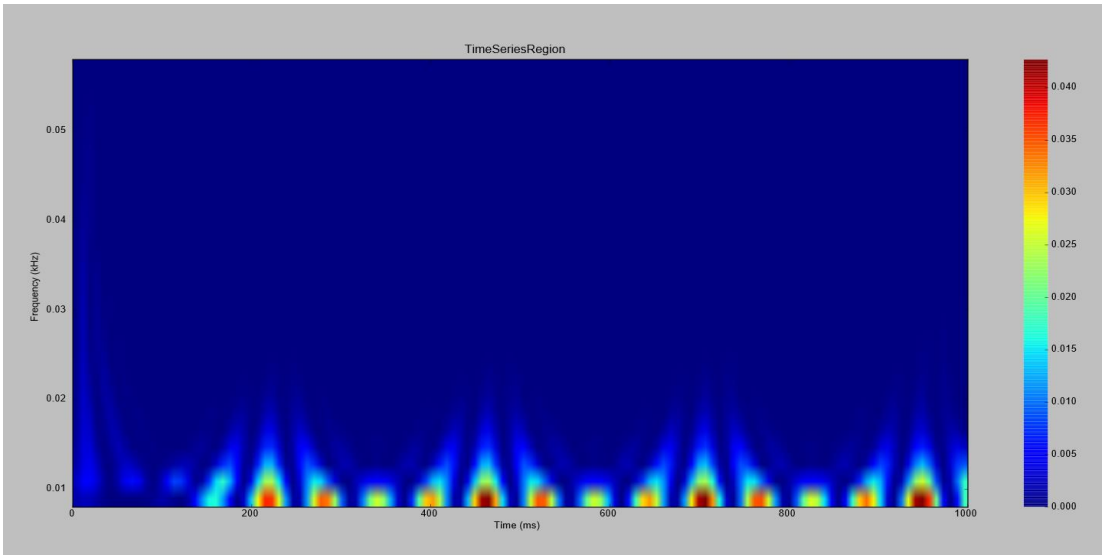

Figure 4.6: Simulation of regular delta–rhythm (1-4Hz). (a-d) Simulated time series for coupled eight brain areas in the left hemisphere (V1,V2, CCR, CCP, CCA, Amyg, A2, A1), respectively with different frequency 1 Hz, 2 Hz, 3 Hz and 4 Hz, respectively (a1-d1) wavelet transform of simulated time series

4.3.2 Generating theta rhythms (4-7 Hz)

To generate a band of regular theta rhythms from 4Hz to 7Hz, we further adjusted the parameters of *A, B, a* and *b* as well as setting different global coupling functions and conduction velocity. With standard numerical values of the Jansen model reported in Section 4.2.3, but low and high values of *A* and *B*, while using the linear function with a slope of 4.2e-12 conduction velocity in 4 mm/ms, the coupled eight brain areas exhibited a regular rhythm around 5Hz. Using small values of *B*, *a* and *b* (22.0, 30s-1, 40s-1, respectively) with linear function with slope 4.2e-10 while set conduction velocity was 3 mm/ms, the coupled eight brain areas exhibited a regular rhythm around 6Hz. Interestingly, as *B* increases (from 22.0 to 28.0) and *a* decreased (from $100s^{-1}$to $40s^{-1}$) with a change in the global coupling from linear to the sigmoid function and conduction velocity in 4 mm/ms, the coupled six brain areas (CCR, CCP, CCA, Amyg, A2, A1, respectively) exhibited a regular rhythm around 6Hz, whilst both areas(V1 and V2) stopped generating the rhythmic oscillation. As shown in Figure 4.7 (a-c), the time series show the simulated theta rhythms (4-7Hz) for eight left interconnected cerebral areas in the network and wavelet transform of the simulated time series (a1-c1).

(a)

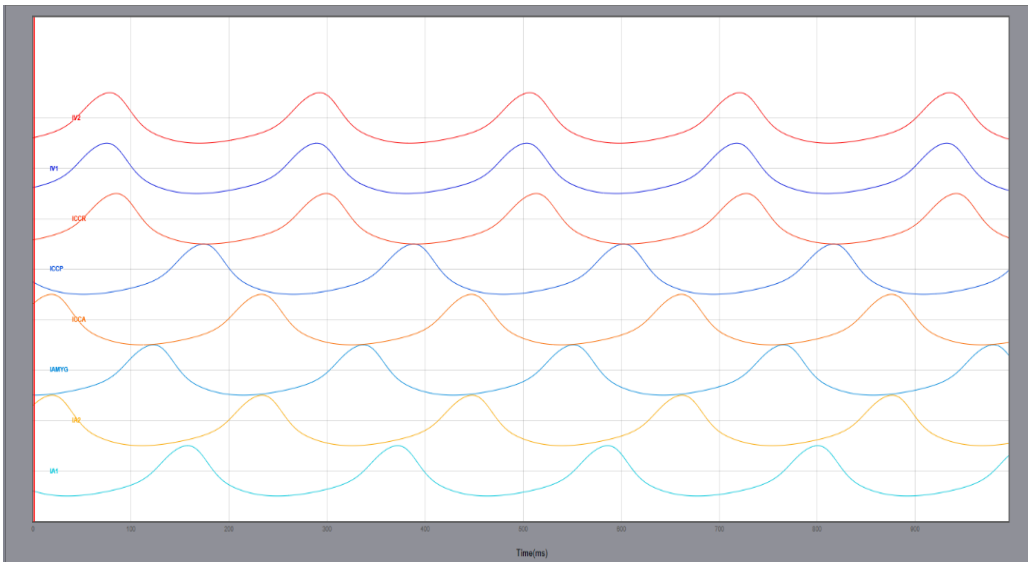
IV2
IV1
ICCK
ICCP
ICCA
IAMYG
IA2
IA1
Time(ms)

(a1)

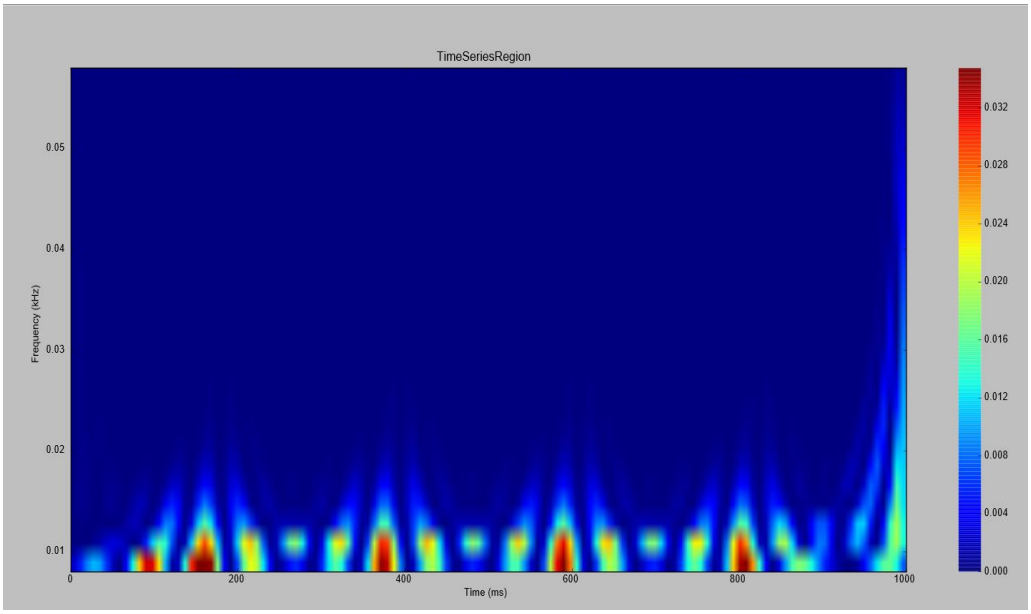
TimeSeriesRegion
Frequency (kHz)
0.05
0.04
0.03
0.02
0.01
0
200
400
600
800
1000
Time (ms)
0.032
0.028
0.024
0.020
0.016
0.012
0.008
0.004
0.000

(b)

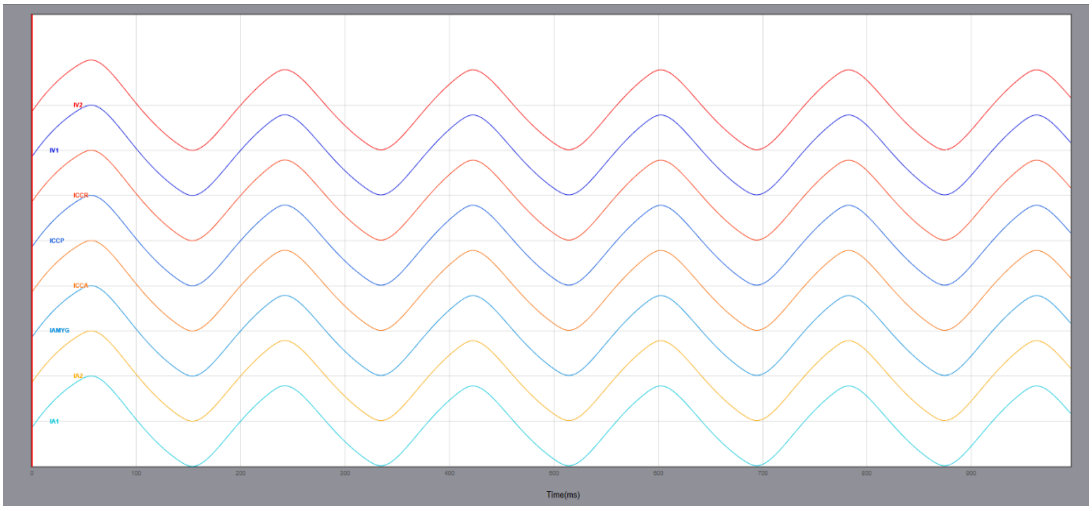
IV2
IV1
ICCR
ICCP
ICCA
IAMYG
IA2
IA1
Time(ms)

(b1)

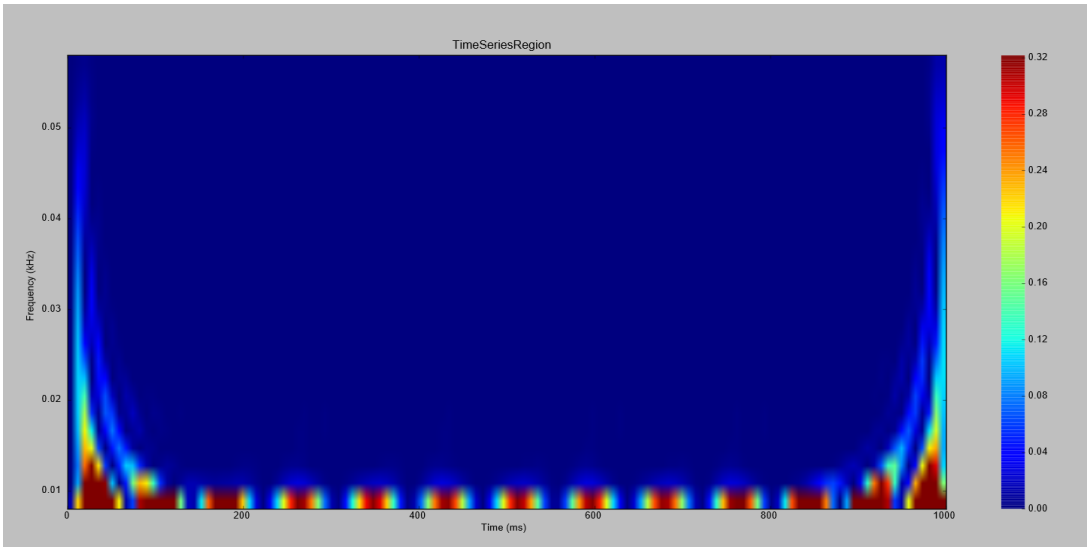
TimeSeriesRegion
Frequency (kHz)
0.05
0.04
0.03
0.02
0.01
0
200
400
600
800
1000
Time (ms)
0.32
0.28
0.24
0.20
0.16
0.12
0.08
0.04
0.00

(c)

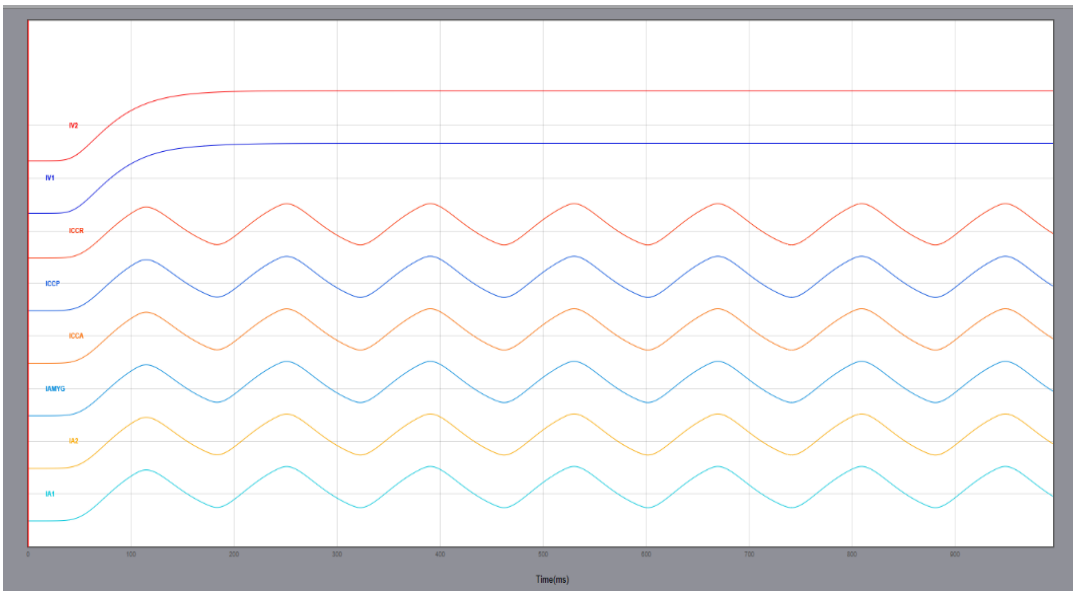

(c1)

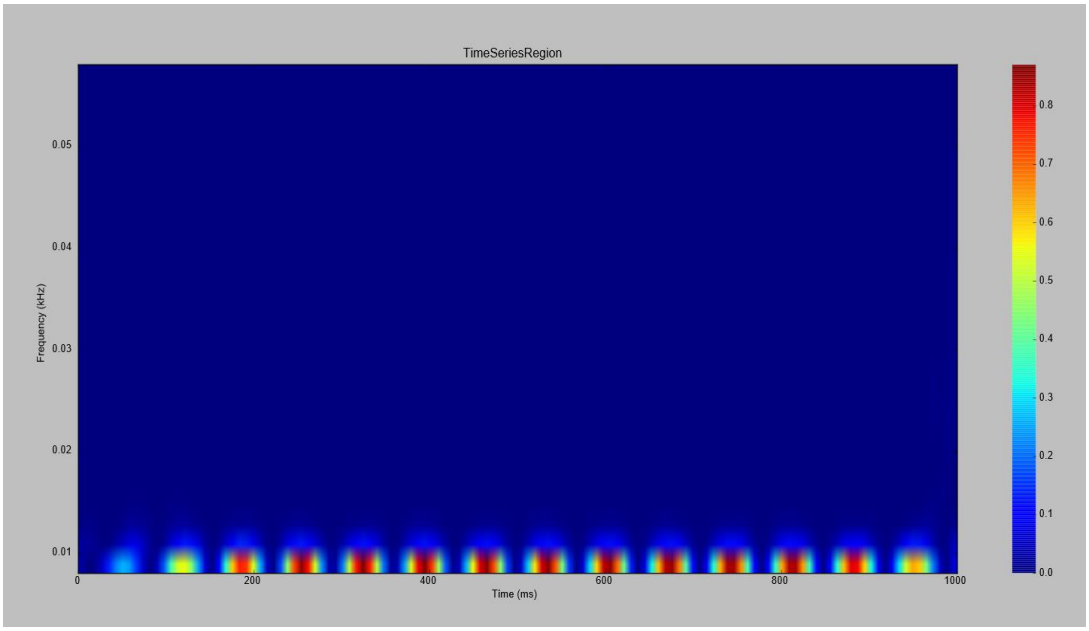

Figure 4.7: Simulation regular theta rhythm (4-7Hz). (a-d) Simulated time series for coupling eight brain areas in the left hemisphere (V1,V2, CCR, CCP, CCA, Amyg, A2, A1), respectively with different frequency 5Hz, 6Hz, 7Hz, respectively. (a1-d1) Wavelet transform of simulated time series

4.3.3 Generating narrowband rhythms ranging from delta to theta (0-5Hz)

Three simulations were performed under different values of *A, B, a* and *b* which revealed a qualitatively rhythmic pattern of the delta combined with a theta at frequency band (0-5 Hz) for eight coupled brain areas. Rhythmic patterns of low band (2-4.5 Hz) were generated, as a decrease in *a* to $40s^{-1}$ and *b* to $20s^{-1}$ and when setting the sigmoid coupling function and conduction velocity at 3 mm/ms while the other local parameters were the same as in Section 4.2.3.

For the next simulation, we set the local parameters as above but set the linear function with slope 4.2e-6 and set conduction velocity in 4 mm/ms. In this case, we noted the generation of narrowband rhythms that had irregular oscillation within the frequency of (4.2-5 Hz) for each cerebral area including low amplitudes within the time window (1000msec).

Finally, frequency band (4.2-5 Hz) was simulated by setting the linear function with slope 4.2e-8 and set conduction velocity in 4 mm/ms; meanwhile, *A* and *B* were set to 3.0 and 26.0, respectively. This band was observed in only six brain areas (CCR, CCP, CCA, Amyg, A2, A1) whilst both areas (V1 and V2) stopped generating the rhythmic oscillation. As shown in Figure 4.8 (a-c), the time series show the simulated narrowband rhythms ranging from delta to theta (0-5Hz) for eight left interconnected cerebral areas in the network and wavelet transform of the simulated time series (a1-c1).

(a)

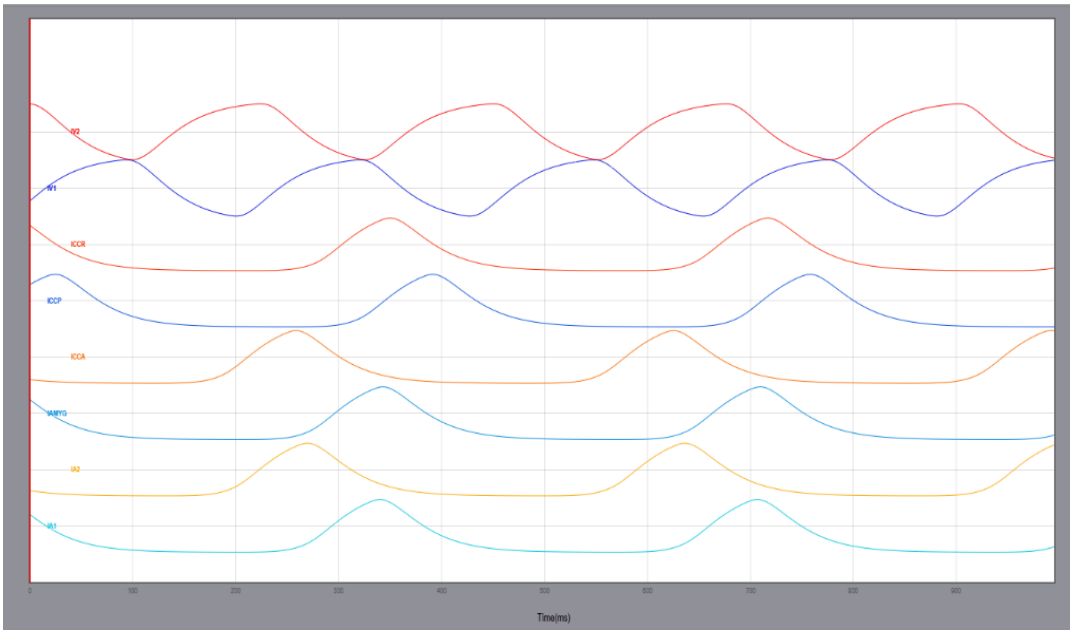
IN2
IN1
ICCR
ICCP
ICCA
IAMYG
IA2
IA1
Time(ms)

(a1)

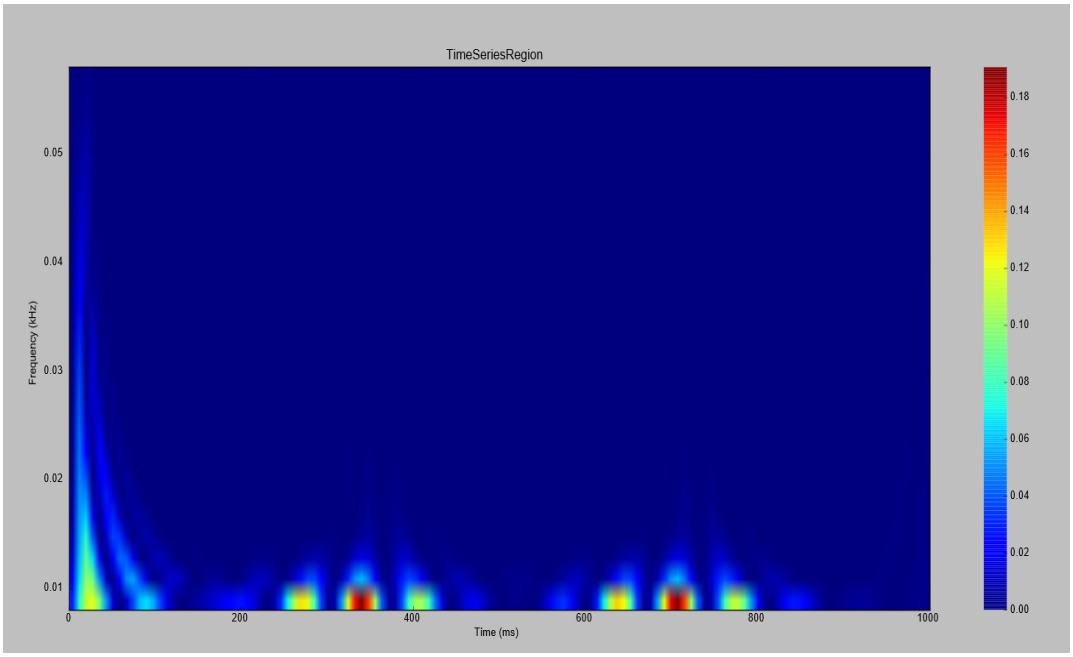
TimeSeriesRegion
Frequency (kHz)
0.05
0.04
0.03
0.02
0.01
0
200
400
600
800
1000
Time (ms)
0.18
0.16
0.14
0.12
0.10
0.08
0.06
0.04
0.02
0.00

(b)

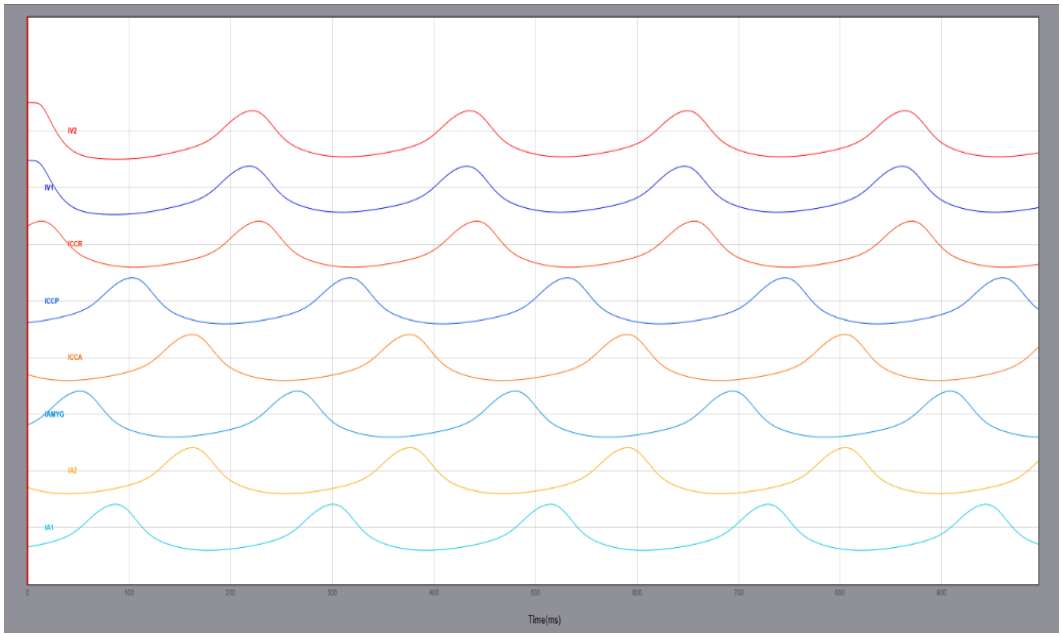
IV2
IV1
ICCR
ICCP
ICCA
IAMYG
IA2
IA1
Time(ms)

(b1)

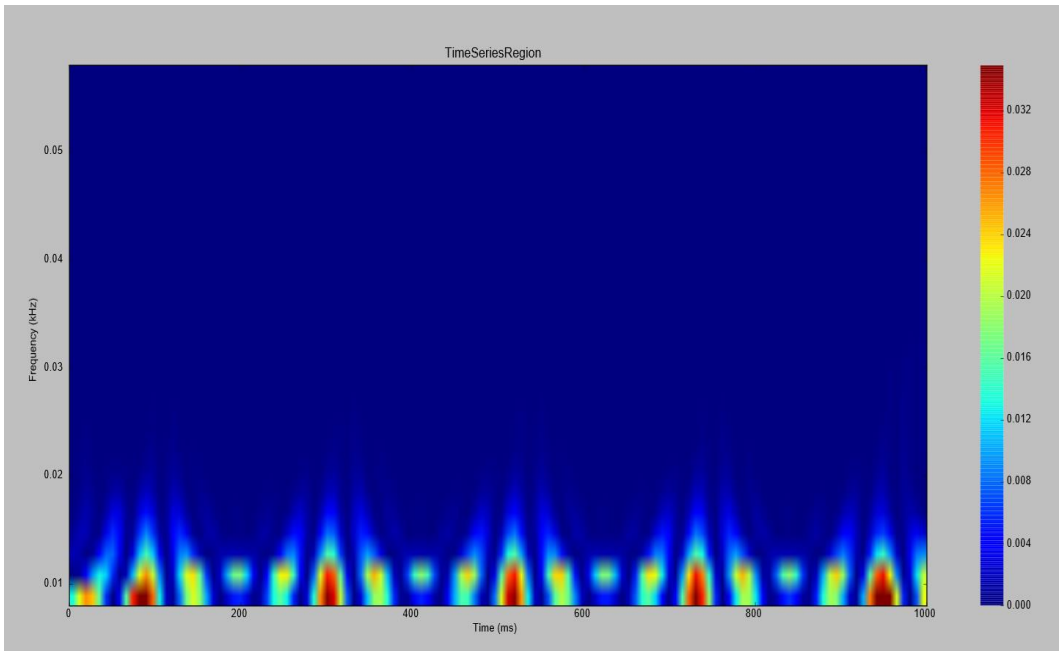
TimeSeriesRegion
Frequency (kHz)
0.05
0.04
0.03
0.02
0.01
0
200
400
600
800
1000
Time (ms)
0.032
0.028
0.024
0.020
0.016
0.012
0.008
0.004
0.000

(c)

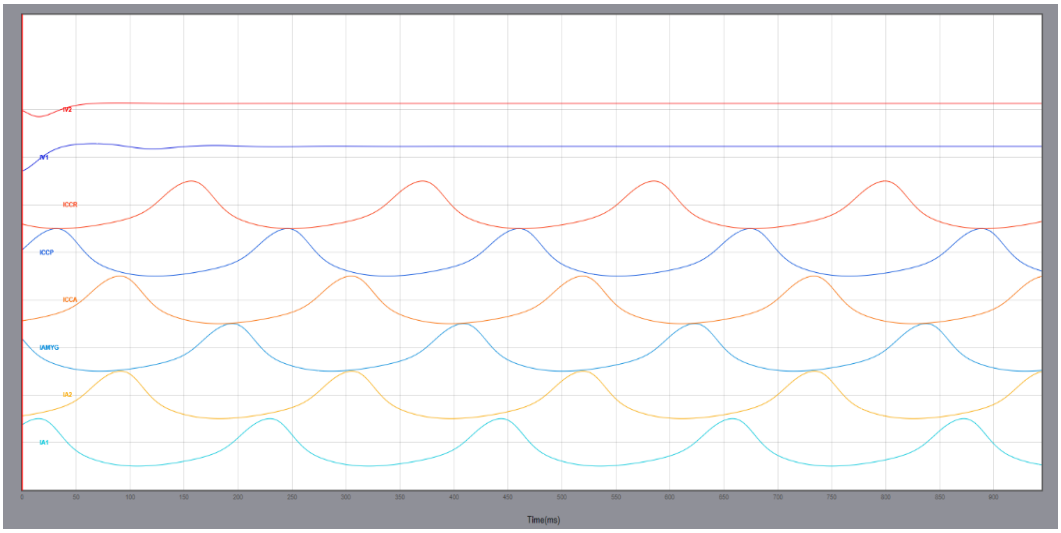

(c1)

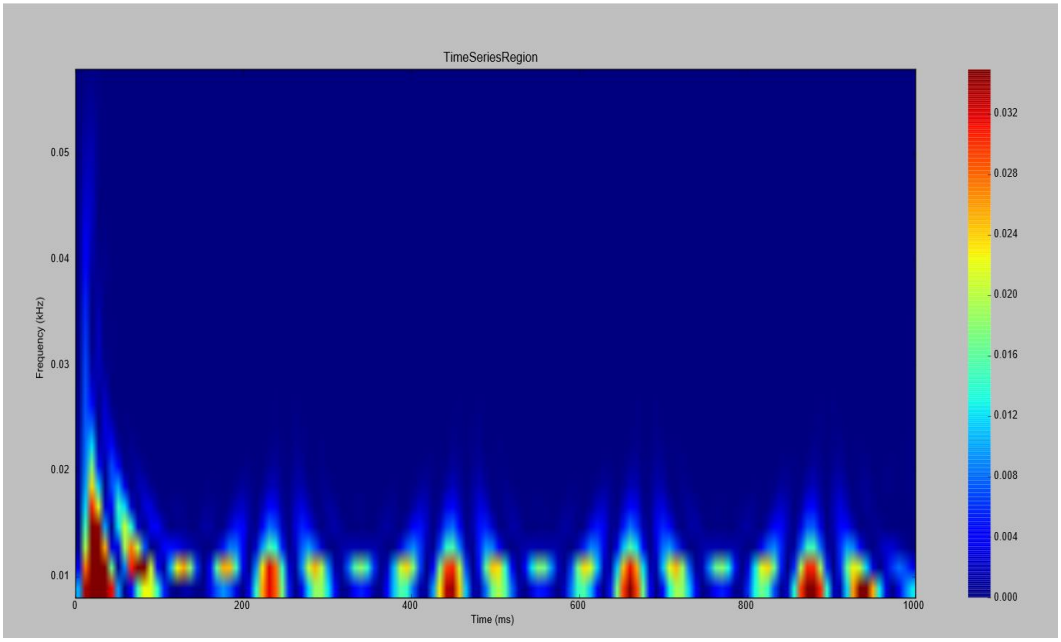

Figure 4.8: Simulated narrowband rhythms ranging from delta to theta (0-5Hz). (a-d) Simulated time series for coupling eight brain areas in the left hemisphere (V1, V2, CCR, CCP, CCA, Amyg, A2, A1), respectively with different frequency bands (2-4.5Hz), (4-5Hz) and 4.2-5Hz), respectively. (a1-d1) Wavelet transform of simulated time series

So far, we have assumed increasing and decreasing the values slightly, represented by local parameters *A, B, a* and *b*. However, there was a strong increase in the value of *b* (*b* =60s^{-1}) and a slight decrease in the value of *A* (3.0); meanwhile other local parameters were set as in Section 4.2.3. This assumption stopped the generation of the rhythmic oscillation for each brain area through setting the global coupling represented by the linear function with different slope (4.2e-10 or 4.2e-12 and conduction velocity in 3 mm/ms), see Figure 4.9.

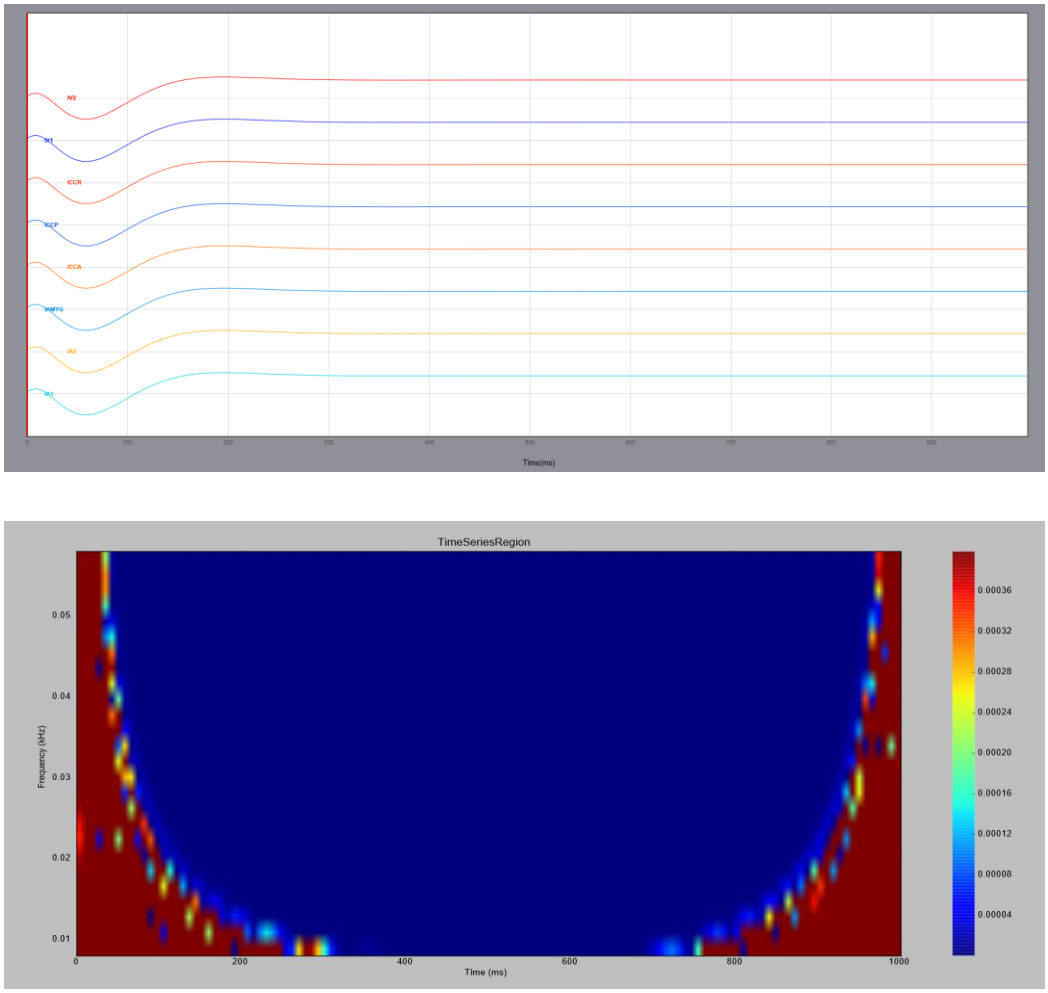

Figure 4.9: Top, non-oscillatory rhythm acquired by greatly increasing the value of *b* (60s^{-1}) and slightly decreasing the value of *A* (3.0mV) for eight coupled brain areas at the left hemisphere (V1, V2, CCR, CCP, CCA, Amyg, A2, A1), respectively. Bottom, frequency plot for simulated time series

We found diverse dynamics oscillations in our network by modifying both the local and global parameters. If we consider this network of n=8 brain areas, each with a dynamic oscillation of m = 11 qualitatively various, the network can feature

n×m=8×11 oscillatory states at the maximum. Thus, based on the results in Figure 4.10, the generated network model can be classified into three distinct frequency bands at the coupling of eight brain areas that were chosen at the left hemisphere of different brain lobes. Hence, these bands can be used to differentiate sleep stages that are distinguished from one another by their frequency. Delta-range frequency of (1-4HZ) is associated with Stage 3 and 4, theta -range frequency of (4-7HZ) is associated with Stages 1 and 2, while delta and theta-range frequency of (0-5HZ) occurred during different stages.

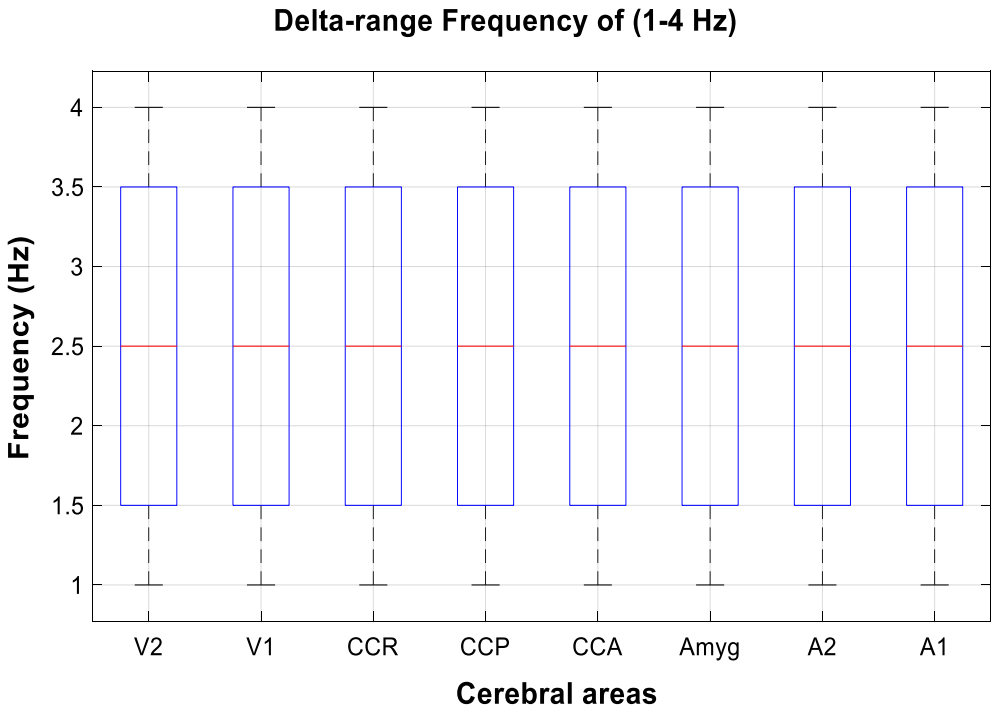

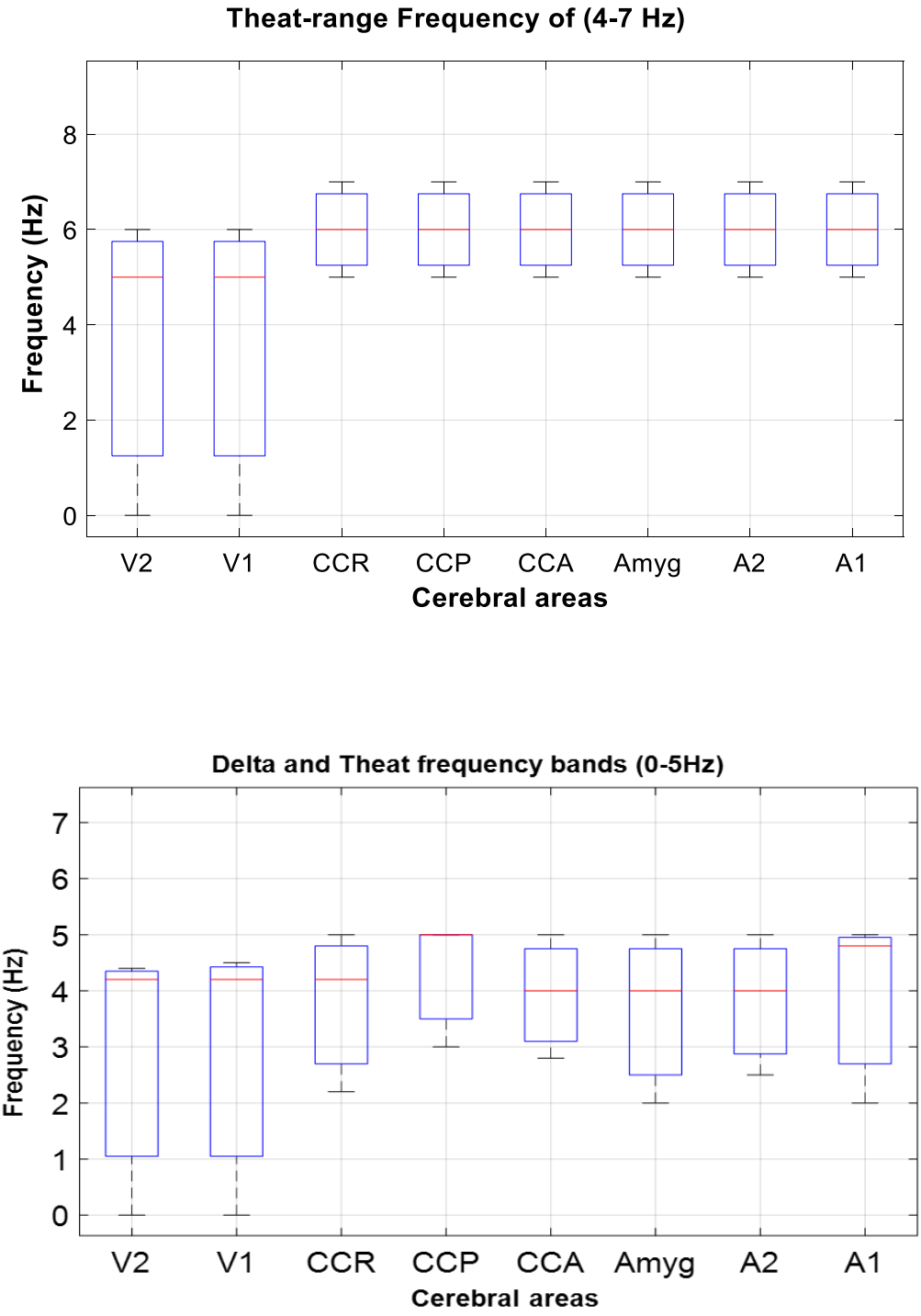

Figure 4. 10: Box plots of the three distinct frequency bands generated from network model at the coupling of eight brain areas (V1, V2, CCR, CCP, CCA, Amyg, A2, A1) that were chosen at the left hemisphere of different brain lobes. Top, Delta-range frequency of (1-4HZ). Middle, theta-range frequency of (4-7HZ).Bottom, delta and theta -range frequency of (0-5HZ)

4.4 Conclusions

The most characteristic EEG patterns, such as delta and theta oscillations have played an important role in studying neurocognitive functions. Further development of BNM at multi-scale is presented in this study to generate these EEG patterns by modifying the local and global parameters of the developed model. We used the model to investigate the influence by modifying local physiological parameters of the local Jansen models (imbalance between excitatory and inhibitory neural populations) and changing the global parameters that take into account the structural connectivity presented by global coupling and dynamic interactions between the eight areas (i.e. conduction velocity). At the local level, each brain area in the large-scale network was simulated in the local regional activity via modification in interconnected excitatory and inhibitory populations of the Jansen models, especially the average excitatory and inhibitory synaptic gain (*A, B)* and time constant of excitatory and inhibitory PSP (*a, b*). The structural connectivity in this study is obtained from a hybrid of DSI and the CoCoMac neuroinformatics database. The modelling and simulation were implemented with TVB, a unique platform for modelling large scale dynamics. The models generated multi-bands of EEG patterns: regular delta–range at a frequency of (1-4 Hz), regular theta at a frequency of (4-7Hz) and diverse narrowband oscillations ranging from delta to theta (0-5Hz). The model outputs are analysed using WT and CWT to investigate the proposed modelling method. The outcomes of the developed network model could be helpful to researchers and clinicians studying slow oscillation activity associated with delta waves of Stages 3 and 4 and theta waves of Stages 1 and 2.

The contents of this chapter was published in the Proceedings of Research Fora 34th International Conference on Science, Engineering & Technology - ICSET 2019, Brisbane, Australia (Al-Hossenat, 2018) and was chosen as an excellent paper. It was then published in the in the International Journal of Electrical, Electronics and Data Communication as an excellent paper (Al-Hossenat, 2019).

CHAPTER 5

NOVEL BRAIN NETWORK MODELS TO SIMULATE AND PREDICT EEG EPILEPTIC PATTERNS

Unlike normal activity in an EEG, epileptiform abnormal activity is characterized by different morphology patterns such as the HFOs of ripples on spikes, spikes and waves, continuous and sporadic spikes, and ploy2 spikes. To predict and investigate these patterns, we have developed three BNMs by linking the NMM of Stefanescu-Jirsa 2D (S-J 2D) with our own structural connectivity derived from the realistic biological data used in previous chapters.

These models include multiple network connectivity of brain regions at different lobes and both hemispheres (left and right). The network node of these models is simulated by the local dynamics of the S-J 2D model generated by adjusting the global coupling between the excitatory and inhibitory populations. We investigated whether adjusting the connection strength between the inhibitory and excitatory neurons of the local model can predict different morphology patterns such as ripples on spikes, spikes, continuous spikes, sporadic spikes and ploy2 spikes ranging from 94-144 Hz. The network model's results were compared with epileptiform abnormal patterns in EEG and those obtained from other BNMs. This study is able to assist researchers and clinical doctors in the field of epilepsy to understand the complex neural mechanisms generating abnormal oscillatory activities and, may open up avenues towards the discovery of new clinical interventions related to epilepsy.

5.1 Background and Related work

The gamma oscillation in EEG can be decomposed into different frequency ranges: slow gamma, typically defined as a frequency from 30 to 80 Hz and HFOs with a frequency >80 Hz. HFOs have been investigated for their important role in health and disease, e.g., their association with cognitive processing in human recognition memory

(Kucewicz el al., 2014). Many studies have shown that HFOs can be novel biomarkers in human epilepsy. For example, Jacobs et al. (2008) reported that HFOs can assist in the identification of abnormal EEG patterns found in the seizure onset zone of human ictal and interictal recordings. These HFOs can be further divided into sub-categories depending on their frequency, ripples (80-250 Hz) and fast ripples (250-500 Hz) (Bragin et al., 1999). The difference between normal and abnormal oscillations can be seen in their patterns. In particular, oscillations observed in the epileptic human brain can be distinguished by different morphology, namely sharp-wave, spikes, spikes and waves, and polyspikes as well as pathological ripples of HFO_S >80 Hz (clinical data[10] of EEG, Chatrian, 1974; Barlow, 1993; Westmoreland, 1996; Noachtar et al. 2004 ; Chang and Drislane, 2007; Jacobs et al., 2008, 2009, 2012; Mathews et al., 2015). Figure 5.1 demonstrates a taxonomy of brain oscillations covering different frequencies with mean ranges (0-500 Hz). From this figure, it is seen that the HFOs are within the 80–500 Hz frequency range and the ripples (80-250 Hz) which are included our study (in this chapter), predict the HFOs of different morphology patterns.

It is very important to understand the complex neural mechanisms generating abnormal oscillatory activity that can cause seizures, and simulate these oscillation with different morphologies. Several modelling approaches have been developed to address these challenging issues.

[10] Epileptic events extracted from EEG data in a patient with temporal lobe epilepsy used in the previous study (Wending et al.2012)

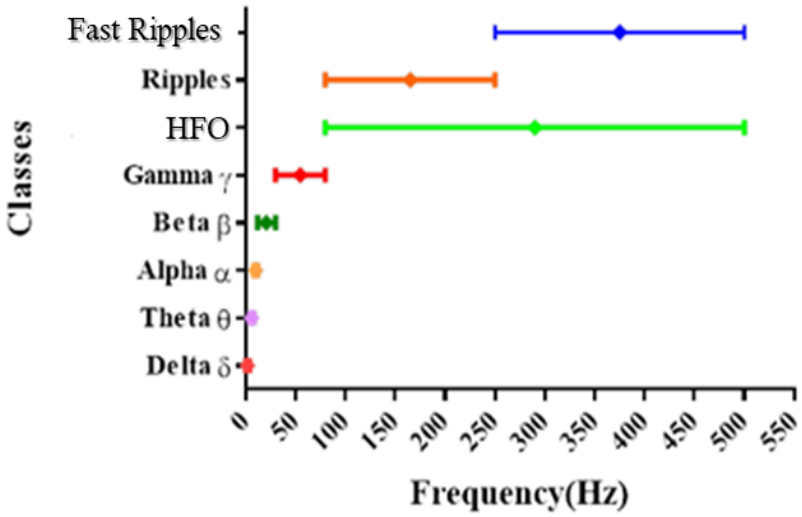

Figure 5.1: Taxonomy of brain oscillations covering frequency mean at range (0-500 Hz)

From the mesoscopic level, considerable work has been devoted to explain rhythms in disease, and reproducing epileptic activities and their patterns as well (Traub et al. 1999; Zetterberg et al., 1978; Wending et al., 2000, 2001; Robinson et al., 2001; Robinson et al., 2002; Liley, and Bojak, 2005; Breakspear et al. 2006; Kim and Robinson, 2007; Touboul et al, 2011; Jedynak et al., 2017; Kameneva et al., 2017; Ahmadizadeh et al., 2018). These models are known as NMMs. For instance, the model proposed by Traub et al. (1999) consists of a network of a large number of pyramidal cells but no interneurons. From this network, interical HFOs, observed as ripples within a range of frequency (120 to 250Hz), were generated. Some models of EEG seizures were developed to simulate different classes of EEG-like activities (Wendling et al., 2000, 2002). For instance, Wendling et al. (2002) introduced a model of seizure-like signals. This model was based on an archicortical structure coupling four neural masses: the pyramidal cell - the main neural cells, fast and slow inhibitory interneurons, and excitatory interneurons. The model outputs showed that the imbalance between excitatory and inhibitory coupling between neural populations produced realistic epileptic EEG signals in the hippocampus. These EEG signals were classified into six different classes of EEG-like activities (Class 1: Background activity, Class 2: Sporadic spikes, Class 3: Sustained spikes–wave discharges, Class 4:

Slow rhythmic activity, Class 5: Low-voltage rapid activity and Class 6: Slow quasi-sinusoidal activity).

These NMMs are popular amongst researchers and many studies have used it. Hebbink (2014) reported that fast and slow inhibitory interneurons had a significant role in generating types of epileptic activities. Comparison was made between the investigated results of activity Classes 4 and 6 produced by Wendling's model. The model was also used by Kameneva et al. (2017), and verified their hypothesis that the brain network of healthy neurons could have regions with seizure-like dynamics, including 16 interconnected columns. They showed that outputs of pathological dynamics were observed when parameters of global connectivity strength were altered.

Wendling et al. (2012) also developed a mesoscopic model for hippocampal activity. Their method described the mechanisms underlying interictal spikes, fast ripples and HFOs that emerged from the neural population-level. From this computational model, the authors demonstrated that generating these activities could depend on model parameters such as increasing the ratio of excitation/inhibition, and they noticed that these activities were similar to real data recorded in the human hippocampus as well as in animal models (vivo and vitro).

Jirsa and colleagues (Jirsa et al., 2014) proposed a NMM derived from the basic principles of coupled dynamical systems. The Epileptor relied on the theory of a slow-fast system in non-linear dynamics described by differential equations and bifurcation theory. This study highlighted the significance of the Epileptor and compiled a seizure taxonomy as a guide to studying epileptic modelling. Other studies utilized the Epilator equations introduced by Jira et al. (2017) to generate typical sequences of an epileptic's neural activities. The neural model consisted of coupled neural networks, including two neural populations (fast-excitatory neurons and inhibitory neurons). Their main results demonstrate that interictal spikes were produced by inhibitory neurons, while generated fast discharges occurred because of the excitatory neurons.

In this thesis, we outline the development of three BNMs by linking the Stefanescu-Jirsa 2D neural mass model (S-J 2D) with the realistic biological data. These models include multiple network connectivity of brain regions at different lobes and hemispheres (left and right). In these models, each network node occupies with local

dynamics generated by adjusting a global coupling between excitatory and inhibitory populations, and edges representing the long-range structural connectivity (SC white matter fibre). In particular, we investigate how the biophysical parameters of the S-J2D local mass model can affect the behaviour of proposed models via unbalancing excitatory and inhibitory coupling strength at the local network. This investigation undertakes to predict oscillatory activities that resembled epileptic seizures with a different morphology of each model where the frequencies of these brain activities ranged from ~94-144 Hz. The technical and conceptual framework for modelling epileptic seizures with TVB proposed in this work, is depicted in Figure 5.2.

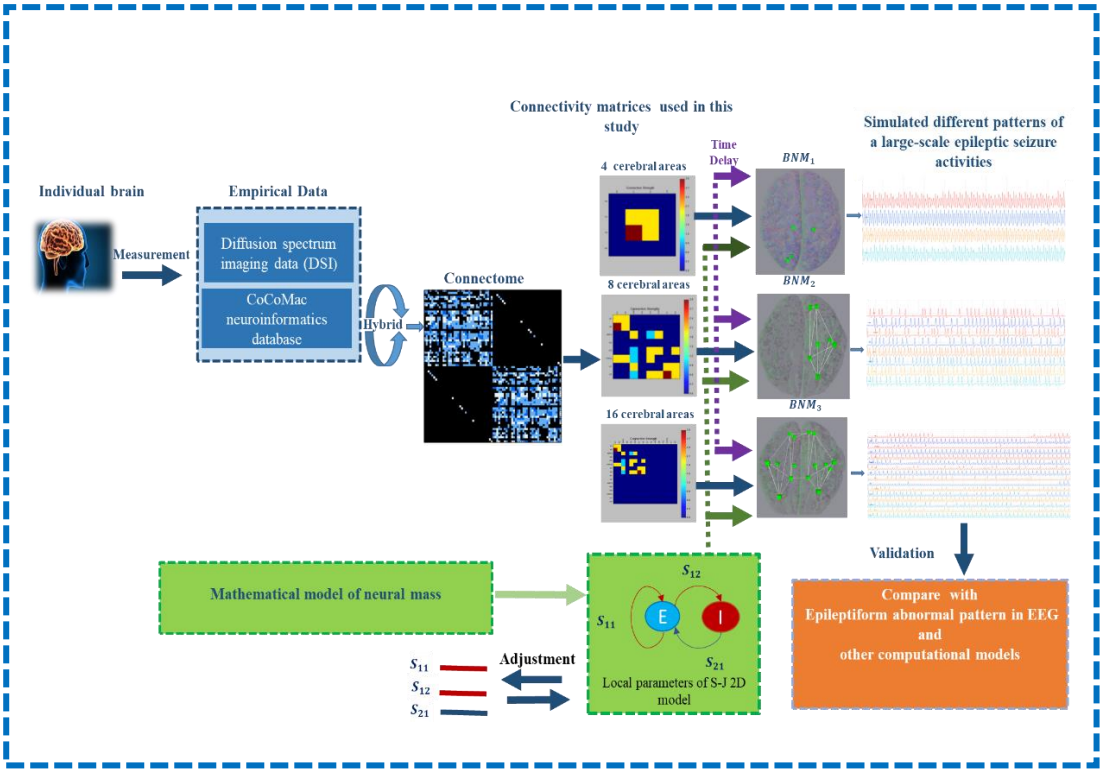

Figure 5.2: The technical and conceptual framework for modelling epileptic activties using TVB

As shown in Figure 5.2, to build our models using TVB, brain structural connectivity (connectome) is combined with the mathematical model of neural mass. This study used structural connectivity generated from a hybrid of DSI data and the neuroinformatics dataset of CoCoMac. From this connectivity, three structural connectivities (N1, N2 and N3) were constructed, each of them represented by its our own connectivity matrix (connection strength) between cerebral areas at different

lobes and in both hemispheres. Each cerebral area was modelled by a S-J2D model via adjustment of the coupling strength between excitation (E) and inhibition (I) neurons: S_{11} (excitatory to excitatory), S_{12} (excitatory to inhibitory) and S_{21} (inhibitory to excitatory). The time delay between all network nodes is also considered in this study. Together, the adjusting parameter values of coupling strength and structural connectivities are (N1, N2 and N3). As a consequence, the three network models' outputs are BNM1, BNM2, and BNM3 respectively. These network models were depicted as simulated time series of different patterns of epileptic seizure activities.

5.2 The architecture of the network models

The architecture of this study is described in three large-scale brain netwok models (BNM_1, BNM_2 and BNM_3) comprising different network connectivies (N_1,N_2,N_3) of neural elements: N1=4, N2=8 and N3=16 cerebral areas or network nodes at different lobes, and in both hemispheres. Each of the network models depends upon long-range and short-range structural connectivity (SC), where the long-range links all elements with each other (heterogeneous connectivity) while the short-range links the nodes within an area (homogeneous connectivity). Heterogeneous connectivity is mediated by fibre tracts which are identified with a hybrid of DSI data and the neuroinformatics dataset of CoCoMac as model input represented by two matrics: the connections matrix between areas and the delay matrix. Each element of the network (i.e., cerebral area) is modelled by a S-J2D model that fully connects homogeneously into excitatory (E) and inhibitory (I) neural populations. In particular, we adjusted the values of local coupling strength between neural excitation (E) and inhibition (I) and global coupling strength between network elements (cerebral areas) to include new values to genetate data of epileptic seizures. Then the network evolution equation of each node (cerebral areas) describing the delay differential system is given as follows:

$$\dot{\Psi}(x_i, t) = f(x_i(t)) + g \sum_{j=1}^{N} w_{ij} x_j\left(t - \Delta t_{ij}\right) \ , \tag{5.1}$$

where $\dot{\Psi}(x_i, t)$ represents the mean field potential of a node *i* at time *t* based on a local dynmic of S-J2D, $f(x_i(t))$, heterogeneous connectivity *w* as connection matrix that

linked brain areas i and j, g which is the global coupling function, and time delay $(t - \Delta t_{ij})$. Here *N= 4,8 and 16* represent the number of nodes of each network used in this model.

5.2.1 Structural layout used in three models

An essential step for building the layout of the BNM is the structural connectivity (SC) of the human connectome that desribes a network map of the structural connections of the human brain derived from different non-invasive neuroimaging techniques (Sporns, 2011). Here, the SC human connectome consists of hybrid data from the DSI data and the CoCoMac database (Kötter, 2004) and defaults on TVB. This dataset used in computational models combines the connection matrices with numerical simulation giving more reliable results, in particular in shaping brain dynamics behaviour due to the use CoCoMac matrix that represents connection strength between brain regions (see Knock et al., 2009). Additionaly, it is widely used by researchers, e.g. Knock et al. (2009), Kunze et al. (2016), Al-Hossenat et al. (2017) and Al-Hossenat et al. (2019). This dataset is considered in a total number of N=76 cerebral areas for both left and right hemispheres, i.e. on the left N= 38 and on the right N= 38 cerebral areas. The details of this dataset are available in Sanz Leon et al. (2015).

According to clinical manifestations and studies in the epilepsy field, seizure-like activities commonly arise anywhere in the temporal and occipital lobes, and their emergence could depend upon areas such as the amygdala and hippocampal cortex (Thom et al., 2012; Javidan, 2012; Aroniadou-Anderjaska et al., 2008 Stafstrom and Carmant, 2015). Remarkably, focal seizures can originate in the temporal lobe.

To obtain realistic models corresponding to clinical manifestations of epilepsy as mentioned above, we have chosen different numbers and locations of cerebral areas from the temporal and occipital lobes. From this default connectivity dataset, that is bi-hemispheres (left and right), three network connectivities are needed to build our network models. The first network connectivity is composed of N=4 cerebral areas in the left and right hemispheres and area choice is dependent upon location. Chosen locations included sites roughly 50% from the occipital lobe and 50% from the temporal lobe. From this structural connectivity, we built the first connectivity matrix.

The second connectivity is composed of N=8 cerebral areas in the right hemisphere and area choice also depended on location which included sites roughly 25% from the occipital lobe and 75% from the temporal lobe. From this structural connectivity, we built the second connectivity matrix. The third network connectivity is comprised of 16 cerebral areas in both hemispheres. Area choice depended on location similar to the second network connectivity in terms of the proportion of selection of cerebral areas within the brain lobes. See Figure 5.3 for depicting and identifying the different brain lobes by color and Table 5.1 for the labels and names of cerebral areas and their locations at lobes used in the network models. See Figure 5.4 for the structural connectivity matrices used to build our network models.

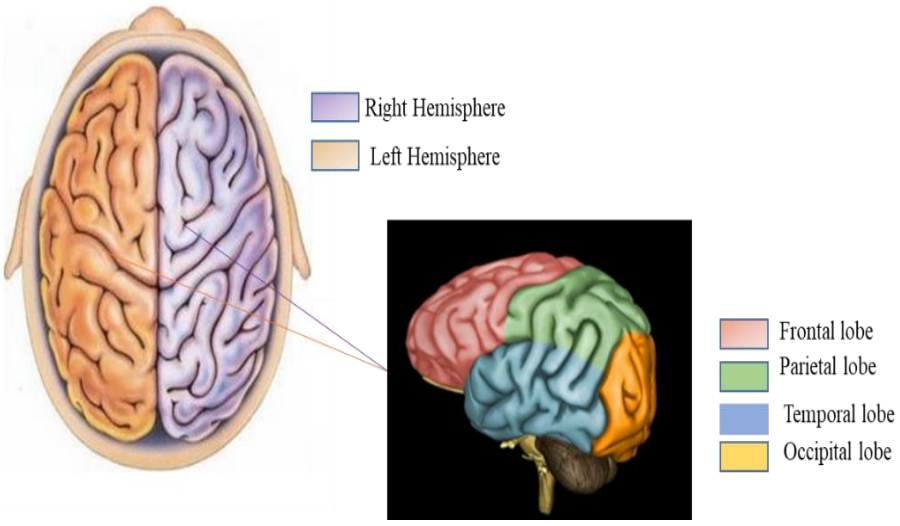

Figure 5.3: Depicting and identifying the different brain lobes by colour

Table 5.1: Abbreviations and names of cerebral areas and their locations including brain lobes and hemispheres used in this network model

Network connectivity	Cerebral Areas		Location	
	Abbreviations	Names	Hemisphere	Lobe
N1	rHC	Hippocampal cortex	R	T
	lV2	Secondary visual cortex	L	O
	lV1	Primary visual cortex	L	O
	lHC	Hippocampal cortex	L	T
N2	rV2	Secondary visual cortex	R	O
	rV1	Primary visual cortex	R	O
	rTCPol	Pole of temporal cortex	R	T
	rTCl	Inferior temporal cortex	R	T
	rHC	Hippocampal cortex	R	T
	rAmyg	Amygdala	R	T
	rA2	Secondary auditory cortex	R	T
	rA1	Primary auditory cortex	R	T
N3	rV2	Secondary visual cortex	R	O
	rV1	Primary visual cortex	R	O
	rTCPol	Pole of temporal cortex	R	T
	rTCI	Inferior temporal cortex	R	T
	rHC	Hippocampal cortex	R	T
	rAmyg	Amygdala	R	T
	rA2	Secondary auditory cortex	R	T
	rA1	Primary auditory cortex	R	T
	lV2	Secondary visual cortex	L	O
	lV1	Primary visual cortex	L	O
	lTCPol	Pole of temporal cortex	L	T
	lTCI	Inferior temporal cortex	L	T
	lHC	Hippocampal cortex	L	T
	lAmyg	Amygdala	L	T
	lA2	Secondary auditory cortex	L	T
	lA1	Primary auditory cortex	L	T
R: Right hemisphere; L: Left hemisphere; T: Temporal lobe; O:Occipital lobe				

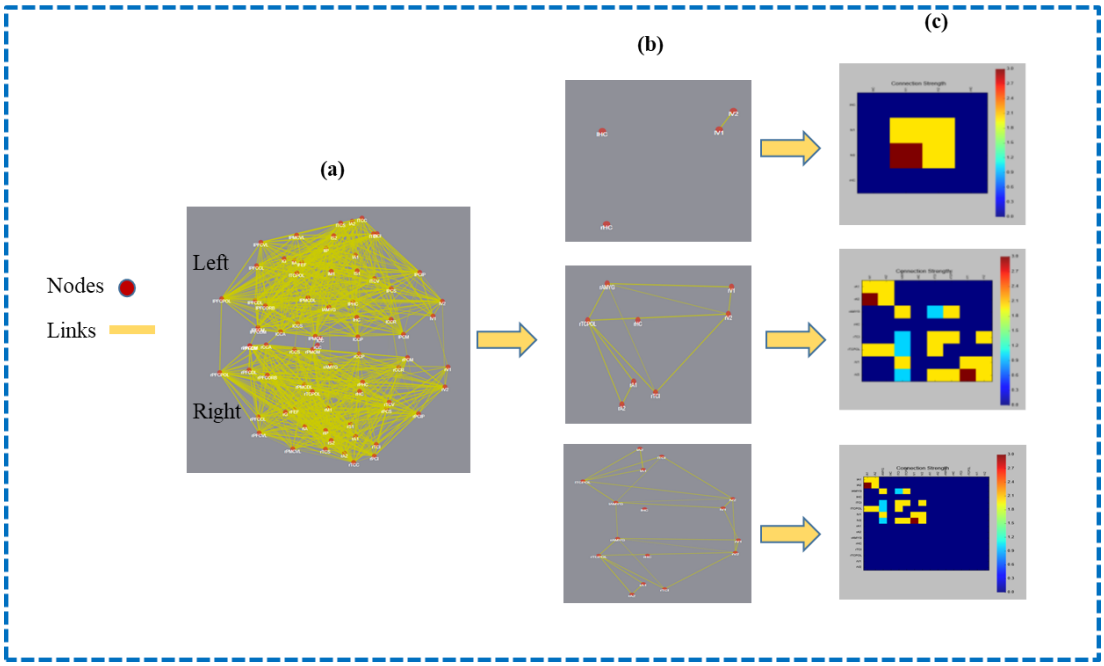

Figure 5.4: Structural connectivity utilized for building network models. (a) Default structural connectivity in TVB including a network of 76 cerebral areas (red circular nodes) and edges (yellow links). (b) From top to bottom structural connectivities between cerebral areas chosen from (a) comprising 4 cerebral areas (rHC, lV2, lV1, lHC) at different brain lobes and both hemispheres, 8 cerebral areas (rV2, rV1, rTCPol, rTCI, rHC, rAmgy, rA2, rA1) at the right hemisphere of different lobes, and 16 cerebral areas (rV2, rV1, rTCPol, rTCI, rHC, rAmgy,rA2, rA1, lV2, lV1, lTCPol, lTCI, lHC, lAmgy, lA2,lA1) at left and right hemispheres of different lobes. (c) From structural connectivities in (b), three connectivity matrices are built (respectively) that weight the strength of the connections between regions ranging from 0-3

5.2.2 Temporal dynamics of a network node: Stefanescu-Jirsa 2D model

The dynamics of the network model of *N* of nodes were defined using the Stefanescu-Jirsa 2D local model (S-J2D) (Stefanescu and Jirsa, 2008) which describes the complex dynamics of the neural population as a two-dimensional flow and also has a complex repertoire of dynamic oscillations. This S-J2D model was developed from the work of the FitzHugh-Nagumo model (FH-N) and is based on a heterogeneous network of coupling excitatory (E) and inhibitory (I) FH-N neurons (FitzHugh, 1961; Nagumoet al., 1962). The reduction of the network of the FH-N is undertaken using mode decomposition techniques (Assisi et al., 2005). The implementation of the local model started by defining the state variable (ST),x_i, y_i describing the dynamics

within the local area for the excitatory mass, while γ_i, $\theta_i$describes the dynamics within that area for the inhibitory mass. The *I* denotes the *i*-th mode, and *c, e, f, b* represent the constant parameters of the model. Coupling strengths between masses are given by S_{11}, S_{12}, *and* S_{21}. The following set of S-J2D equations that describe the dynamics of network node $f(x_i(t)) = f(x_i, y_i, \gamma_i, \theta_i)$ in Eq. (5.1) are given as follows:

$$\left.\begin{aligned} \dot{x}_i &= c\left(x_i - e_i\frac{x_i^3}{3} - y_i\right) + S_{11}\left(\sum_{r=1}^{3} A_{ir}x_r - x_i\right) - S_{12}\left(\sum_{r=1}^{3} B_{ir}\gamma_r - x_i\right) + cIE_i \quad (5.2)\\ \dot{y}_i &= \frac{(x_i - by_i + m_i)}{c} \quad (5.3)\end{aligned}\right\} \textit{For excitatory mass}$$

$$\left.\begin{aligned} \dot{\gamma}_i &= c\left(\gamma_i - f_i\frac{\gamma_i^3}{3} - \theta_i\right) + S_{21}\left(\sum_{r=1}^{3} C_{ir}x_r - \gamma_i\right) + cII_i \quad (5.4)\\ \dot{\theta}_i &= \frac{(\gamma_i - b\theta_i + n_i)}{c} \quad (5.5)\end{aligned}\right\} \textit{For inhibitory mass}$$

In accordance with current hypotheses, imbalance between excitatory and inhibitory couplings could be generating seizure signals, so we set different values of S_{11}, S_{12}, *and* S_{21} parameters and also parameter distribution (standard deviation of Gaussian distribution), while keeping other parameters with standard numerical values through different simulations. Table 5.2 shows the abbreviated description of the S-J2D model and its classical and adjusted values parameters utilized in our model.

Table 5.2**:** Abbreviated description of S-J2D model and its classical and adjusted values parameters utilized in our model

Derived model	**Neural mass (NM)**	**State variables (ST)**	**Modes (M)**	**Dimensionality of this model (D)**
FitzHugh-Nagumo model	2	2	3	12
Classical parameterised Stefanescu-Jirsa 2D model				
Parameters	**Value**	**Description of parameters**		
c	3	Time-scale separation		
a	0.45	Derived from FH-N model constants affecting faster ion channels		
b	0.9			
μ	0	Mean distribution of membrane excitability for the excitatory and inhibitory masses		
σ	0.35	Gaussian distribution of membrane excitability for the excitatory and inhibitory masses (standard deviation)		
II	Derived from σ & μ	Model excitability of each node and mode for inhibitory input		
IE	Derived from σ & μ	Model excitability of each node and mode for excitatory input		
x_i, y_i γ_i,θ_i	ST of excitatory mass ST of inhibitory mass			
S_{11} S_{12} S_{21}	0.5 Excitatory-excitatory Coupling strengths-between two masses 0.15 Excitatory-inhibitory Coupling strengths-between two masses 0.15 Inhibitory-excitatory Coupling strengths-between two masses			
Using adjusted parameters in our network model				
Parameters	**Value**			
S_{11}	0.2, 0.5, 0.7, 0.8, 0.97			
S_{12}	0.15, 0.2, 0.4, 0.5 , 0.8, 1.0			
S_{21}	0.15, 0.2, 0.22, 0.3, 0.38, 0.4, 0.95, 0.0.1			
σ	0,3,0.35,0.4,0.5			

5.2.3 Simulations

Figure 5.5 shows a typical flowchart for simulating three models with TVB platform using sequential steps. We started the simulations with BNM1, then BNM2 and finally BNM3; each fed with different inputs. As previously mentioned (see Subsection 5.2.1), each of these inputs was given two metrics, a weighted matrix- the connection strengths between regions and a delay matrix. At the beginning of a simulation, there were three inputs. If the model input consisted of its our own connectivity matrix (CM) of four cerebral areas at left and right hemispheres, the simulation of BNM1 was started and the input was then imported into TVB simulator. Afterwards, it was necessary to select a local model of S-J2D that describes brain dynamics within nodes (cerebral areas) with its original parameterisations in the first simulation.

The next step was to join the local dynamics of the S-J2D model over the connection between four areas by setting a long-range coupling function. In this simulation, the global coupling function of all simulations of the model was a linear function with a slope a = 0.00390625, with the conduction velocity for long-range connectivity for four areas of 3.0mm/ms. The system of difference equations of this model was then solved using stochastic Heun's method with an integration step size of 0.01220703125ms. Next, we used an EEG monitor to record the relevant data from the simulations with a sampling period of 1.0ms and then obtained the length of the simulation that ran a default value of 1000ms. Finally, we achieved the BNM1 output for the first simulation.

Our goal for the next simulation was to predict the most notable characteristics of the seizure dynamics. To do this, we repeated the sequential steps, but with the adjustment of some numerical values of the local S-J2D model. In this case, all parameters of the local model of S-J2D model kept numerical standard values except for the strength of coupling (S_{11}, S_{12}, *and* S_{21}) between the excitatory (E) and inhibitory (I) neurons and parameter distribution σ (see Table 5.2). Note that each simulation used one value of S_{11}, S_{12}, S_{21} and σ. After finishing all the simulations of BNM1 that represented the model outputs of BNM1, and then the second input of our BNM model began with the connectivity matrix (CM) of eight cerebral areas in the right hemisphere.

We carried out a set of simulations using the sequential steps above, but specifically varied the numerical values of each of the parameters of S_{11}, S_{12}, S_{21} and σ by a few percentages from those used in BNM 1. In the first simulation, we lowered the values of connection strength within excitatory to inhibitory subpopulations S_{12} and inhibitory to excitatory subpopulations S_{21} to be half their values rather than the values used in the BNM1, as displayed in Table 5. 2. If the simulation results of BNM2 were achieved (e.g. end-all of simulations related to BNM2), the third inputs of BNM3 that comprised 16 cerebral areas at both hemispheres were brought to TVB simulator, and repeat the simulations again.

These models were also built up based on procedures that had previously been performed, but there were differences in the step regarding the selection of the local model. We modified the values of coupling strength so they were higher values than the previous values used in each step, BNM1 and BNM2 during the first simulation. In addition, the long-range coupling function (used in this simulation) was set to a different function from that used in BNM1 and BNM2. In this case, the sigmoid coupling function was set with the maximum and minimum of the sigmoid function, and standard deviation of the sigmoid function at values of -1.0, 1.0 and 230.0, respectively. In the second simulation, other modifications of interest were done by setting the values of coupling strength lower than all simulations previously performed.

It must be noted that, for each simulation, we used the phase plane tool to ensure that the dynamics of the physical model of S-J2D were changed as a function of its parameters. Therefore, we determined and tuned the parameters that were used in each simulation before embedding a local model of S-J2D's model in the network. Figure 5.6 provides an example of the phase plane to the original and then adjustment of the parameterised S-J2D model in BNM3 used in the second simulation. Here, when we clicked on the point approximately (1, -1.5) for each case, the trajectories were sketched representing the state variables of the local model.

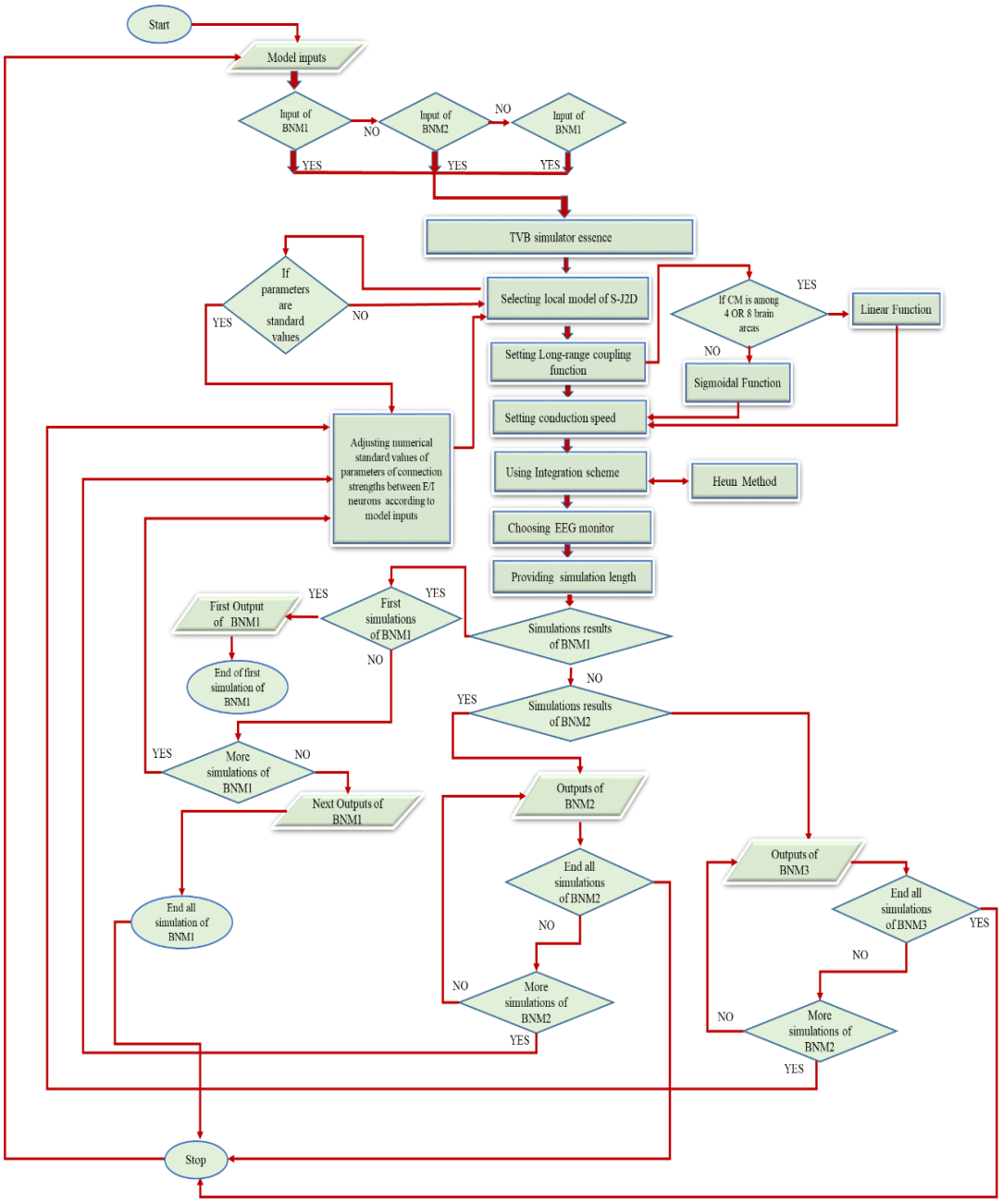

Figure 5.5: A typical flowchart for simulating three models BNM1, BNM2 and BNM3 with TVB platform using sequential steps

(a)

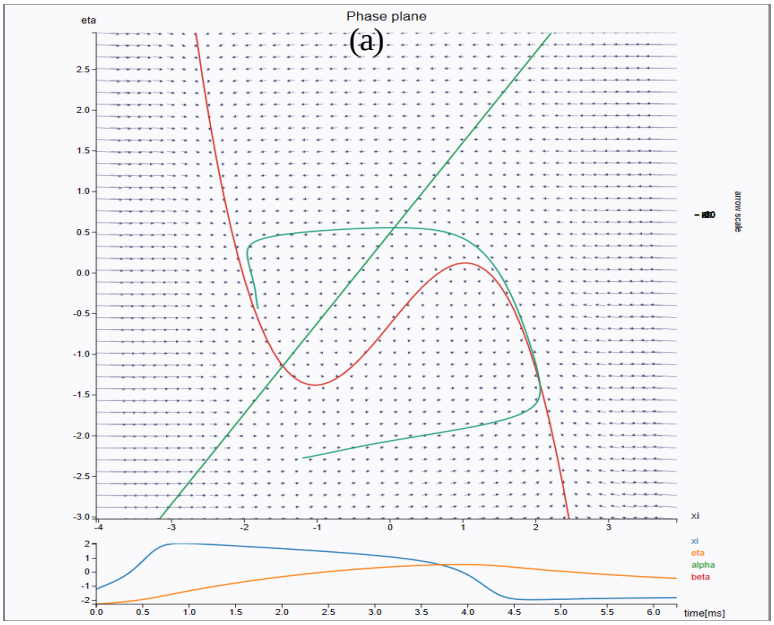

(b)

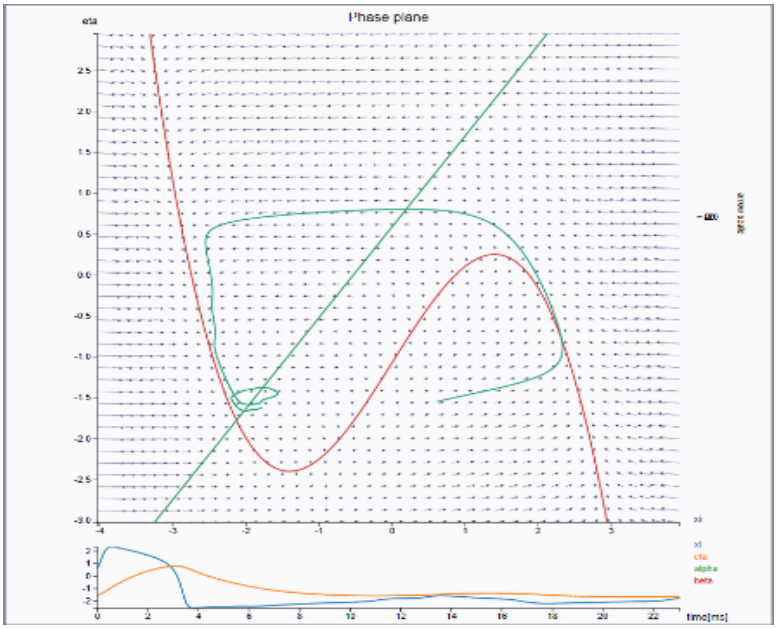

Figure 5.6: An example of phase plane to the original (a) and adjusted parameterised of S-J2D model (b)

5.3 Results and analysis

After carrying out the simulations using TVB platform, the results of each of BNM1, BNM2 and BNM3 were analysed using a wavelet spectrogram that is a suitable and powerful tool for evaluating the dominant frequency generated by network models. These results showed a number of predictions of seizure oscillatory morphologies which represent the general characteristics of seizure dynamics, and are summarised in Table 5.3.

To achieve a realistic model, we began our simulations by considering which areas of the brain might be involved in seizures and their anatomic locations, including the left and right cerebral hemispheres, and the lobes of the brain considering their known associations with the occurrence of seizures, as advised by International League against Epilepsy (ILAE) (Engel, 2001). The ILAE[11] has reported that possible seizure classifications could be based on anatomical locations. For instance, temporal lobe seizures most commonly begin in the temporal lobe that is located on the bottom section of the brain, comprising the primary and secondary auditory cortex (V1, V2) which have important functions for processing auditory information. Moreover, occipital lobe epilepsy is the most common issue affecting the occipital lobe.

5.3.1 Outputs of BNM1

In BNM1, the predicted outputs were based on the structural connectivity composed of four cerebral areas in the left and right hemispheres where the chosen areas depended on the locations that included roughly 50% from the occipital lobe and 50% from the temporal lobe (see Table 5.1). They were also based on modified biophysical model parameters of the neural mass of the S-J2D model. Our specific predictions were conditional on chosen parameters, especially for strength of coupling (S_{11}, S_{12},

[11]The 2017 ILAE Classification of Seizures Available: https://www.epilepsy.com/sites/core/files/atoms/files/Presentation%20Illustrating%20the%202017%20Classification%20of%20Seizure%20Types.pdf [Accessed 1.8.2018]

and S_{21}) between the excitatory (E) and inhibitory (I) neurons. Additionally, parameter distribution σ were achieved using several simulations.

In the first simulation, we set classical value parameters of the S-J2D model as given in Table 5.2. In this case, a normal oscillatory pattern that generated fast activity with low amplitude and high frequency (~100 Hz) emerged from each cerebral area in both hemispheres (rHC, lV2, lV1, lHC), unlike the abnormal EEG recordings which were characterized by abnormal patterns such as spikes with different shapes and sharp waves, Spike-and-Slow-Wave Complex and Polyspikes (clinical data of EEG; Chatrian, 1974; Barlow, 1993; Westmoreland et al., 1994; Westmoreland, 1996; Chang and Drislane, 2007; Jacobs et al., 2008, 2009, 2012; Mathews et al., 2015). Figure 5.7 depicts predicted time series of normal oscillation with frequency of ~100 Hz and the wavelet transform plot for this time series.

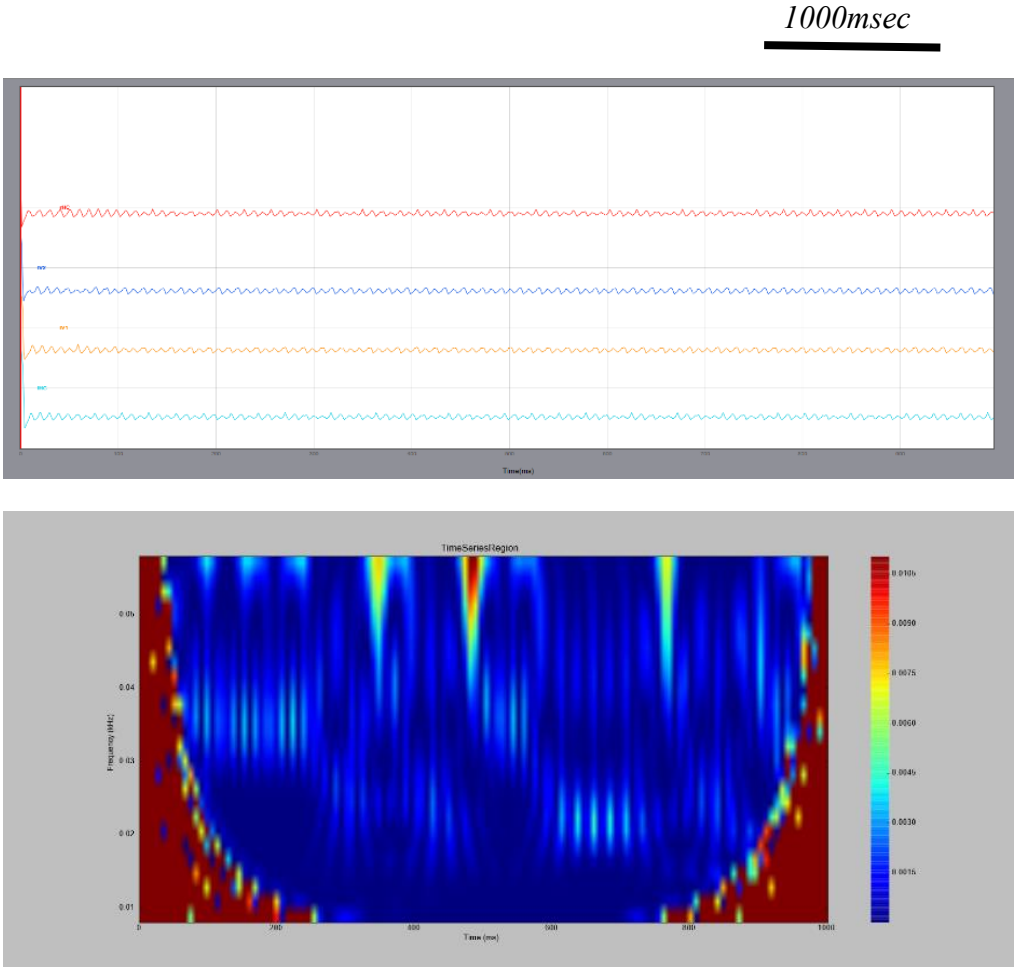

Figure 5.7: Prediction of normal oscillation with frequency of ~100 Hz. Top: Predicted time series using the classical parameterized S-J2D model for cerebral areas in both hemispheres (rHC: red, lV2: blue, lV1: yellow, lHC: green, respectively). Bottom: Wavelet transform plot

Our goal for the next simulations was to test whether we can predict most characteristics of the seizure dynamics. The dynamic features of this model were achieved by increasing and decreasing local parameters' values of connection strength within the excitatory subpopulations S_{11}, from excitatory to inhibitory subpopulations S_{12}, and from inhibitory to excitatory subpopulations S_{21}, in additional to parameter distribution σ, as in Table 5.2. Figure 5.8(a-d)-(a1-d1) illustrates the effects of the variation of parameter, S_{11}, S_{12}, S_{21} and σ, on BNM1 behaviour.

Firstly, this diagram shows that complex HFOs with irregular waves within the frequency range of ~117-125 Hz for each cerebral area in both hemispheres (rHC, lV2, lV1, lHC) were predicted, when we varied both parameters' values S_{11}, S_{12}, *and* S_{21} from 0.5, 0.15 , 0.15 to 0.2, 0.2 0.3, respectively. At the same time, the rest of the parameters' values set the same values. This type of HFO was composed of ripple waves (R) which included high and low amplitudes within the time window (1000msec), as depicted in Figure 5.8(a).

Secondly, by increasing the numerical values of both S_{11}, S_{12} and S_{21} to 0.8, 0.2 and 0.38, whilst the value of parameter distribution σ is decreased to, σ =3 while the settings of the other parameters are constant, two types of HFO rhythmic activity of BNM1 are generated. One type mainly consists of spike waves (SW) with large amplitude spikes at ~112 Hz and within the duration of 1000msec observed in rHC and lHC areas, while the other type generates a high amplitude of HFO in other regions (lV,lV2) bearing a striking similarity to quasi-sinusoidal activity (Q-S) at approximately ~ 94 Hz, as depicted in Figure 5.8(b).

Thirdly, another two classes of complex HFO appeared with regular and irregular oscillations. Oscillatory behaviour in this case depended on changing just two of the parameters' values of S_{21} and σ from 0.15 and 0.35 to 0.2 and 0.4. These classes occupied the poly 2 spike waves (p2SW) observed in rHC, lV2, lV1 with high amplitudes in the frequency above ~ 96 Hz along a fixed duration (1000msec), and the fast waves of continuous sharp spikes (SSW) were observed in lHC with low amplitudes and frequency ~ 109 Hz per 1000msec, as depicted in Figure 5.8(c). Interestingly, for increasing both $S_{11} = 0.8$ and $S_{12} = 0.8$ in of $S_{21} = 0.3$ higher than the default values of the local model, fast HFOs with regular waves in the peak frequency in the ~130 Hz per 1000mesc were predicted. These fast HFOs reflected high

amplitudes of continuous spike-wave activity (S-W) that are observed in each brain area (rHC, lV2, lV1, lHC), as depicted in Figure 5.8(d).

These predictions of different types of complex HFOs produced by BNM1 with a frequency of ~ 94-130 Hz were analysed as valid using WT (see Figure 5.8(a1-d1)

5.3: Summary of simulations results produced by BNM1, BNM2 and BNM3

	Adjusted parameters of S-J2D model in this study	Oscillatory wave	Frequency Oscillations	Amplitude	Morphology	Window
BNM_1	S_{11}=*0.2*,S_{12}=*0.2*,S_{21}=*0.3* and σ =*0.35*	Complex HFO with irregular waves	~ 117-125 Hz	High and low amplitudes	Ripple waves	1000msec
	S_{11}=*0.8*,S_{12}=*0.2*,S_{21}=*0.38* and σ =*0.3*	Complex HFO with regular and irregular waves	~94-112 Hz	High and low amplitudes	Spike waves Quasi-sinusoidal waves	100-1000msec 100-1000msec
	S_{11}=0.5,S_{12}=0.15,S_{21}=0.2 and σ =0.4	Complex HFO with regular and irregular waves	~ 96 Hz ~109 Hz	High amplitudes High and low amplitudes	Poly 2 spike waves Continuous sharp spikes	100-700msec 1000mesc
	S_{11}=0.8,S_{12}=0.8,S_{21}=0.3 and σ =0.4	Complex HFO with regular	~130 Hz	High amplitudes	Spike and wave	100-1000msec

BNM2	S_{11}=0.2,S_{12}=0.2,S_{21}=0.22 and σ =0.4	Complex HFO with irregular waves	~121 Hz	High and low amplitudes	Ripple on spikes waves	100-1000msec 450-625msec
	S_{11}=0.8,S_{12}=0.4,S_{21}=0.15 and σ =0.4	Complex HFO with regular waves	~115 Hz	High amplitudes	Spike and waves	100-1000msec 400msec
	S_{11}=0.7,S_{12}=0.5,S_{21}=0.95 and σ =0.35	Complex HFO with irregular waves	~144 Hz	High and low amplitudes	Continuous spike	1000msec
	S_{11}=0.8,S_{12}=0.2,S_{21}=0.1 and σ =0.3	Complex HFO with irregular waves	~ 96 Hz	High and low amplitudes	Sporadic spikes	1000msec
BNM3	S_{11}=0.97,S_{12}=0.2,S_{21}=0.4 and σ =0.5	Complex HFO with regular and irregular waves	~104-124 Hz	High amplitudes	Sustained spikes wave discharges irregular spiking	1000msec
	S_{11}=0.97,S_{12}=1.0,S_{21}=0.1 and σ =0.5	Complex HFO with regular and irregular waves	~110 Hz ~104 Hz	Highly varying amplitudes	Regular spike and waves Irregular spike and waves	1000msec

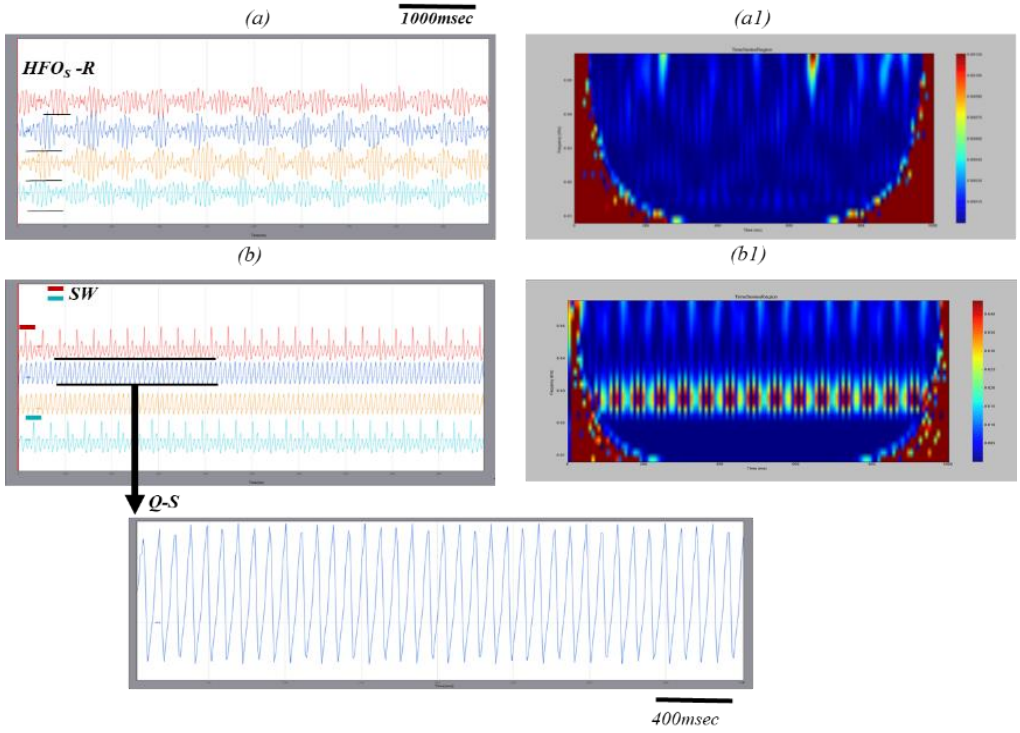
(a)
1000msec
(a1)
HFO$_S$ -R
(b)
(b1)
SW
Q-S
400msec

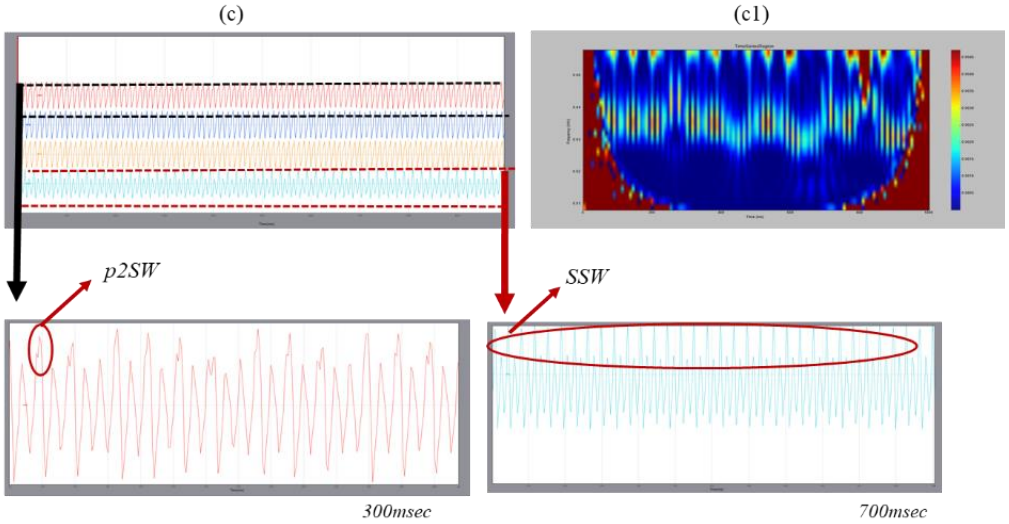
(c)
(c1)
p2SW
SSW
300msec
700msec

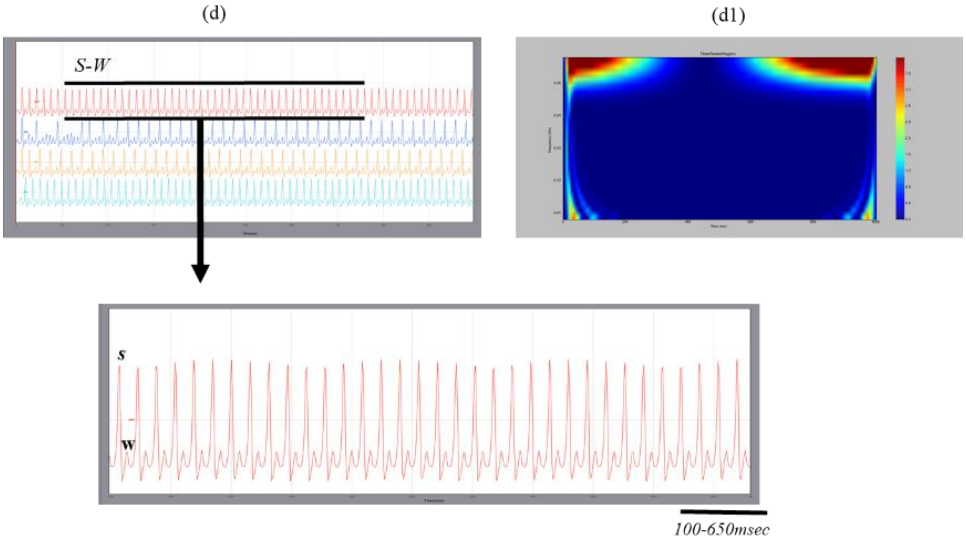

Figure 5.8: (a-d) Prediction of different types of complex HFOs produced by BNM1 with frequency of ~ 94-130 Hz when the numerical values of S_{11}, S_{12},, S_{21} and σ of S-J2D model parametres are altered. (a) Predictions of time series of HFOs as ripple (R) for cerebral areas in both hemispheres (rHC: red, lV2: blue, lV1: yellow, lHC: green, respectively). (b) Predictions of time series of HFOs as spike (SW) for two areas (rHC: red, lHC: green) and quasi-sinusoidal (Q-S) for lV2: blue, see zooming at 400msec and lV1: yellow). (c) Predictions of time series of HFOs as ploy2 spike (p2SW) for areas (rHC: red, lV2: blue and lV1: yellow, see zooming for rHC at 300msec) and sharp spike for area in the left (lHC: green, see zooming at 700msec). (d) Predictions of time series of HFOs as spike-wave for each areas in both hemispheres (rHC: red, lV2: blue, lV1: yellow, lHC: green, see zooming at 100-650msec). (a1)-(d1): wavelet transform plot for each times series produced by BNM1

5.3.2 Outputs of BNM2

The structural connectivity of BNM2 used in this model included eight cerebral areas in the right hemisphere where the cerebral areas were chosen roughly 25% from the occipital lobe and 75% from the temporal lobe (see Table 5. 1). Depending on the same technique used in BNM1, including variations of the biophysical model parameters of the local model were utilised in the previous simulations (see specific part of BNM2 listed in Table 5.3), various shapes of HFOS were predicted. Figure 5.9(a-f)-(a1-f1) illustrate the influence of the change of some numerical parameter values of the S-J2D model on BNM2 behaviour.

To predict these different shapes of HFOs, we did several simulations; each utilised some parameters of the S-J2D model which were quite different from the parameters used in the original model and BNM1. In the first simulation, we hypothesised

decreasing the values of connection strength within the inhibitory to excitatory subpopulations S_{21} to 0.22 and increasing parameter distribution σ to 0.4 (more than the values used in BNM1), while the other parameter values were kept constant, as in the first simulation of BNM1. In this case, we noted the generation of ripples on spikes (SR) of HFOs that had regular and irregular waves within the frequency of ~121 Hz for each cerebral area (rV2, rV1, rTCPol, rTCI, rHC, rAmgy, rA2, rA1, respectively) in the right hemisphere and different lobes including higher and low amplitudes within the time window (1000msec). Interestingly, we found that the amplitude, number and frequency ripples output from BNM2 (see zooming on rTCPol observed in Figure8 (a, bottom)) were higher compared with BNM1ripples (see zooming on lV1observed in Figure8 (b, bottom)), especially in the duration between 450 and 625msec. In the second simulation, we presumed that that there would be an effect of lowering both of the values of connection strength within excitatory to inhibitory subpopulations *S12* and inhibitory to excitatory subpopulations *S21*. The lower value was half the values used in the BNM1 through the last simulation (S_{12} from 0.8 to 0.4 and S_{21} from 0.3 to 0.15, see Table 5.3, BNM1-- the fourth box of parameters of the S-J2D model) whilst keeping the other parameters at the same values as used in the BNM1. This simulation predicted diverse S-W of complex HROs that had regular and irregular waves within the frequency range of ~115 Hz. We observed the production of a spike of higher amplitude immediately followed by a different number and frequency with low amplitude. For example, the cerebral area (rV2) had irregular sharp spikes followed by around 15, 2, 6, 5 and 3 Hz (see Figure8 (c, bottom)) whereas, lV1 (in the BNM1) had a regular and continuous S-W-one sharp spike followed by 2Hz (see Figure 5.9 (d). In the third simulations, clear transient of continuous spikes can also be observed by varying just the values of S_{11}, S_{12}, S_{21} to 0.7, 0.5 and 0.95 (increased with S_{21} more than its values used in the BNM1) for eight brain areas in the right hemisphere. This pattern was characterised by continuous spikes of regular waves of complex HFO (~144 Hz) at the time window (1000msec), as depicted in Figure5.9 (e).

In the final simulation, a spontaneous transition to the other epileptic type occurred when the values of S_{11}, S_{12}, S_{21} and σ were adjusted to 0.8, 0.2, 0.1 and 0.3 (strongly deceased with S_{21} when its values used the original model in the BNM1). This type could be called sporadic spikes which have complex HFO (~96Hz) at period 1000msec, as can be seen in Figure 5.9(f).

These predictions of HFOs produced by BNM2 with frequency of ~ 96-144 Hz were analysed using WT for each of these time series (see Figure 5.9(a1-f1)).

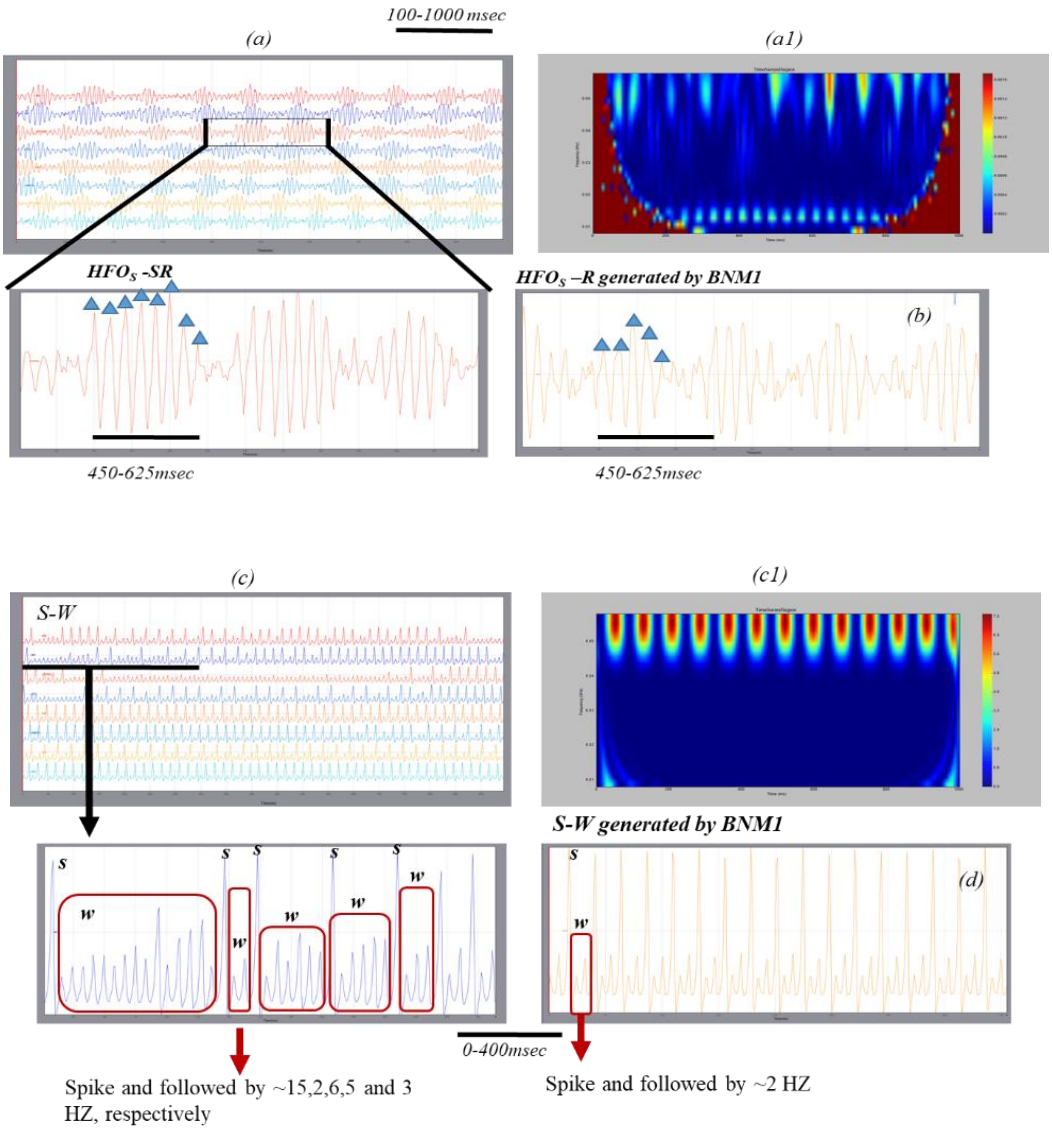

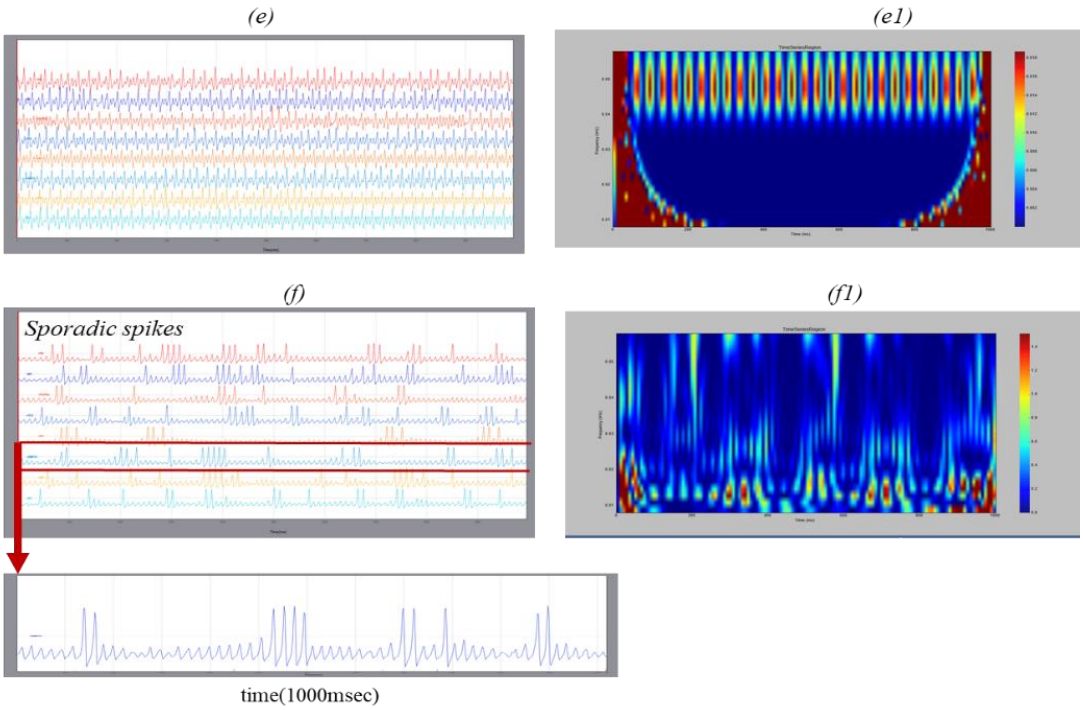

Figure 5.9 : (a-f) Prediction of different shapes of complex HFOs produced by BNM2 with frequency of ~ 96-144 Hz by increasing and decreasing values of S_{11}, S_{12}, S_{21} and σ compared to those used in BNM1. (a) Predictions of time series of sharp wave ripples on spikes (SR) for each cerebral area (rV2: dark red, rV1: dark blue, rTCPol: light red, rTCI: light blue, rHC: orange, rAmgy: blue, rA2: yellow, rA1: green, respectively) in the right hemisphere and produced in different lobes. (a,bottom) Example of generation of higher amplitude, number and frequency (SR) outputting from right rTCPol in the BNM2 compared with ripples of BNM1(see Figure 5.8(a)), especially in the duration between 450 and 625msec observed in left lV1 in the BNM1 (b). (c) Predictions of time series of spike with higher amplitude followed by different number and frequency with low amplitude for each cerebral area (rV2: dark red, rV1: dark blue, rTCPol: light red, rTCI: light blue , rHC: orange, rAmgy: blue, rA2: yellow, rA1: green, respectively). (c, bottom) Example of generating S-W with higher amplitude followed by around 15, 2, 6, 5, and 3 Hz outputting from right left lV1 in the BNM2 compared with S-W of BNM1 especially in duration (400msec) observed in right rV1 in the BNM1(d). (e) Predictions of time series of continuous spike for 8 brain areas in the right hemisphere area (rV2: dark red, rV1: dark blue, rTCPol: light red, rTCI:light blue, rHC: orange , rAmgy: blue , rA2: yellow, rA1:green, respectively. (f) Predictions of time series of sporadic spikes for 8 brain areas in the right hemisphere area (rV2: dark red, rV1: dark blue, rTCPol: light red, rTCI:light blue, rHC: orange, rAmgy: blue, rA2: yellow, rA1:green, respectively. (a1- f1) Wavelet transform plot time series for each times series produced by BNM2

5.3.3 Outputs of BNM3

From the experimental results of BNM3, we noticed that the effect of varying maximum coupling strength of S_{11}, S_{12}, and σ were more significantly than that in the BNM1 and BNM2 (see Table 5.3, BNM3-- the box of parameters of S-J2D model),

can predict other abnormal patterns as recorded during epileptic seizures. In addition new morphologies of HFOs were different from those in BNM2 and BNM3. Starting from this point, the parameter values of S_{11} and σ corresponding to the original values (S_{11}= 0.5, σ =0.35) were adjusted higher in values during the first simulation. S_{11} was increased to 0.97 and σ to 0.5 while S_{12} was slightly increased from its numerical standard value (from 0.15 to 0.2) and S_{21} was changed to 0.4, producing HFO (~104-124 Hz) of sustained spike wave discharges (SWD) with regular waves at around a time of 1000msec for the eight cerebral areas in the right hemisphere (rV2, rV1, rTCPol, rTCI, rHC, rAmgy, rA2, rA1). In addition, irregular spiking oscillations were produced but for eight cerebral areas in the left hemisphere (lV2,lV1,lTCPol,lTCI,lHC,lAmgy,lA2,lA1) with higher–amplitude spiking activities, as depicted in Figure 5.10 (a). However, the next simulation, when S_{12} was increased more than in BNM1 and BNM2, keeping both S_{11} and σ at the same values in the first simulation, we found that BNM3 can predict different morphologies of spike and wave than those observed in BNM1and BNM2. One of the wave shapes was a regular sequence of spikes and waves (~110 Hz) for the eight cerebral areas in the right hemisphere (rV2, rV1, rTCPol, rTCI, rHC, rAmgy, rA2, rA1) but the second shape comprised irregular waves (~104 Hz) that began with a different number of spikes and which were immediately followed by two slow waves for the eight cerebral areas in the left hemisphere (lV2, lV1, lTCPol, lTCI, lHC, lAmgy, lA2, lA1). All of these oscillations were complex HFOs with highly varying amplitudes within the time window (1000msec), as depicted in Figure 5.10 (b).

Again, new morphologies of complex HFOs produced by BNM3 with a frequency of ~ 104-124 Hz were analysed using WT for each of these time series (see Figure 5.10(a1- b1)).

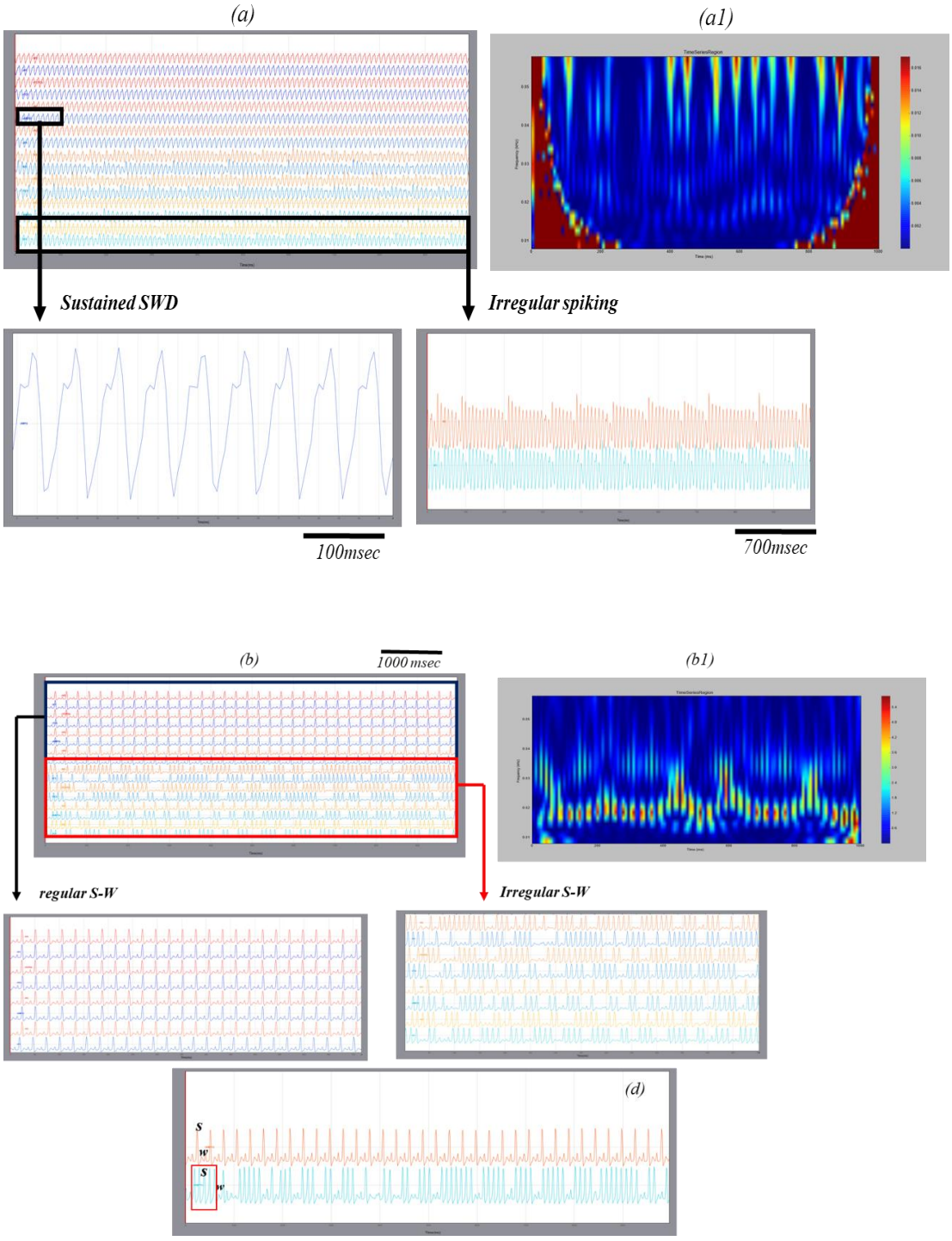

Figure 5.10: (a-b) Prediction of other abnormal patterns as recorded during epileptic seizures and new morphologies of complex HFOs produced by BNM3 with frequency of ~ 104-124 Hz dependeding on an increase both of S_{11} and σ greater than in the BNM1 and BNM2 (a) predictions of time series of sustained SWD observed in eight right areas (rV2: red, rV1: blue, rTCPol: red, rTCI: blue, rHC: red, rAmgy: blue, A2: red, rA1:green, respectively), and irregular spiking oscillations observed in left areas (lV2: red, lV1: blue, lTCPol: red, lTCI:

blue, lHC: light red, lAmgy: light blue, lA2: orange lA1, respectively) (a, bottom, left). Zooming on sustained SWD within the period of time (100msec) for area rAmgy in the right hemispheres (a, bottom, right). Zooming on irregular spiking oscillations within a period of time (700msec) for two areas in the left lA2, lA1. (b) Predictions of time series of different morphologies of S-W. (b, bottom, left) Zooming on regular S-W for 8 areas in the right areas (rV2: red, rV1: blue, rTCPol: red, rTCI: blue, rHC: red, rAmgy: blue, rA2: red, rA1:green, respectively). (b, bottom, right) Zooming on irregular S-W for 8 areas in the left hemisphere lV2: red, lV1: blue, lTCPol:red, lTCI: blue, lHC: light red, lAmgy: light blue, lA2: orange, lA1, respectively). (d) Zooming on two areas rAmgy at right hemisphere and lAmgy at left hemisphere as compared with them through the different number of spikes and waves. (a1- b1) Wavelet transform plot time series for each times series produced by BNM3

5.4 Comparisons

To evaluate the proposed network models, we made two kinds of comparisons. First, our data generated by these models, BNM1, BNM2 and BNM3 were compared with epileptiform abnormal patterns in the EEG. Second, model outputs that represented simulated oscillatory activities were compared with other models.

5.4.1 Comparison with epileptiform abnormal patterns in EEG

Investigations were made between the simulated results and the epileptiform abnormal patterns in the EEG in terms of EEG morphology of epileptic seizures and frequency. From the results produced by BNM1, BNM2 and BNM3 (see brain areas rHC and lHC brain areas in Figure 5. 8(b-SW) and lHC in Figure 5.8(c-SSW)), Figure 5. 9(e-continuous spikes) as well as areas in lA2and lA1in Figure 5.10(a- Irregular spiking oscillations), it can be noticed that, in a fast appearing oscillatory pattern, so-called spikes due to their wave shape on the EEG and in additional by definition, have a duration less than 70ms (from 20-70ms), and bore a striking similarity to epileptiform spikes according to the Mayo Clinic for medical education and research and experimental studies specialising in the field of epilepsy (Westmoreland et al., 1994; Chatrian,1974; Barlow, 1993; Westmoreland, 1996; Noachtar et al. 2004; chang and Drislane, 2007; Jacobs et al., 2008, 2009, 2012; Mathews et al., 2015). Another effective way to verify simulated spikes is by comparing them with real EEG data for morphological similarity between them. Interestingly, we observed that the frequent

repetitive spikes, so called continuous spikes produced by BNM2, were quite similar to continuous spike discharges recorded in EEGs in a patient with generalized tonic-clonic status epilepticus (see Figure 5.11). Further investigation was made in terms of the HFO (>80 Hz) with ripples on spikes recorded from EEG which could be novel markers of the epileptogenic zone. Based on the studies of Jacobs et al. (2008, 2009, 2012), we found these types of ripples on spikes in the outputs produced by BNM1 (Figure5. 8(a-HFO-R)) and BNM2 (Figure 5.9(a-HFO-R)) that had a frequency above 80Hz (see Results section, HFO was identified in the frequency range ~117-125 Hz at1000msec).

To prove the point more clearly in this case, we compared simulated ripples. For example, BNM1 produced ripples on epileptic spikes through the wave shape (see Figure 5.12). Next, we found that our results were characterized by spikes followed immediately by one slow wave or complex waves (see Figure 5.8(d-S-W). Figure 5.9(c-S-W) and Figure 5.10(b) were morphologically similar to that description and an interpretation of the EEG that was reported by the literature (Chatrian, 1974; Gloor, 1977; Westmoreland, 1996; Noachtar et al. 2004; Avoli, 2012; Seneviratne et al., 2012). This EEG clinical interpretation was given in light of the diagnosis and the questions of the physician. Figure 5.13 showed the similarity between EEG tracings of spike epileptiform discharges and was followed immediately by one slow wave, e.g., produced by BNM1.

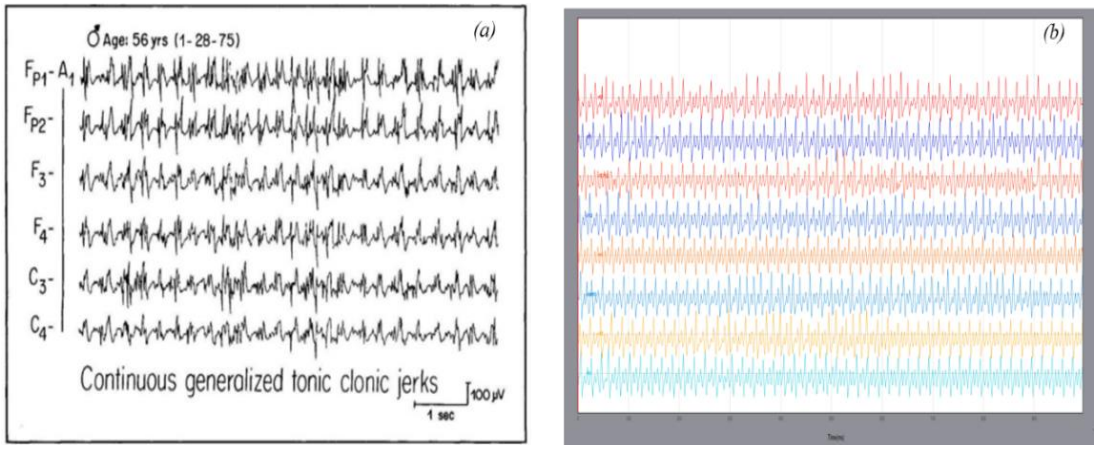

Figure 5.11: (a) Example of electroencephalographic tracings of the patient with generalized tonic-clonic status epilepticus, showing continuous spike discharges (Figure7, Westmoreland et al., 1994). (b) Simulated continuous spike produced by BNM2 (Figure 5. 9 (e))

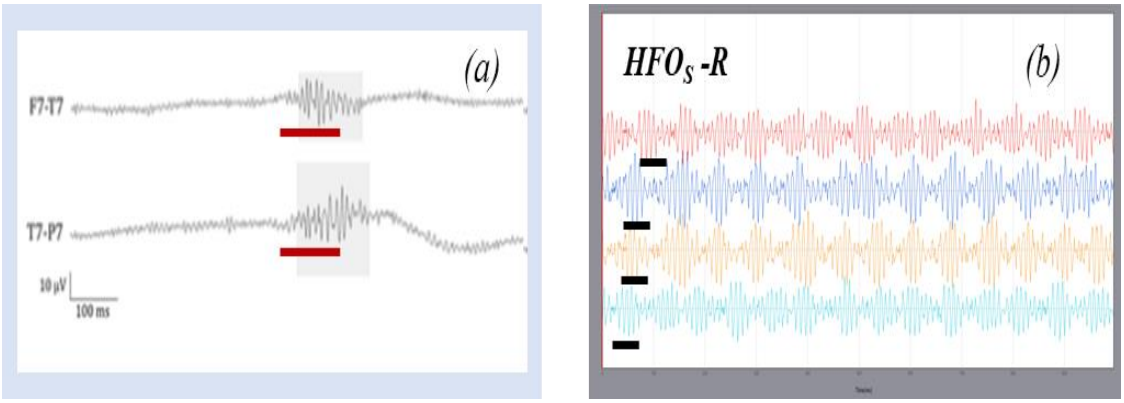

Figure 5.12: (a) Examples of ripples on epileptic spikes marked in study (Mooij et al., 2017, see Figure2). (b) Simulated ripples on spikes produced by BNM1 (Figure 5.8(a))

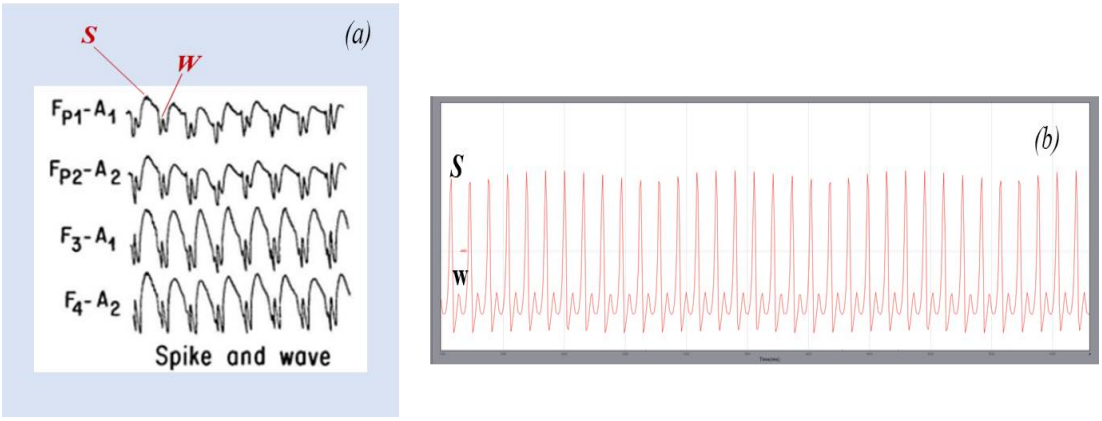

Figure 5.13: (a) Example of electroencephalographic tracings of spike and wave epileptiform discharges (Figure 1, Westmoreland et al., 1994). (b) Simulated spike and wave produced by BNM1(Figure 5.8(d, bottom)

5.4.2 Comparison with other computational models

Next, we compared our simulated models to the Wendling models (Wendling et al., 2000, 2002) which have been used extensively as the comparative study due to their simulation of very realistic activities, and also compared with the previous study (Blenkinsop et al., 2012).

The evaluation between our simulated results and the results of Wendling et al. was under a similar hypothesis, i.e., epileptic activities may generate a network consisting

of coupled neural populations (multiple neural populations). Each area in our models was composed of globally coupled both excitatory (E) and inhibitory (I) populations (see Section 5.2.2). For the results obtained from BNM1 (Figure 5.8(b, bottom)), we observed similarity to Type 6 that referred to slow quasi-sinusoidal activity produced by the Wendling model (Wendling, et al., 2002) that was compared with the real depth EEG recording, as shown in Figure 5.14. As well, comparing Figure 5.8(c, bottom) with the previous study (Blenkinsop et al., 2012), its results were compared with a real clinical iEEG of temporal lobe epilepsy, and it was noticed that a run of two spikes followed by a wave, so-called polyspikes, could have the same form as shown in Figure 5.15.

For the results obtained from the BNM2 (Figure 5.9(f)) example in the right brain area, Amygdala (rAmgy), we also noticed sporadic spikes like those reproduced by Wendling et al. (2000), as shown in Figure 5.16. Finally, for the results obtained from BNM3 (Figure 5.10(a, bottom)), as exemplified in the rAmgy, one can also observe that the Type 3 simulated by Wendling et al. (2002) was quite accurately simulated by this model, as shown in Figure 5.17.

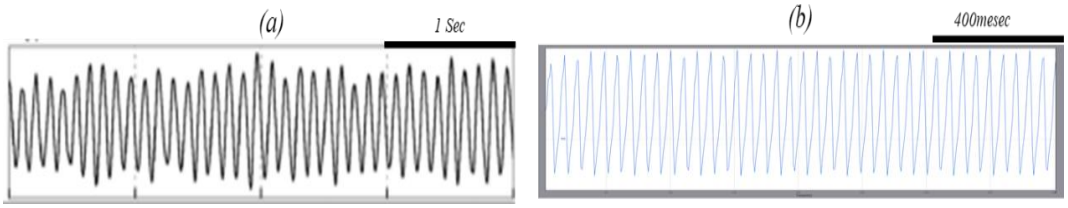

Figure 5.14: (a) Type 6 that was referred to as slow quasi-sinusoidal activity produced by model of Wendling et al. (Wendling et al., 2000) (b) Simulated Q-S produced by BNM1 (Figure 5.8(b, bottom))

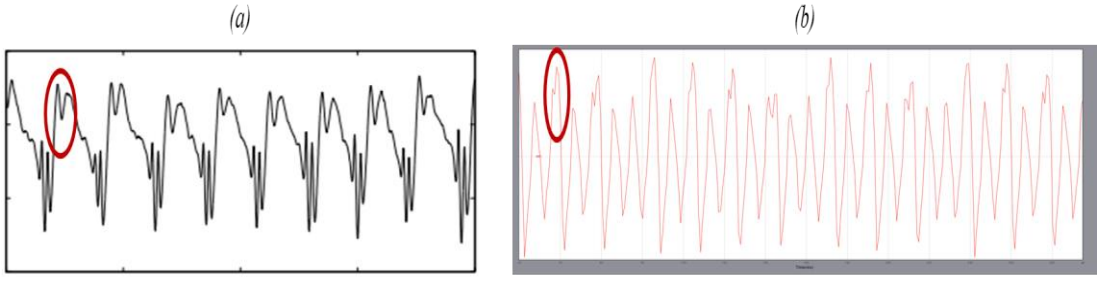

Figure 5. 15: (a) Two spikes followed by a wave produced by Blenkinsop et al. (2012). (b) Simulated p2SW produced by BNM1 (Figure 5.8 (c, bottom))

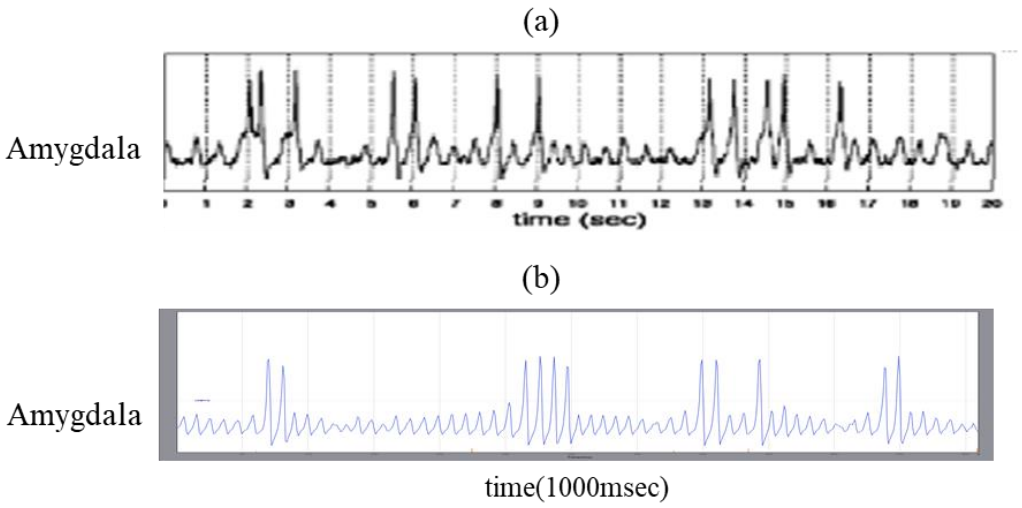

Figure 5.16: (a) Sporadic spikes reproduced by Wendling et al., (2000), see Figure 6(c, top). (b) Simulated sporadic spikes produced by BNM2 (Figure 5.9(f, bottom))

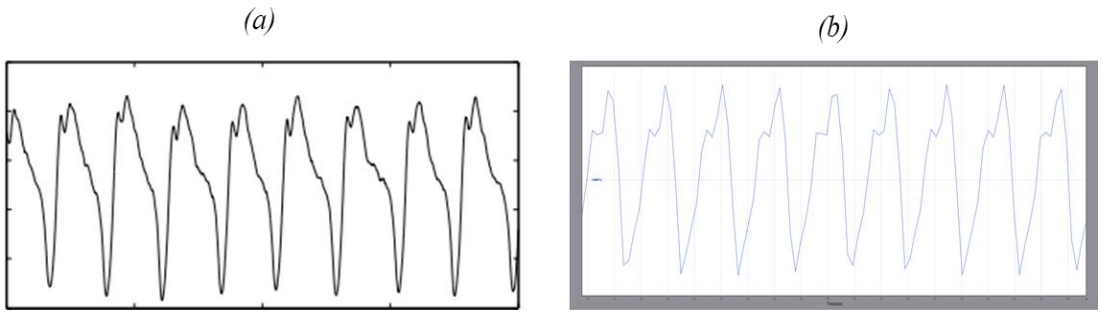

Figure 5.17: (a) Type 3 that was referred to sustained spikes wave discharges reproduced by Wendling et al. (2002). (b) Simulated sustained SWD was produced by BNM3 (Figure 5.10(a, bottom))

5.5 Perspectives and limitations of the present study

Based on the available literature, neither experimental studies nor computational models address HFOs in multiple frequency ranges (~ 94-144 Hz) within the limited time window (1000msec) generated in this study, as seen in Table 5.3. From this insight, we conclude that these oscillations could be considered to be new morphologies of HFO and may be included in the classification of seizures for identification of epileptiform abnormal waveforms. Moreover, according to the

classification of seizures made by the Commission on Classification and Terminology of the International League Against Epilepsy (1981), the Commission on Classification and Terminology of the International League Against Epilepsy 1989 ; Engel, 2001), epileptic seizures are generally classified into two categories: focal and generalized seizures. Focal seizures start in one hemisphere of brain, while, generalized seizures start in both hemispheres of the brain. From this point, we can classify our models into both categories which are verified (see Section 5.4): the focal seizures model generates patterns of epileptic seizures in part of the brain (left or right hemisphere), whereas BNM1 and BNM3 can be called generalized models because they generate epileptic seizure patterns in both hemispheres of the brain (see Section 5.2.1 and Table 5.1). This study is dependent on the concept of making the imbalance strengths of coupling between the excitatory and inhibitory populations for a local mass model through highly/slightly increased and deceased parameters. From this concept, we conclude that these parameters of coupling strengths are quite sensitive when there are variations of a few percentages as explained in the results, thus these results can be used as guidelines (see, the summary in Table 5.3) to help researchers and physicians to understand and study these types of activities.

Large-scale neural predication models that predict large-scale neural activity, can be conditioned on the choice of parameters (see the excellent review of Breakspear (2017). It is likely that model parameters, whether local or global, can have effects on the behaviour of our model. In all simulations of our models, we set a long-range coupling function that is a linear function with a slope that has very small values (see Section 5.2.3). However, when setting this slope with a large value, as used in this study, we noticed a ceasing of neural oscillations in some brain areas.

5.6 Conclusions

Simulations and evaluations of abnormal patterns of brain activities were made by developing three BNMs: BNM1, BNM2 and BNM3 at different scale. Each of them is modelled by combining the NMM with the realistic biological data connectome that is used for the structural layout of our BNMs derived from hybrid data from DSI data and the CoCoMac database. The local network of the NMM of S-J 2D is used to

describe the temporal dynamics of a network node (ie. cerebral areas). In particular, we investigated how to adjust the connections strength between the inhibitory and excitatory neurons of the local model to predict different morphology patterns. BNM1 predicts HFOs that occupied the ripples on spikes (~117-125 Hz), spikes and quasi-sinusoidal waves (~94-11 2Hz), ploy2 spikes (~96), continuous sharp spikes (~109Hz) and spikes and wave (~130 Hz). BNM2 predicts other patterns of complex HFOs with different frequencies such as sharp ripples (~121 Hz), spikes and waves (~115Hz), continuous spikes (~144 Hz) and sporadic spikes (~96 Hz), while BNM3 also predicts morphologies of HFO as a sustained spikes wave discharges irregular spiking with a range of (~104-124 Hz) and regular and irregular spike and waves at range of (~104-110 Hz).

These models are verified by comparing them with epileptiform abnormal patterns in EEGs and other computational models. The simulation of each model was performed on the basis of the unique platform, The Virtual Brain. The significance of the network models is that they can assist researchers and clinical doctors in the epilepsy field to understand the complex neural mechanisms of abnormal oscillatory activity generation and, thus, may open up avenues towards the discovery of new clinical interventions related to these types of activities. Moreover, they point out the potential of TVB to identify epilepsy biomarkers and, thus, will attract further attention over years to come.

The contents of this chapter have been submitted for publication to the Journal of Expert Systems with Application on 2020.

CHAPTER 6

CONCLUSIONS AND FUTURE DIRECTIONS

With the availability of realistic biological data, the so-called connectome of human brain regions, a new type of network model of human brain has emerged such as the BNM or LSBNM. This type of brain model leads to systematic approximations of the neural field, and possesses a significant number of parameters governing its structure. These parameters are represented by a long-range connections between brain regions (global parameter) and dynamic activity that is generated from NMMs occurs at the local level.

In this project, we developed brain network models at multi-scales to include novel network structures of the human brain to investigate how local and global parameters affect the proposed network models' behaviour and corresponding EEG patterns for healthy and disease states. This thesis describes the work we carried out in order to address the main contributions.

6.1 Main Contributions

1. A LSBNM was developed to include four human cerebral areas at the left hemisphere of different brain lobes by:

    a. Building a connectivity matrix representing the connection strength between four brain regions
    b. Investigating the embedding of the oscillator JR model of a single cortical region in its original parameters with the connectivity matrix to generate EEG patterns for health: alpha rhythms within a low frequency at 7Hz

c. Analysing and validating model outputs represented in time series using fast Fourier transforms for four brain areas.

2. Extending this network model to include six cerebral areas was carried out by:
    a. Building a connectivity matrix to determine the coupling strengths between six areas and consider time-delay in this extended network model
    b. Modifying the parameters of the JR model, especially with the synaptic gains represented by *A* parameter
    c. Linking modified parameters of *A* with the connectivity matrix via specific connections and time delays between the six areas to simulate multi-patterns, the alpha band of EEG rhythms at different ranges of frequencies 7–8 Hz, 8–9 Hz and 10–11 Hz
    d. Validating the extended model outputs using FFT.
3. A new network model for simulating multi-bands of EEG patterns: delta–range frequency of (1-4 Hz), theta at a frequency of (4-7Hz) and diverse narrowband oscillations ranging from delta to theta (0-5Hz) were constructed by:
    a. Building two metrics representing the coupling strengths and time delay between eight cerebral areas at various brain lobes in the left hemisphere
    b. Further modifying on JR equations to include new values for interconnected excitatory and inhibitory populations of JR model, especially the maximum amplitude of the excitatory and other inhibitory neurons (*A and B*) as well as the time constant of excitatory and inhibitory neurons (*a and b)*
    c. Using different global coupling with modification values that join the local dynamics of the JR model to transform the neural activity from source areas into target areas
    d. Analysing the simulated time series representing multi-bands of EEG patterns for validation is accomplished using WT.

4. Novel BNM at different scales to simulate and predict the EEG epileptic patterns were developed by:

a. Building three connectivity matrices. The first determines the coupling strengths and time delay between four cerebral areas at left and right hemispheres, including area roughly 50% from the occipital lobe and 50% from the temporal lobe. The second determines the coupling strengths and time delay between eight cerebral areas in the right hemisphere, including areas sites roughly 25% from the occipital lobe and 75% from the temporal lobe. The third determines the coupling strengths and time delay between 16 cerebral areas in the left and right hemispheres, including area sites roughly 50% from the occipital lobe and 50% from the temporal lobe
b. Adjusting some parameters of S-J2D's model to include new values, especially the strength of coupling (S_{11}, S_{12}, *and* S_{21}) between excitatory (E) and inhibitory (I) neurons and also parameter distribution σ
c. Simulating different morphology patterns of abnormal EEEs such as ripples on spikes, spikes, continuous spikes, sporadic spikes and ploy2 spikes ranging from 94 to 144 Hz
d. Analysing network models' outputs using WT
e. Comparing different morphology patterns of abnormality generated from novel BNMs with epileptiform abnormal pattern obtained in real EEG and other computational models.

6.2 Limitations and future directions

Future research can be done to facilitate further developments of the proposed network models by considering the following points.

Firstly, this study explained that our large-scale neural models predicting large-scale neural activity, can be conditioned with the choice of parameters. It is likely that model parameters, whether local or global, can have effects on the behaviour of network

models similar to those of Chapter 5 which predicted the EEG epileptic patterns. To go further in this direction, intensive study of both of these parameters could lead to further predictions of special EEG signals such as those associated with anaesthetic, sleep, etc.

Second, the JR model of a single cortical column that we in Chapters 3 and 4 can be extended. Further research in this direction can be done by expanding into coupling two columns (double-column) of the JR model. In this way it would determine the strength of the connection between columns by adding a time delay between neurons. To the best of our knowledge, this method has not yet been used to model the brain network at multi-scale. The proposed network model will incorporate the extended local JR model using the original parameters or the modified parameters from Chapters 3 or 4, and own structural connectivity. In this case, we would use bifurcation analysis which is a valuable tool used to describe the local model's behaviours when investigating the effect of an extended local JR model with modified parameters (as in previous chapters) on the generated dynamic oscillations from the proposed network model. In addition, we think that TVB is limited with specific NMMs. We would investigate the extension, to embed JR's double-column model in TVB simulator as well as the script of this method as part of a demonstration package for using TVB to easily reproduce results.

In this thesis, all our proposed BNMs comprise large-scale our own connectivity and neural local mass models, as the network nodes. Each network node is modelled by different local models, each with a variety of features and parameters. However, it could be interesting to develop a new version of BNM comprising 50 cerebral areas in the left and right hemispheres. The left hemisphere would include 25 cerebral areas at different brain lobes, each of them will modelled by a NMM in its original parameters while the right hemisphere would include 25 cerebral areas at different brain lobes, each of them will be modelled by neural mass model in modified parameters. Therefore, with this proposal, it may be possible to predict new oscillatory patterns.

In above direction of further researches can be efficient to the exploration and generation of a new and rich repertoire of multi-frequency EEG rhythms and they

could use in the different applications to diagnosing diseases such as sleep disorders, Alzheimer's disease (AD) or cognitive processes.

At present, a few computational models are used to investigate the spatiotemporal changes in brain dynamics by applying brain stimulation techniques in a large-scale brain network modelling. The systematic application of Transcranial Magnetic Stimulation (TMS), which is a non-invasive technique used to stimulate or suppress nerves in specific regions of the brain, could be taken into account to test brain stimulation and its effect on functional brain activity.

At most, mathematical models for human brain are used to approximate the system of the neural field and its complex phenomena. The model parameters can exert the greatest influence on model results. Therefore, conducting a sensitivity analysis of these parameters is critical for model evaluation to determine which inputs contribute most to output variability, and to determine which parameters are most highly correlated with the output. So, this analysis should be included in future study.

REFERENCES

Abo-Zahhad, M, Ahmed, SM & Abbas, SN 2015, 'A new EEG acquisition protocol for biometric identification using eye blinking signals', *International Journal of Intelligent Systems and Applications*, vol. 7, no. 6, pp. 48-54.

Acebrón, JA, Bonilla, LL, Vicente, CJP, Ritort, F & Spigler, R 2005, 'The Kuramoto model: A simple paradigm for synchronization phenomena', *Reviews of modern physics*, vol. 77, no. 1, pp. 137-186.

Achard, S & Bullmore, E 2007, 'Efficiency and cost of economical brain functional networks', *PLoS computational biology*, vol. 3, no. 2, pp. 0174-0183.

Achard, S, Salvador, R, Whitcher, B, Suckling, J & Bullmore, E 2006, 'A resilient, low-frequency, small-world human brain functional network with highly connected association cortical hubs', *Journal of Neuroscience*, vol. 26, no. 1, pp. 63-72.

Adeli, H, Zhou, Z & Dadmehr, N 2003, 'Analysis of EEG records in an epileptic patient using wavelet transform', *Journal of neuroscience methods*, vol. 123, no. 1, pp. 69-87.

Adhikari, MH, Beharelle, AR, Griffa, A, Hagmann, P, Solodkin, A, McIntosh, AR, Small, SL & Deco, G 2015, 'Computational modeling of resting-state activity demonstrates markers of normalcy in children with prenatal or perinatal stroke', *Journal of Neuroscience*, vol. 35, no. 23, pp. 8914-8924.

Aerts, H, Schirner, M, Jeurissen, B, Van Roost, D, Achten, E, Ritter, P & Marinazzo, D 2018, 'Modeling brain dynamics in brain tumor patients using The Virtual Brain', *eNeuro*, vol. 5, no. 3, pp 0083, viewed 30 July 2018, https://www.ncbi.nlm.nih.gov/pmc/articles/PMC6001263/.

Aerts, H, Schirner, M, Dhollander, T, Jeurissen, B, Achten, E, Van Roost, D, Ritter, P & Marinazzo, D 2019, 'Modeling brain dynamics after tumor resection using The Virtual Brain', *BioRxiv*, p. 752931, viewed 30 September 2019, https://www.biorxiv.org/content/10.1101/752931v2.abstract.

Ahmadizadeh, S, Karoly, PJ, Nešić, D, Grayden, DB, Cook, MJ, Soudry, D & Freestone, DR 2018, 'Bifurcation analysis of two coupled Jansen-Rit neural mass models', *PloS one*, vol. 13, no. 3, p. 0192842, viewed 30 June 2019, https://www.ncbi.nlm.nih.gov/pmc/articles/PMC5870965/.

Al-Hossenat, A, Wen, P & Li, Y 2017, 'Simulation α of EEG using brain network model' in *Proceedings of the 1st MoHESR and HCED Iraqi Scholars Conference in Australasia 2017 (ISCA 2017)*, Swinburne University of Technology, pp.336-345.

Al-Hossenat, A, Wen, P & Li, Y 2019, 'Modelling and simulating different bands of EEG signals with the virtual brain', *International Journal of Electrical, Electronics and Data Communication*, vol. 7, no. 5, pp. 66-70.

Al-Qazzaz, NK, Ali, SHB, Ahmad, SA, Chellappan, K, Islam, MS & Escudero, J 2014, 'Role of EEG as biomarker in the early detection and classification of dementia', *The Scientific World Journal*, Volume 2014, viewed 1 January 2016, http://downloads.hindawi.com/journals/tswj/2014/906038.pdf.

Alstott, J, Breakspear, M, Hagmann, P, Cammoun, L & Sporns, O 2009, 'Modeling the impact of lesions in the human brain', *PLoS Comput Biol*, vol. 5, no. 6, p. 1000408, viewed 1 January 2016, https://www.ncbi.nlm.nih.gov/pmc/articles/PMC2688028/.

Aroniadou-Anderjaska, V, Fritsch, B, Qashu, F & Braga, MF 2008, 'Pathology and pathophysiology of the amygdala in epileptogenesis and epilepsy', *Epilepsy research*, vol. 78, no. 2-3, pp. 102-116.

Assisi, CG, Jirsa, VK & Kelso, JS 2005, 'Synchrony and clustering in heterogeneous networks with global coupling and parameter dispersion', *Physical review letters*, vol. 94, no. 1, p. 018106, viewed 1 January 2017, https://journals.aps.org/prl/abstract/10.1103/PhysRevLett.94.018106.

Atwood, HL & MacKay, WA 1989, *Essentials in Neurophysiology*, BC Decker.

Avoli, M 2012, 'A brief history on the oscillating roles of thalamus and cortex in absence seizures', *Epilepsia*, vol. 53, no. 5, pp. 779-89.

Barlow, JS 1993, *The electroencephalogram: its patterns and origins*, MIT press.

Bassett, DS & Bullmore, E 2006, 'Small-world brain networks', *The neuroscientist*, vol. 12, no. 6, pp. 512-523.

Bassett, DS & Bullmore, ET 2009, 'Human brain networks in health and disease', *Current opinion in neurology*, vol. 22, no. 4, pp. 340-347.

Becker, R, Knock, S, Ritter, P & Jirsa, V 2015, 'Relating alpha power and phase to population firing and hemodynamic activity using a thalamo-cortical neural mass

model', *PLoS computational biology*, vol. 11, no. 9, p. 100435, viewed 30 January 2017, https://www.ncbi.nlm.nih.gov/pmc/articles/PMC4559309/.

Beurle, RL 1956, 'Properties of a mass of cells capable of regenerating pulses', *Philosophical Transactions of the Royal Society of London. Series B, Biological Sciences*, vol.240, no. 669, pp. 55-94.

Bezgin, G, Solodkin, A, Bakker, R, Ritter, P & McIntosh, AR 2017, 'Mapping complementary features of cross-species structural connectivity to construct realistic "Virtual Brains"', *Human brain mapping*, vol. 38, no. 4, pp. 2080-93.

Biswal, BB, Mennes, M, Zuo, X-N, Gohel, S, Kelly, C, Smith, SM, Beckmann, CF, Adelstein, JS, Buckner, RL & Colcombe, S 2010, 'Toward discovery science of human brain function', *Proceedings of the National Academy of Sciences*, vol. 107, no. 10, pp. 4734-4739.

Blenkinsop, A, Valentin, A, Richardson, MP & Terry, JR 2012, 'The dynamic evolution of focal-onset epilepsies–combining theoretical and clinical observations', *European Journal of Neuroscience*, vol. 36, no. 2, pp. 2188-2200.

Bohland, JW, Wu, C, Barbas, H, Bokil, H, Bota, M, Breiter, HC, Cline, HT, Doyle, JC, Freed, PJ & Greenspan, RJ 2009, 'A proposal for a coordinated effort for the determination of brainwide neuroanatomical connectivity in model organisms at a mesoscopic scale', *PLoS computational biology*, vol. 5, no. 3, p.1000334, viewed 30 June 2017, https://www.ncbi.nlm.nih.gov/pmc/articles/PMC2655718/.

Bragin, A, Engel Jr, J, Wilson, CL, Fried, I & Buzsáki, G 1999, 'High-frequency oscillations in human brain', *Hippocampus*, vol. 9, no. 2, pp. 137-142.

Braun, U, Plichta, MM, Esslinger, C, Sauer, C, Haddad, L, Grimm, O, Mier, D, Mohnke, S, Heinz, A & Erk, S 2012, 'Test–retest reliability of resting-state connectivity network characteristics using fMRI and graph theoretical measures', *NeuroImage*, vol. 59, no. 2, pp. 1404-1412.

Breakspear, M 2017, 'Dynamic models of large-scale brain activity', *Nature neuroscience*, vol. 20, no. 3, pp. 340-352.

Breakspear, M & Stam, CJ 2005, 'Dynamics of a neural system with a multiscale architecture', *Philosophical Transactions of the Royal Society B: Biological Sciences*, vol. 360, no. 1457, pp. 1051-1074.

Breakspear, M, Terry, JR & Friston, KJ 2003, 'Modulation of excitatory synaptic coupling facilitates synchronization and complex dynamics in a biophysical model of neuronal dynamics', *Network: Computation in Neural Systems*, vol. 14, no. 4, pp. 703-732.

Breakspear, M, Roberts, J, Terry, J, Rodrigues, S & Robinson, P 2006, 'A unifying explanation of generalized seizures via the bifurcation analysis of a dynamical brain model', *Cerebral Cortex*, vol. 16, pp. 1296-1313.

Britton, JW, Frey, LC, Hopp, J, Korb, P, Koubeissi, M, Lievens, W, Pestana-Knight, E & St, EL 2016, *Electroencephalography (EEG): An introductory text and atlas of normal and abnormal findings in adults, children, and infants*, American Epilepsy Society, Chicago.

Brodmann, K 1909, *Vergleichende Lokalisationslehre der Grosshirnrinde in ihren Prinzipien dargestellt auf Grund des Zellenbaues*, Barth.

Bronzino, JD 1995, 'Principles of electroencephalography', *The biomedical engineering handbook*, CRC press.

Bronzino, JD 1999, *Biomedical engineering handbook*, CRC press.

Bullmore, E & Sporns, O 2009, 'Complex brain networks: graph theoretical analysis of structural and functional systems', *Nature Reviews Neuroscience*, vol. 10, no. 3, pp. 186-198.

Bullmore, ET & Bassett, DS 2011, 'Brain graphs: graphical models of the human brain connectome', *Annual review of clinical psychology*, vol. 7, pp. 113-140.

Buzsáki, G & Draguhn, A 2004, 'Neuronal oscillations in cortical networks', *science*, vol. 304, no. 5679, pp. 1926-1929.

Cabral, J, Kringelbach, M & Deco, G 2012a, 'Functional graph alterations in schizophrenia: a result from a global anatomic decoupling?', *Pharmacopsychiatry*, vol. 45, no. , pp. 57-64.

Cabral, J, Hugues, E, Sporns, O & Deco, G 2011, 'Role of local network oscillations in resting-state functional connectivity', *NeuroImage*, vol. 57, no. 1, pp. 130-139.

Cabral, J, Hugues, E, Kringelbach, ML & Deco, G 2012b, 'Modeling the outcome of structural disconnection on resting-state functional connectivity', *NeuroImage*, vol. 62, no. 3, pp. 1342-1353.

Cabral, J, Fernandes, HM, Van Hartevelt, TJ, James, AC, Kringelbach, ML & Deco, G 2013, 'Structural connectivity in schizophrenia and its impact on the dynamics of spontaneous functional networks', *Chaos: An Interdisciplinary Journal of Nonlinear Science*, vol. 23, no. 4, p. 046111-9, , viewed 30 June 2016, https://aip.scitation.org/doi/abs/10.1063/1.4851117.

Cabral, J, Luckhoo, H, Woolrich, M, Joensson, M, Mohseni, H, Baker, A, Kringelbach, ML & Deco, G 2014, 'Exploring mechanisms of spontaneous functional connectivity in MEG: how delayed network interactions lead to structured amplitude envelopes of band-pass filtered oscillations', *NeuroImage*, vol. 90, pp. 423-435.

Carlson, NR 2005, *Foundations of physiological psychology*, Pearson Education New Zealand.

Carlson, NR & Braun, J 1995, *Foundations of physiological psychology*, Allyn and bacon Boston.

Chang, BS & Drislane, FW 2007, 'Epileptiform abnormalities', in *The Clinical Neurophysiology Primer*, Springer, pp. 101-125.

Chatrian, G 1974, 'A glossary of terms most commonly used by clinical electroencephalographers', *Electroenceph. clin. Neurophysiol.*, vol. 37, pp. 538-548.

Collura, TF 1993, 'History and evolution of electroencephalographic instruments and techniques', *Journal of clinical neurophysiology*, vol. 10, no. 4, pp. 476-504.

Coombes, S 2010, 'Large-scale neural dynamics: simple and complex', *NeuroImage*, vol. 52, no. 3, pp. 731-739.

Da Silv, FL 2005, *Electroencephalography: basic principles, clinical applications, and related fields*, Lippencott Wlliams & Wilkins.

da Silva, FL 2005, 'Computer-assisted EEG diagnosis: pattern recognition and brain mapping', *Electroencephalography: Basic Principles, Clinical Applications, and Related Fields, E. Niedermeyer and F. Lopes da Silva, Editors. Lippincott Williams and Wilkins, Philadelphia* (2005), pp. 1203-1226.

Da Silva, FL, Van Rotterdam, A, Barts, P, Van Heusden, E & Burr, W 1976, 'Models of neuronal populations: the basic mechanisms of rhythmicity', in *Progress in brain research*, Elsevier, vol. 45, pp. 281-308.

Daducci, A, Gerhard, S, Griffa, A, Lemkaddem, A, Cammoun, L, Gigandet, X, Meuli, R, Hagmann, P & Thiran, J-P 2012, 'The connectome mapper: an open-source processing pipeline to map connectomes with MRI', *PloS one*, vol. 7, no. 12, p. 48121, viewed 30 June 2017, https://www.ncbi.nlm.nih.gov/pmc/articles/PMC3525592/.

Damoiseaux, JS & Greicius, MD 2009, 'Greater than the sum of its parts: a review of studies combining structural connectivity and resting-state functional connectivity', *Brain structure and function*, vol. 213, no. 6, pp. 525-533.

Dauwels, J, Vialatte, F & Cichocki, A 2010, 'Diagnosis of Alzheimer's disease from EEG signals: where are we standing?', *Current Alzheimer Research*, vol. 7, no. 6, pp. 487-505.

David, O & Friston, KJ 2003, 'A neural mass model for MEG/EEG:: coupling and neuronal dynamics', *NeuroImage*, vol. 20, no. 3, pp. 1743-1755.

David, O, Cosmelli, D & Friston, KJ 2004, 'Evaluation of different measures of functional connectivity using a neural mass model', *NeuroImage*, vol. 21, no. 2, pp. 659-673.

David, O, Harrison, L & Friston, KJ 2005, 'Modelling event-related responses in the brain', *NeuroImage*, vol. 25, no. 3, pp. 756-770.

Deco, G & Corbetta, M 2011a, 'The dynamical balance of the brain at rest', *The neuroscientist*, vol. 17, no. 1, pp. 107-123.

Deco, G & Jirsa, VK 2012, 'Ongoing cortical activity at rest: criticality, multistability, and ghost attractors', *Journal of Neuroscience*, vol. 32, no. 10, pp. 3366-3375.

Deco, G, Jirsa, VK & McIntosh, AR 2011b, 'Emerging concepts for the dynamical organization of resting-state activity in the brain', *Nature Reviews Neuroscience*, vol. 12, no. 1, pp. 43-56.

Deco, G, Jirsa, VK & McIntosh, AR 2013a, 'Resting brains never rest: computational insights into potential cognitive architectures', *Trends in neurosciences*, vol. 36, no. 5, pp. 268-274.

Deco, G, Hagmann, P, Hudetz, AG & Tononi, G 2013b, 'Modeling resting-state functional networks when the cortex falls asleep: local and global changes', *Cerebral Cortex*, vol. 24, no. 12, pp. 3180-3194.

Deco, G, Kringelbach, ML, Jirsa, VK & Ritter, P 2017, 'The dynamics of resting fluctuations in the brain: metastability and its dynamical cortical core', *Scientific reports*, vol. 7, no. 1, p. 3095, viewed 30 June 2017, https://www.nature.com/articles/s41598-017-03073-5.pdf.

Deco, G, Jirsa, VK, Robinson, PA, Breakspear, M & Friston, K 2008, 'The dynamic brain: from spiking neurons to neural masses and cortical fields', *PLoS computational biology*, vol. 4, no. 8, p. 1000092, viewed 25 July 2016, https://journals.plos.org/ploscompbiol/article/file?type=printable&id=10.1371/journal.pcbi.1000092.

Deco, G, Jirsa, V, McIntosh, AR, Sporns, O & Kötter, R 2009, 'Key role of coupling, delay, and noise in resting brain fluctuations', *Proceedings of the National Academy of Sciences*, vol. 106, no. 25, pp. 10302-10307.

Deco, G, Ponce-Alvarez, A, Mantini, D, Romani, GL, Hagmann, P & Corbetta, M 2013c, 'Resting-state functional connectivity emerges from structurally and dynamically shaped slow linear fluctuations', *Journal of Neuroscience*, vol. 33, no. 27, pp. 11239-1152.

Deco, G, Cabral, J, Saenger, VM, Boly, M, Tagliazucchi, E, Laufs, H, Van Someren, E, Jobst, B, Stevner, A & Kringelbach, ML 2018, 'Perturbation of whole-brain dynamics in silico reveals mechanistic differences between brain states', *NeuroImage*, vol. 169, pp. 46-56.

Dong, E & Liang, Z 2014, 'The multi-frequency EEG rhythms modeling based on two-parameter bifurcation of neural mass model', in *2014 IEEE International Conference on Mechatronics and Automation*, IEEE, pp. 1564-1569.

Engel Jr, J 2001, 'A proposed diagnostic scheme for people with epileptic seizures and with epilepsy: report of the ILAE Task Force on Classification and Terminology', *Epilepsia*, vol. 42, no. 6, pp. 796-803.

Falcon, MI, Jirsa, V & Solodkin, A 2016a, 'A new neuroinformatics approach to personalized medicine in neurology: The Virtual Brain', *Current opinion in neurology*, vol. 29, no. 4, pp. 429-436.

Falcon, MI, Riley, JD, Jirsa, V, McIntosh, AR, Chen, EE & Solodkin, A 2016b, 'Functional mechanisms of recovery after chronic stroke: modeling with the Virtual

Brain', *eNeuro*, vol. 3, no. 2, pp. 0158, viewed 15 July 2016, https://www.ncbi.nlm.nih.gov/pmc/articles/PMC4819288/.

Falcon, MI, Riley, JD, Jirsa, V, McIntosh, AR, Shereen, AD, Chen, EE & Solodkin, A 2015, 'The virtual brain: modeling biological correlates of recovery after chronic stroke', *Frontiers in neurology*, vol. 6, p. 228, viewed July 30 2017, https://www.frontiersin.org/articles/10.3389/fneur.2015.00228/full

Fisch, BJ & Spehlmann, R 1999, 'EEG primer: basic principles of digital and analog EEG', *Elsevier Health Sciences*, pp. 23-7, viewed 15 July 2016, https://onlinelibrary.wiley.com/doi/pdf/10.1002/bem.20209.

FitzHugh, R 1961, 'Impulses and physiological states in theoretical models of nerve membrane', *Biophysical journal*, vol. 1, no. 6, pp. 445-466.

Fornito, A, Zalesky, A & Breakspear, M 2013, 'Graph analysis of the human connectome: promise, progress, and pitfalls', *NeuroImage*, vol. 80, pp. 426-444.

Freeman, WJ 1975, *Mass action in the nervous system*, vol. 2004, Citeseer.

Freeman, W 1978, 'Models of the dynamics of neural populations', *Electroencephalography and clinical neurophysiology. Supplement*, no. 34, pp. 9-18.

Freeman, WJ 1987, 'Simulation of chaotic EEG patterns with a dynamic model of the olfactory system', *Biological cybernetics*, vol. 56, no. 2-3, pp. 139-50.

Geng, S, Zhou, W, Zhao, X, Yuan, Q, Ma, Z & Wang, J 2014, 'Bifurcation and oscillation in a time-delay neural mass model', *Biological cybernetics*, vol. 108, no. 6, pp. 747-756.

Ghosh, A, Rho, Y, McIntosh, A, Kötter, R & Jirsa, V 2008a, 'Cortical network dynamics with time delays reveals functional connectivity in the resting brain', *Cognitive neurodynamics*, vol. 2, no. 2, pp. 115-120.

Ghosh, A, Rho, Y, McIntosh, AR, Kötter, R & Jirsa, VK 2008b, 'Noise during rest enables the exploration of the brain's dynamic repertoire', *PLoS computational biology*, vol. 4, no. 10, p. 1000196, viewed 15 July 2016, https://www.ncbi.nlm.nih.gov/pmc/articles/PMC2551736/.

Glasser, MF & Van Essen, DC 2011, 'Mapping human cortical areas in vivo based on myelin content as revealed by T1-and T2-weighted MRI', *Journal of Neuroscience*, vol. 31, no. 32, pp. 11597-11616.

Glasser, MF, Goyal, MS, Preuss, TM, Raichle, ME & Van Essen, DC 2014, 'Trends and properties of human cerebral cortex: correlations with cortical myelin content', *NeuroImage*, vol. 93, pp. 165-175.

Glasser, MF, Sotiropoulos, SN, Wilson, JA, Coalson, TS, Fischl, B, Andersson, JL, Xu, J, Jbabdi, S, Webster, M & Polimeni, JR 2013, 'The minimal preprocessing pipelines for the Human Connectome Project', *NeuroImage*, vol. 80, pp. 105-124.

Glasser, MF, Smith, SM, Marcus, DS, Andersson, JL, Auerbach, EJ, Behrens, TE, Coalson, TS, Harms, MP, Jenkinson, M & Moeller, S 2016, 'The human connectome project's neuroimaging approach', *Nature neuroscience*, vol. 19, no. 9, pp. 1175-1187.

Gloor, P 1977, 'The EEG and differential diagnosis of epilepsy', *Current concepts in clinical neurophysiology*.

Gong, G, Rosa-Neto, P, Carbonell, F, Chen, ZJ, He, Y & Evans, AC 2009, 'Age-and gender-related differences in the cortical anatomical network', *Journal of Neuroscience*, vol. 29, no. 50, pp. 15684-15693.

Grabska-Barwińska, A & Żygierewicz, J 2006, 'A model of event-related EEG synchronization changes in beta and gamma frequency bands', *Journal of theoretical biology*, vol. 238, no. 4, pp. 901-913.

Gray, FJ 2002, *Anatomy for the medical clinician*, FJ Gray.

Grimbert, F & Faugeras, O 2006, 'Bifurcation analysis of Jansen's neural mass model', *Neural computation*, vol. 18, no. 12, pp. 3052-3068.

Grosse-Wentrup, M, Liefhold, C, Gramann, K & Buss, M 2009, 'Beamforming in noninvasive brain–computer interfaces', *IEEE Transactions on Biomedical Engineering*, vol. 56, no. 4, pp. 1209-1219.

Hagmann, P, Kurant, M, Gigandet, X, Thiran, P, Wedeen, VJ, Meuli, R & Thiran, J-P 2007, 'Mapping human whole-brain structural networks with diffusion MRI', *PloS one*, vol. 2, no. 7, p. 597, viewed 15 January 2016, https://journals.plos.org/plosone/article%3Fid%3D10.1371/journal.pone.0000597.

Hagmann, P, Cammoun, L, Gigandet, X, Meuli, R, Honey, CJ, Wedeen, VJ & Sporns, O 2008, 'Mapping the structural core of human cerebral cortex', *PLoS Biol*, vol. 6, no. 7, p. 159, viewed 15 January 2016, https://journals.plos.org/plosbiology/article/file?type=printable&id=10.1371/journal.pbio.0060159.

Harmony, T 2013, 'The functional significance of delta oscillations in cognitive processing', *Frontiers in integrative neuroscience*, vol. 7, p. 83.

Hebbink, G 2014, 'Activity types in a neural mass model', University of Twente.

Holmes, GL & Khazipov, R 2007, 'Basic neurophysiology and the cortical basis of EEG', in *The clinical neurophysiology primer*, Springer, pp. 19-33.

Honey, CJ, Thivierge, J-P & Sporns, O 2010, 'Can structure predict function in the human brain?', *NeuroImage*, vol. 52, no. 3, pp. 766-776.

Honey, CJ, Kötter, R, Breakspear, M & Sporns, O 2007, 'Network structure of cerebral cortex shapes functional connectivity on multiple time scales', *Proceedings of the National Academy of Sciences*, vol. 104, no. 24, pp. 10240-10245.

Honey, C, Sporns, O, Cammoun, L, Gigandet, X, Thiran, J-P, Meuli, R & Hagmann, P 2009, 'Predicting human resting-state functional connectivity from structural connectivity', *Proceedings of the National Academy of Sciences*, vol. 106, no. 6, pp. 2035-2040.

Horwitz, B, Hwang, C & Alstott, J 2013, 'Interpreting the effects of altered brain anatomical connectivity on fMRI functional connectivity: a role for computational neural modeling', *Frontiers in human neuroscience*, vol. 7, p. 649, viewed 15 January 2016, https://www.frontiersin.org/articles/10.3389/fnhum.2013.00649/full.

Houmani, N, Vialatte, F, Gallego-Jutglà, E, Dreyfus, G, Nguyen-Michel, V-H, Mariani, J & Kinugawa, K 2018, 'Diagnosis of Alzheimer's disease with Electroencephalography in a differential framework', *PloS one*, vol. 13, no. 3, p. 0193607, viewed 15 January 2016, https://www.ncbi.nlm.nih.gov/pmc/articles/PMC5860733/.

Hsieh, L-T & Ranganath, C 2014, 'Frontal midline theta oscillations during working memory maintenance and episodic encoding and retrieval', *NeuroImage*, vol. 85, pp. 721-729.

Jacobs, J, LeVan, P, Chander, R, Hall, J, Dubeau, F & Gotman, J 2008, 'Interictal high-frequency oscillations (80–500 Hz) are an indicator of seizure onset areas independent of spikes in the human epileptic brain', *Epilepsia*, vol. 49, no. 11, pp. 1893-1907.

Jacobs, J, LeVan, P, Châtillon, C-É, Olivier, A, Dubeau, F & Gotman, J 2009, 'High frequency oscillations in intracranial EEGs mark epileptogenicity rather than lesion type', *Brain*, vol. 132, no. 4, pp. 1022-1037.

Jacobs, J, Staba, R, Asano, E, Otsubo, H, Wu, J, Zijlmans, M, Mohamed, I, Kahane, P, Dubeau, F & Navarro, V 2012, 'High-frequency oscillations (HFOs) in clinical epilepsy', *Progress in neurobiology*, vol. 98, no. 3, pp. 302-315.

Jansen, BH & Rit, VG 1995, 'Electroencephalogram and visual evoked potential generation in a mathematical model of coupled cortical columns', *Biological cybernetics*, vol. 73, no. 4, pp. 357-366.

Jansen, BH, Zouridakis, G & Brandt, ME 1993, 'A neurophysiologically-based mathematical model of flash visual evoked potentials', *Biological cybernetics*, vol. 68, no. 3, pp. 275-283.

Jasper, HH 1958a, 'The ten-twenty electrode system of the International Federation', Electroencephalogr. Clin. Neurophysiol. vol. 10, pp. 367-380..

Jasper, H 1958b, 'Report of the committee on methods of clinical examination in electroencephalography', *Electroencephalogr Clin Neurophysiol*, vol. 10, no. 2, pp. 371-375.

Javidan, M 2012, 'Electroencephalography in mesial temporal lobe epilepsy: a review', *Epilepsy research and treatment*, vol. 2012, p 17, viewed 15 January 2016, http://downloads.hindawi.com/archive/2012/637430.pdf.

Jedynak, M, Pons, AJ, Garcia-Ojalvo, J & Goodfellow, M 2017, 'Temporally correlated fluctuations drive epileptiform dynamics', *NeuroImage*, vol. 146, pp. 188-196.

Jensen, O & Tesche, CD 2002, 'Frontal theta activity in humans increases with memory load in a working memory task', *European Journal of Neuroscience*, vol. 15, no. 8, pp. 1395-1399.

Jensen, O, Gelfand, J, Kounios, J & Lisman, JE 2002, 'Oscillations in the alpha band (9–12 Hz) increase with memory load during retention in a short-term memory task', *Cerebral Cortex*, vol. 12, no. 8, pp. 877-882.

Jirsa, VK 2009, 'Neural field dynamics with local and global connectivity and time delay', *Philosophical Transactions of the Royal Society of London A: Mathematical, Physical and Engineering Sciences*, vol. 367, no. 1891, pp. 1131-1143.

Jirsa, VK, Jantzen, KJ, Fuchs, A & Kelso, JS 2002, 'Spatiotemporal forward solution of the EEG and MEG using network modeling', *IEEE Transactions on Medical Imaging*, vol. 21, no. 5, pp. 493-504.

Jirsa, VK, Stacey, WC, Quilichini, PP, Ivanov, AI & Bernard, C 2014, 'On the nature of seizure dynamics', *Brain*, vol. 137, no. 8, pp. 2210-2230.

Jirsa, VK, Proix, T, Perdikis, D, Woodman, MM, Wang, H, Gonzalez-Martinez, J, Bernard, C, Bénar, C, Guye, M & Chauvel, P 2017, 'The virtual epileptic patient: individualized whole-brain models of epilepsy spread', *NeuroImage*, vol. 145, pp. 377-388.

Kahle, W & Frotscher, M 2003, *Nervous System and Sensory Organs. Color Atlas and Textbook of Human Anatomy*, Thieme Medical Publishers, Stuttgart New York.

Kameneva, T, Ying, T, Guo, B & Freestone, DR 2017, 'Neural mass models as a tool to investigate neural dynamics during seizures', *Journal of computational neuroscience*, vol. 42, no. 2, pp. 203-215.

Kim, J & Robinson, P 2007, 'Compact dynamical model of brain activity', *Physical Review E*, vol. 75, no. 3, p. 031907, viewed 15 January 2016, https://journals.aps.org/pre/abstract/10.1103/PhysRevE.75.031907.

Kingsley, RE, Gable, SR & Kingsley, T 2000, *Concise text of neuroscience*, Lippincott Williams & Wilkins Philadelphia.

Klimesch, W 1997a, 'EEG-alpha rhythms and memory processes', *International Journal of Psychophysiology*, vol. 26, no. 1-3, pp. 319-340.

Klimesch, W 1999, 'EEG alpha and theta oscillations reflect cognitive and memory performance: a review and analysis', *Brain research reviews*, vol. 29, no. 2-3, pp. 169-195.

Klimesch, W 2012, 'Alpha-band oscillations, attention, and controlled access to stored information', *Trends in cognitive sciences*, vol. 16, no. 12, pp. 606-617.

Klimesch, W, Schimke, H & Pfurtscheller, G 1993, 'Alpha frequency, cognitive load and memory performance', *Brain topography*, vol. 5, no. 3, pp. 241-251.

Klimesch, W, Doppelmayr, M, Schimke, H & Ripper, B 1997b, 'Theta synchronization and alpha desynchronization in a memory task', *Psychophysiology*, vol. 34, no. 2, pp. 169-176.

Klimesch, W, Doppelmayr, M, Stadler, W, Pöllhuber, D, Sauseng, P & Roehm, D 2001, 'Episodic retrieval is reflected by a process specific increase in human electroencephalographic theta activity', *Neuroscience letters*, vol. 302, no. 1, pp. 49-52.

Knock, S, McIntosh, A, Sporns, O, Kötter, R, Hagmann, P & Jirsa, V 2009, 'The effects of physiologically plausible connectivity structure on local and global dynamics in large scale brain models', *Journal of neuroscience methods*, vol. 183, no. 1, pp. 86-94.

Kötter, R 2004, 'Online retrieval, processing, and visualization of primate connectivity data from the CoCoMac database', *Neuroinformatics*, vol. 2, no. 2, pp. 127-144.

Kötter, R 2007, *Anatomical Concepts of Brain Connectivity. Handbook of Brain Connectivity, Understanding Complex Systems*, Springer, Berlin, Heidelberg.

Kötter, R & Wanke, E 2005, 'Mapping brains without coordinates', *Philosophical Transactions of the Royal Society of London B: Biological Sciences*, vol. 360, no. 1456, pp. 751-766.

Kraft, U 2006, 'Train your brain', *Scientific American Mind*, vol. 17, no. 1, pp. 58-63.

Kringelbach, ML, McIntosh, AR, Ritter, P, Jirsa, VK & Deco, G 2015, 'The rediscovery of slowness: exploring the timing of cognition', *Trends in cognitive sciences*, vol. 19, no. 10, pp. 616-628.

Kucewicz, MT, Cimbalnik, J, Matsumoto, JY, Brinkmann, BH, Bower, MR, Vasoli, V, Sulc, V, Meyer, F, Marsh, W & Stead, S 2014, 'High frequency oscillations are associated with cognitive processing in human recognition memory', *Brain*, vol. 137, no. 8, pp. 2231-2244.

Kunze, T, Hunold, A, Haueisen, J, Jirsa, V & Spiegler, A 2016, 'Transcranial direct current stimulation changes resting state functional connectivity: a large-scale brain network modeling study', *NeuroImage*, vol. 140, pp. 174-187.

Kuramoto, Y 2003, *Chemical oscillations, waves, and turbulence*, Courier Corporation.

Kuramoto, Y 1984, *Chemical oscillations, waves, and turbulence*. Spriger-Verlag, Berlin.

Lally, N, Mullins, PG, Roberts, MV, Price, D, Gruber, T & Haenschel, C 2014, 'Glutamatergic correlates of gamma-band oscillatory activity during cognition: A concurrent ER-MRS and EEG study', *NeuroImage*, vol. 85, pp. 823-833.

Larter, R, Speelman, B & Worth, RM 1999, 'A coupled ordinary differential equation lattice model for the simulation of epileptic seizures', *Chaos: An Interdisciplinary* Journal of Nonlinear Science, vol. 9, no. 3, pp. 795-804.

Leon, PS, Knock, SA, Woodman, MM, Domide, L, Mersmann, J, McIntosh, AR & Jirsa, V 2013, 'The Virtual Brain: a simulator of primate brain network dynamics', Frontiers in neuroinformatics, vol. 7, viewed 15 February 2015, https://www.ncbi.nlm.nih.gov/pmc/articles/PMC3678125/.

Leung, L-W & Borst, J 1987, 'Electrical activity of the cingulate cortex. I. Generating mechanisms and relations to behavior', *Brain research*, vol. 407, no. 1, pp. 68-80.

Liley, DT & Bojak, I 2005, 'Understanding the transition to seizure by modeling the epileptiform activity of general anesthetic agents', *Journal of clinical neurophysiology*, vol. 22, no. 5, pp. 300-313.

Liu, Y, Liang, M, Zhou, Y, He, Y, Hao, Y, Song, M, Yu, C, Liu, H, Liu, Z & Jiang, T 2008, 'Disrupted small-world networks in schizophrenia', *Brain*, vol. 131, no. 4, pp. 945-961.

Lizio, R, Vecchio, F, Frisoni, GB, Ferri, R, Rodriguez, G & Babiloni, C 2011, 'Electroencephalographic rhythms in Alzheimer's disease', International Journal of Alzheimer's Disease, vol. 2011, viewed 25 May 2016, http://dx.doi.org/10.4061/2011/927573.

Lopes da Silva, F, Hoeks, A, Smits, H & Zetterberg, L 1974, 'Model of brain rhythmic activity', *Biological cybernetics*, vol. 15, no. 1, pp. 27-37.

Lynall, M-E, Bassett, DS, Kerwin, R, McKenna, PJ, Kitzbichler, M, Muller, U & Bullmore, E 2010, 'Functional connectivity and brain networks in schizophrenia', *Journal of Neuroscience*, vol. 30, no. 28, pp. 9477-9487.

Mathews, LM & Sethu, G 2015, 'Interpretation of EEG in Epileptic Patients, A Review', *Journal of Pharmaceutical Sciences and Research*, vol. 7, no. 10, pp. 893-894.

Mattia, M & Del Giudice, P 2002, 'Population dynamics of interacting spiking neurons', *Physical Review E*, vol. 66, no. 5, p. 051917, viewed 25 May 2016, https://journals.aps.org/pre/abstract/10.1103/PhysRevE.66.051917.

Medithe, JWC & Nelakuditi, UR 2016, 'Study of normal and abnormal EEG', in *2016 3rd International conference on advanced computing and communication systems (ICACCS)*, IEEE, pp. 1-4.

Mooij, AH, Raijmann, RC, Jansen, FE, Braun, KP & Zijlmans, M 2017, 'Physiological ripples (±100 Hz) in spike-free scalp EEGs of children with and without epilepsy', *Brain topography*, vol. 30, no. 6, pp. 739-746.

Morris, C & Lecar, H 1981, 'Voltage oscillations in the barnacle giant muscle fiber', *Biophysical journal*, vol. 35, no. 1, pp. 193-213.

Nagumo, J, Arimoto, S & Yoshizawa, S 1962, 'An active pulse transmission line simulating nerve axon', *Proceedings of the IRE*, vol. 50, no. 10, pp. 2061-2070.

Noachtar, S & Rémi, J 2009, 'The role of EEG in epilepsy: a critical review', *Epilepsy & Behavior*, vol. 15, no. 1, pp. 22-33.

Noachtar, S, Binnie, C, Ebersole, J, Mauguière, F, Sakamoto, A & Westmoreland, B 2004, 'A glossary of terms most commonly used by clinical electroencephalographers and proposal for the report form for the EEG findings', *Klinische Neurophysiologie*, vol. 35, no. 1, pp. 5-21.

Nunez, PL 1974, 'The brain wave equation: a model for the EEG', *Mathematical Biosciences*, vol. 21, no. 3, pp. 279-297.

Nunez, PL & Srinivasan, R 1982, 'Electric Fields of the Brain: The neurophysics of EEG', *Physics Today*, vol. 35, no. 6, pp. 1-59.

Nunez, PL & Srinivasan, R 2006, *Electric fields of the brain: the neurophysics of EEG*, Oxford University Press, USA.

Paulus, W & Rothwell, JC 2016, 'Membrane resistance and shunting inhibition: where biophysics meets state-dependent human neurophysiology', The Journal of physiology, vol. 594, no. 10, pp. 2719-2728.

Proix, T, Bartolomei, F, Guye, M & Jirsa, VK 2017, 'Individual brain structure and modelling predict seizure propagation', *Brain*, vol. 140, no. 3, pp. 641-654.

Proix, T, Jirsa, VK, Bartolomei, F, Guye, M & Truccolo, W 2018, 'Predicting the spatiotemporal diversity of seizure propagation and termination in human focal epilepsy', *Nature communications*, vol. 9, no. 1, p. 1088, viewed 25 May 2017, https://www.nature.com/articles/s41467-018-02973-y.

Proix, T, Spiegler, A, Schirner, M, Rothmeier, S, Ritter, P & Jirsa, VK 2016, 'How do parcellation size and short-range connectivity affect dynamics in large-scale brain network models?', *NeuroImage*, vol. 142, pp. 135-149.

Purves, D, Augustine, GJ, Fitzpatrick, D, Hall, W, LaMantia, A, McNamara, J & White, L 2004, 'Neuroscience, Sinauer Associates', *Inc., USA*.

Ritter, P, Schirner, M, McIntosh, AR & Jirsa, VK 2013, 'The virtual brain integrates computational modeling and multimodal neuroimaging', *Brain connectivity*, vol. 3, no. 2, pp. 121-145.

Ritter, P, Jirsa, V, McIntosh, AR & Breakspear, M 2015, 'State-dependent brain computation', *Frontiers in computational neuroscience*, vol. 9, p. 77, viewed 25 May 2017, https://www.frontiersin.org/articles/10.3389/fncom.2015.00077/full.

Roberts, JA, Perry, A, Lord, AR, Roberts, G, Mitchell, PB, Smith, RE, Calamante, F & Breakspear, M 2016, 'The contribution of geometry to the human connectome', *NeuroImage*, vol. 124, pp. 379-393.

Robinson, P, Rennie, C & Rowe, D 2002, 'Dynamics of large-scale brain activity in normal arousal states and epileptic seizures', *Physical Review E*, vol. 65, no. 4, p. 041924, viewed 25 May 2016, https://journals.aps.org/pre/abstract/10.1103/PhysRevE.65.041924.

Robinson, P, Loxley, P, O'connor, S & Rennie, C 2001, 'Modal analysis of corticothalamic dynamics, electroencephalographic spectra, and evoked potentials', *Physical Review E*, vol. 63, no. 4, p. 041909, viewed 25 March 2016, https://journals.aps.org/pre/abstract/10.1103/PhysRevE.63.041909.

Roy, D, Sigala, R, Breakspear, M, McIntosh, AR, Jirsa, VK, Deco, G & Ritter, P 2014, 'Using the virtual brain to reveal the role of oscillations and plasticity in shaping brain's dynamical landscape', *Brain connectivity*, vol. 4, no. 10, pp. 791-811.

Rubinov, M & Sporns, O 2011, 'Weight-conserving characterization of complex functional brain networks', *NeuroImage*, vol. 56, no. 4, pp. 2068-2079.

Rykhlevskaia, E, Gratton, G & Fabiani, M 2008, 'Combining structural and functional neuroimaging data for studying brain connectivity: a review', *Psychophysiology*, vol. 45, no. 2, pp. 173-187.

Salvador, R, Suckling, J, Schwarzbauer, C & Bullmore, E 2005, 'Undirected graphs of frequency-dependent functional connectivity in whole brain networks', *Philosophical Transactions of the Royal Society B: Biological Sciences*, vol. 360, no. 1457, pp. 937-946.

Sanei, S & Chambers, JA 2007, 'EEG signal processing'.

Sanz Leon, P 2014, 'Development of a computational and neuroinformatics framework for large-scale brain modelling', Aix-Marseille.

Sanz-Arigita, EJ, Schoonheim, MM, Damoiseaux, JS, Rombouts, SA, Maris, E, Barkhof, F, Scheltens, P & Stam, CJ 2010, 'Loss of 'small-world'networks in Alzheimer's disease: graph analysis of FMRI resting-state functional connectivity', *PloS one*, vol. 5, no. 11, p. 13788, viewed 25 March 2018, https://www.ncbi.nlm.nih.gov/pmc/articles/PMC2967467/.

Sanz-Leon, P, Knock, SA, Spiegler, A & Jirsa, VK 2015, 'Mathematical framework for large-scale brain network modeling in The Virtual Brain', *NeuroImage*, vol. 111, pp. 385-430.

Schirner, M, Rothmeier, S, Jirsa, VK, McIntosh, AR & Ritter, P 2015, 'An automated pipeline for constructing personalized virtual brains from multimodal neuroimaging data', *NeuroImage*, vol. 117, pp. 343-357.

Schirner, M, McIntosh, AR, Jirsa, V, Deco, G & Ritter, P 2018, 'Inferring multi-scale neural mechanisms with brain network modelling', *Elife*, vol. 7, p. 28927, viewed 25 March 2019, https://elifesciences.org/articles/28927.

Seneviratne, U, Cook, M & D'Souza, W 2012, 'The electroencephalogram of idiopathic generalized epilepsy', *Epilepsia*, vol. 53, no. 2, pp. 234-248.

Sharma, N, Kolekar, M & Chandra, S 2016, 'The role of EEG signal processing in detection of neurocognitive disorders', *International Journal of Behavioural and Healthcare Research, vol.* 6, no. 1,p. 081073, viewed 25 March 2018, https://www.inderscienceonline.com/doi/pdf/10.1504/IJBHR.2016.081073.

Shen, K, Bezgin, G, Schirner, M, Ritter, P, Everling, S & McIntosh, R 2019, 'A macaque connectome for large-scale network simulations in TheVirtualBrain', *BioRxiv*, p. 480905, viewed 25 October 2019, https://www.nature.com/articles/s41597-019-0129-z.

Sigala, R, Haufe, S, Roy, D, Dinse, HR & Ritter, P 2014, 'The role of alpha-rhythm states in perceptual learning: insights from experiments and computational models', *Frontiers in computational neuroscience*, vol. 8, p. 36, viewed 25 October 2017, https://www.frontiersin.org/articles/10.3389/fncom.2014.00036/full.

Sotero, RC, Trujillo-Barreto, NJ, Iturria-Medina, Y, Carbonell, F & Jimenez, JC 2007, 'Realistically coupled neural mass models can generate EEG rhythms', *Neural computation*, vol. 19, no. 2, pp. 478-512.

Spiegler, A 2011, 'Dynamics of biologically informed neural mass models of the brain', Universitätsverlag Ilmenau.

Spiegler, A & Jirsa, V 2013, 'Systematic approximations of neural fields through networks of neural masses in the virtual brain', *NeuroImage*, vol. 83, pp. 704-725.

Spiegler, A, Kiebel, SJ, Atay, FM & Knösche, TR 2010, 'Bifurcation analysis of neural mass models: Impact of extrinsic inputs and dendritic time constants', *NeuroImage*, vol. 52, no. 3, pp. 1041-1058.

Spiegler, A, Hansen, EC, Bernard, C, McIntosh, AR & Jirsa, VK 2016, 'Selective activation of resting-state networks following focal stimulation in a connectome-based network model of the human brain', *eNeuro*, vol. 3, no. 5, p.0068, viewed 12 October 2017, https://www.ncbi.nlm.nih.gov/pmc/articles/PMC5052665/.

Sporns, O 2007, 'Brain connectivity', *Scholarpedia*, vol. 2, no. 10, p. 4695, viewed 12 October 2015, http://var.scholarpedia.org/article/Brain_connectivity.

Sporns, O 2010, *Networks of the Brain*, MIT press.

Sporns, O 2011, 'The human connectome: a complex network', *Annals of the New York Academy of Sciences*, vol. 1224, no. 1, pp. 109-125.

Sporns, O 2013, 'The human connectome: origins and challenges', *NeuroImage*, vol. 80, pp. 53-61.

Sporns, O, Tononi, G & Kötter, R 2005, 'The human connectome: a structural description of the human brain', *PLoS computational biology*, vol. 1, no. 4, p. 42, viewed 12 March 2016, https://www.ncbi.nlm.nih.gov/pmc/articles/PMC1239902/.

Sporns, O, Chialvo, DR, Kaiser, M & Hilgetag, CC 2004, 'Organization, development and function of complex brain networks', *Trends in cognitive sciences*, vol. 8, no. 9, pp. 418-425.

Stafstrom, CE & Carmant, L 2015, 'Seizures and epilepsy: an overview for neuroscientists', *Cold Spring Harbor perspectives in medicine*, vol. 5, no. 6, p.022426, viewed 12 March 2017, http://perspectivesinmedicine.cshlp.org/content/5/6/a022426.short.

Stefanescu, RA & Jirsa, VK 2008, 'A low dimensional description of globally coupled heterogeneous neural networks of excitatory and inhibitory neurons', *PLoS Comput Biol*, vol. 4, no. 11, p.1000219, viewed 12 March 2016, https://www.ncbi.nlm.nih.gov/pmc/articles/PMC2574034/.

Stefanovski, L, Ghani, A, McIntosh, AR & Ritter, P 2016, 'Linking connectomics and dynamics in the human brain', *e-Neuroforum*, vol. 22, no. 3, pp. 64-70.

Stefanovski, L, Triebkorn, P, Spiegler, A, Diaz-Cortes, M-A, Solodkin, A, Jirsa, V, McIntosh, AR, Ritter, P & Initiative, AsDN 2019, 'Linking molecular pathways and large-scale computational modeling to assess candidate disease mechanisms and pharmacodynamics in Alzheimer's disease', *BioRxiv*, p. 600205, viewed 15 August 2019, https://www.frontiersin.org/articles/10.3389/fncom.2019.00054/full.

Stern, JM 2005, *Atlas of EEG patterns*, Lippincott Williams & Wilkins.

Supekar, K, Menon, V, Rubin, D, Musen, M & Greicius, MD 2008, 'Network analysis of intrinsic functional brain connectivity in Alzheimer's disease', *PLoS computational biology*, vol. 4, no. 6, p. 1000100, viewed 25 August 2016, https://www.ncbi.nlm.nih.gov/pmc/articles/PMC2435273/.

Swartz, BE & Goldensohn, ES 1998, 'Timeline of the history of EEG and associated fields', *Electroencephalography and clinical Neurophysiology*, vol. 106, no. 2, pp. 173-176.

Tallon-Baudry, C 2004, 'Attention and awareness in synchrony', *Trends in cognitive* sciences, vol. 8, no. 12, pp. 523-525.

Tamilia, E, Madsen, JR, Grant, PE, Pearl, PL & Papadelis, C 2017, 'Current and emerging potential of magnetoencephalography in the detection and localization of high-frequency oscillations in epilepsy', Frontiers in neurology, vol. 8, p. 14 , viewed 25 August 2016, https://www.frontiersin.org/articles/10.3389/fneur.2017.00014/full.

Tanaka, H, Hayashi, M & Hori, T 1997, 'Topographical characteristics and principal component structure of the hypnagogic EEG', *Sleep*, vol. 20, no. 7, pp. 523-534.

Teplan, M 2002, 'Fundamentals of EEG measurement', *Measurement science review*, vol. 2, no. 2, pp. 1-11.

Thom, M & Bertram, EH 2012, 'Temporal lobe epilepsy', *Handbook of clinical neurology*, vol. 107, pp. 225-240.

Touboul, J, Wendling, F, Chauvel, P & Faugeras, O 2011, 'Neural mass activity, bifurcations, and epilepsy', *Neural computation*, vol. 23, no. 12, pp. 3232-3286.

Traub, RD, Schmitz, D, Jefferys, JG & Draguhn, A 1999, 'High-frequency population oscillations are predicted to occur in hippocampal pyramidal neuronal networks interconnected by axoaxonal gap junctions', *Neuroscience*, vol. 92, no. 2, pp. 407-426.

Tzourio-Mazoyer, N, Landeau, B, Papathanassiou, D, Crivello, F, Etard, O, Delcroix, N, Mazoyer, B & Joliot, M 2002, 'Automated anatomical labeling of activations in SPM using a macroscopic anatomical parcellation of the MNI MRI single-subject brain', *NeuroImage*, vol. 15, no. 1, pp. 273-289.

van den Heuvel, MP, Mandl, RC, Stam, CJ, Kahn, RS & Pol, HEH 2010, 'Aberrant frontal and temporal complex network structure in schizophrenia: a graph theoretical analysis', *Journal of Neuroscience*, vol. 30, no. 47, pp. 15915-15926.

Van Essen, DC & Ugurbil, K 2012a, 'The future of the human connectome', *NeuroImage*, vol. 62, no. 2, pp. 1299-1310.

Van Essen, DC, Ugurbil, K, Auerbach, E, Barch, D, Behrens, T, Bucholz, R, Chang, A, Chen, L, Corbetta, M & Curtiss, SW 2012b, 'The Human Connectome Project: a data acquisition perspective', *NeuroImage*, vol. 62, no. 4, pp. 2222-2231.

Van Hartevelt, TJ, Cabral, J, Deco, G, Møller, A, Green, AL, Aziz, TZ & Kringelbach, ML 2014, 'Neural plasticity in human brain connectivity: the effects of long term deep brain stimulation of the subthalamic nucleus in Parkinson's disease', *PloS one*, vol. 9, no. 1, p. 86496, viewed 25 August 2017, https://www.ncbi.nlm.nih.gov/pmc/articles/PMC3899266/.

van Rotterdam, A, Da Silva, FL, Van den Ende, J, Viergever, M & Hermans, A 1982, 'A model of the spatial-temporal characteristics of the alpha rhythm', *Bulletin of mathematical biology*, vol. 44, no. 2, pp. 283-305.

Vanrumste, B 2002, 'EEG dipole source analysis in a realistic head model', Ghent University.

Webster, JG 2014, *The physiological measurement handbook*, CRC Press.

Wendling, F, Bellanger, J-J, Bartolomei, F & Chauvel, P 2000, 'Relevance of nonlinear lumped-parameter models in the analysis of depth-EEG epileptic signals', *Biological cybernetics*, vol. 83, no. 4, pp. 367-378.

Wendling, F, Bartolomei, F, Bellanger, J & Chauvel, P 2002, 'Epileptic fast activity can be explained by a model of impaired GABAergic dendritic inhibition', *European Journal of Neuroscience*, vol. 15, no. 9, pp. 1499-1508.

Wendling, F, Bartolomei, F, Mina, F, Huneau, C & Benquet, P 2012, 'Interictal spikes, fast ripples and seizures in partial epilepsies–combining multi-level computational models with experimental data', *European Journal of Neuroscience*, vol. 36, no. 2, pp. 2164-2177.

Westmoreland, BF 1996, 'Epileptiform electroencephalographic patterns', in *Mayo Clinic Proceedings*, Elsevier, vol. 71, no. 5, pp. 501-11.

Westmoreland, BF, Benarroch, EE & Reagan, TJ 1994, *Medical neurosciences: An approach to anatomy, pathology, and physiology by systems and levels*, Lippincott Williams & Wilkins.

Wilson, HR & Cowan, JD 1972, 'Excitatory and inhibitory interactions in localized populations of model neurons', *Biophysical journal*, vol. 12, no. 1, pp. 1-24.

Womelsdorf, T & Fries, P 2007, 'The role of neuronal synchronization in selective attention', *Current opinion in neurobiology*, vol. 17, no. 2, pp. 154-160.

Woodman, MM, Pezard, L, Domide, L, Knock, SA, Sanz-Leon, P, Mersmann, J, McIntosh, AR & Jirsa, V 2014, 'Integrating neuroinformatics tools in TheVirtualBrain', Frontiers in neuroinformatics, vol. 8, p. 36, viewed 12 January 2016, https://www.frontiersin.org/articles/10.3389/fninf.2014.00036/full.

Zalesky, A, Fornito, A, Harding, IH, Cocchi, L, Yücel, M, Pantelis, C & Bullmore, ET 2010, 'Whole-brain anatomical networks: does the choice of nodes matter?', *NeuroImage*, vol. 50, no. 3, pp. 970-983.

Zetterberg, L, Kristiansson, L & Mossberg, K 1978, 'Performance of a model for a local neuron population', *Biological cybernetics*, vol. 31, no. 1, pp. 15-26.

Zimmermann, J, Griffiths, J, Schirner, M, Ritter, P & McIntosh, AR 2018a, 'Subject specificity of the correlation between large-scale structural and functional connectivity', *Network Neuroscience*, vol. 3, no. 1, pp. 90-106.

Zimmermann, J, Perry, A, Breakspear, M, Schirner, M, Sachdev, P, Wen, W, Kochan, NA, Mapstone, M, Ritter, P & McIntosh, AR 2018b, 'Differentiation of Alzheimer's disease based on local and global parameters in personalized Virtual Brain models', *NeuroImage: Clinical*, vol. 19, pp. 240-251.

Zuo, X-N, Ehmke, R, Mennes, M, Imperati, D, Castellanos, FX, Sporns, O & Milham, MP 2011, 'Network centrality in the human functional connectome', *Cerebral Cortex*, vol. 22, no. 8, pp. 1862-1875.